Software Development for Integrating Molpro with Newton-X for Adiabatic and Non-adiabatic Excited State Dynamics

by

Zhibo Wang

A thesis submitted in partial fulfillment of the requirements for the degree of

Master of Science

Department of Chemistry

University of Alberta

Abstract

An interface between the non-adiabatic dynamics software Newton-X and the quantum chemistry software package Molpro has been created for select methods: second order local coupled cluster (LCC2), second order local algebraic diagrammatic construction (LADC(2)), and complete active space self-consistent field (CASSCF). This interface incorporates Molpro electronic structure methods for the generation of absorption spectra, adiabatic dynamics, and non-adiabatic dynamics via surface hopping. Functionality of the interface was tested with (i) absorption spectra generation using LCC2 and LADC(2) sampling of a Wigner distribution of the ground state for thiophene and the B-Te-6-B tellurophene, (ii) absorption spectra for thiophene using CASSCF, and (iii) non-adiabatic dynamics for methaniminium and thiophene using CASSCF.

For the LCC2/LADC(2) integration, CAM-B3LYP/cc-pVDZ optimized geometries and normal modes were used as the initial seed for the ensemble of Wigner distribution sampled geometries. These sampled geometries were then processed with LCC2/LADC(2) to generate UV-Vis absorbance spectra for the two aforementioned molecules: thiophene and B-Te-6-B. Spectra generated compare reasonably well with experimentally measured spectra, although there are blue-shifts possibly due to the use of modest-sized basis sets for computational efficiency. There are also discrepancies in peak intensities for B-Te-6-B but these could be accounted for by incorporating more excited states, at increased computational cost.

Simulations using the integration of Molpro for CASSCF dynamics were successful in replicating literature results for a methaniminium trajectory and of a thiophene ring opening

involving a non-adiabatic transition from the first excited state to the ground state. This CASSCF implementation also permits UV-Vis spectrum generation via sampling a ground state Wigner distribution and adiabatic dynamics, where trajectories are propagated on a single potential energy surface.

Preface

The code for passing initial conditions from Newton-X to Molpro was implemented with the help of undergraduate student Zhan Tong Zhang who built the first functional interface. Optimization of the initial conditions implementation was completed by myself along with code portability adjustments and the main body of the programming, including all work for CASSCF adiabatic and non-adiabatic dynamics. All research reported in this thesis involves the sole contributions by myself with aid from my supervisor, Dr. Alex Brown.

Acknowledgements

Thanks to Dr. Alex Brown who acted as my supervisor and guide. Additional acknowledgements to Zhan Tong Zhang who laid the groundwork for the project, Dr. Ali Reza Ilkhani for supporting my endeavours, and the whole of the Brown group for the amicable environment. Additional thanks to NSERC Discovery Grant to Alex Brown and the Queen Elizabeth II Scholarship for funding this research and thesis, Compute Canada for the use of their computing resources and storage, and the University of Alberta's Chemistry department for providing the workspace. Finally, thank you to my friends for motivation and my sanity during research, and my family for the everlasting support and presence.

Table of Contents

List of Tables

List of Figures

List of Abbreviations and Acronyms

Abbreviations

ΔE	Energy difference
AD	Adiabatic dynamics
ADC(2)	Second order (canonical) algebraic diagrammatic construction
AIMD	Ab initio molecular dynamics
aVDZ	aug-cc-pVDZ, Dunning's augmented, correlation-consistent valence double-zeta basis set
B3LYP	Becke, 3 parameter, Lee-Yang-Parr
BO	Born-Oppenheimer
CAM-B3LYP	Coulomb-attenuating method, Becke, 3 parameter, Lee-Yang-Parr
CASPT2	Complete active space second order perturbation theory
CASSCF	Complete active space self-consistent field
CC	Coupled cluster
CC2	Second order approximate coupled cluster
CC3	Third order approximate coupled cluster
CCSD	Coupled cluster singles and doubles
CI	Configuration interaction
DF	Density fitting

DFT	Density functional theory
EOM	Equation of motion
FWHM	Full width at half maximum
HF	Hartree-fock
HO	Harmonic oscillator
LADC(2)	Second order local algebraic diagrammatic construction
LCC2	Second order local approximate coupled cluster
LT-DF	Laplace transformed density fitting
MQC	Mixed quantum-classical
MRCI	Multireference configuration interaction
NACV	Non-adiabatic coupling vectors
NAD	Non-adiabatic dynamics
NSERC	Natural Sciences and Engineering Research Council (of Canada)
NVE	Fixed energy
NVT	Fixed temperature
Osc	Oscillator strength
PES	Potential energy surface
QCS	Quantum chemistry software
RHF	Restricted Hartree-Fock
RI	Resolution of identity
S_N	N^{th} (singlet) state, 0 is ground
SA-CASSCF	State-averaged complete active space self consistent field
TD-DFT	Time dependent density functional theory
UV-Vis	Ultraviolet and visible spectrum
VDZ	Valence double-zeta
ZPE	Zero point energy

Chapter 1

Introduction

1.1 Motivation

Molecules in their electronically excited states play important roles in a diverse range of phenomena including vision, atmospheric chemistry, photodriven devices, and biological imaging.[1–6] While a multitude of experimental methods have been developed to study excited states, most require complementary theoretical analysis to interpret the information gathered. Therefore, it is important to develop tools for understanding molecular behaviour on both ground and electronically excited states, to simulate molecular spectra, and to explore potential reaction pathways, especially those initiated on electronically excited states.[4]

Excited electronic states can be computed using a myriad of quantum chemistry methods. At a fixed geometry, there are a number of single reference wavefunction-based approaches built upon ground state Hartree-Fock theory (HF), multi-reference methods such as multi-configuration self-consistent field (MCSCF) as well as post-MCSCF techniques to add in dynamic electronic correlation, and time-dependent density functional theory (TD-DFT), which is constructed upon ground state density functional theory (DFT).[7–9] The most basic wavefunction method of obtaining an excited state wavefunction and corresponding properties from a HF ground state is the configuration interaction approach.[9,10] Other methods

used to obtain excited states in this work are summarized briefly in this chapter.

Molecular dynamics focuses on the intramolecular and/or intermolecular motions including how molecules behave in their expected environments, e.g., gas phase, liquid phase. For example, the consideration of intramolecular forces that guide dynamical behaviour (atomic motions) away from the equilibrium structure can provide insight into a diversity of processes.[11,12] The frame of reference is then moved away from a static image of a molecule, i.e., a single rigid structure, and into the dynamic. This change in thinking allows one to follow the structural transformations a molecule may undergo upon being subject to external stimuli and, importantly, the modification of corresponding properties.

When considering molecular dynamics in the excited electronic state, two important components must be considered: the slow moving molecular dynamics (nuclear motion) and the faster electronic transitions.[13] A number of computational approaches can be taken to deal with these different dynamical processes. Of interest in this thesis are the mixed quantum-classical methods (MQC) which lower the computational cost by using classical mechanics for nuclear motion (Newton's equations of motion) and quantum mechanics to deal with the electronic properties of the molecule.[14–16] This approach, in turn, creates a number of possible representations from (i) dynamics evolving on a single potential energy surface (PES) as adiabatic dynamics, (ii) dynamics occurring on average PESs (Ehrenfest dynamics),[17,18] or (iii) as an area of focus in this thesis, dynamics occurring on a single PES at a time but with the possibility for non-classical transitions (hops) to occur between PESs.

The following sections will briefly introduce the electronic structure theory methods used in this thesis (Section 1.2) as well as the approaches for determining spectra and performing adiabatic and non-adiabatic dynamics. Section 1.3 includes a discussion of the semi-classical Wigner distribution which provides the initial conditions (geometries, and, if needed, momenta) for the generation of UV-Vis spectra or for initiating classical trajectories in the excited state. In Section 1.4, a very brief description of classical dynamics is provided, including details of how to incorporate non-adiabatic transitions. Finally, an overview of the

two research and conclusions chapters of the thesis is provided in Section 1.5.

1.2 Electronic Structure Computation

The computation of molecular properties all stem from the core concept of solving the Schrödinger equation:

$$\hat{H}(\vec{r},\vec{R})\Psi(\vec{r},\vec{R}) = E\Psi(\vec{r},\vec{R}). \tag{1.1}$$

Here, the Hamiltonian operator ($\hat{H}(\vec{r},\vec{R})$) and the wavefuntion ($\Psi(\vec{r},\vec{R})$) both depend on the coordinates of the constituent electrons ($\vec{r}$) and nuclei ($\vec{R}$) of the molecule. The Hamiltonian operator contains the kinetic energy operator for both the nuclei and electrons, as well as potential energy terms involving Coulomb interactions for all the charged particles (electrons and nuclei) making up the molecule. Within the molecule, electrons interact with all other electrons (Coulomb repulsion), the electrons also interact with all nuclei (Coulomb attraction), and the nuclei also interact with each other (Coulomb repulsion). However, approximations are made to make the solution of the Schrödinger equation tractable. The Born-Oppenheimer (BO) approximation is commonly used as it allows for the separation of electronic and nuclear wavefunctions. This approximation is based on the fact that nuclei are much more massive than electrons, and hence move much more slowly. Therefore, the electronic Schrödinger equation can be solved with fixed positions of the nuclei; i.e.,

$$\hat{H}_{el}(\vec{r};\vec{R})\Psi(\vec{r};\vec{R}) = E_{el}(\vec{R})\Psi(\vec{r};\vec{R}). \tag{1.2}$$

The Born-Oppenheimer approximation will be explored further in a later section.

To solve the electronic Schrödinger equation, additional approximations are required, although most methods begin with Hartree-Fock (HF) theory, see Section 1.2.1, where the Coulomb electron correlation is neglected. A variety of post-HF methods use different algorithms to include electron correlation. As each method makes different approximations,

resulting in varying computational accuracy and costs, there are benefits and disadvantages intrinsic to each. Some of the quantum chemistry methods utilized in this thesis to solve the electronic structure problem are briefly outlined in the following subsections; references to the relevant literature for further details are provided. In the end, these methods all aim to determine the electronic wavefunction for the molecule at the relevant geometry, from which one can obtain the molecular properties. Of course, computation of electronic spectra or photoinduced dynamics also demands that the methods used permit the determination of excited electronic state properties (energies and transition strengths).

The majority of excited state computations in this thesis have been carried out with the Molpro quantum chemistry package.[19,20] Some comparison excited state computations, as well as ground state computations, have been performed with Gaussian.[21] For specific quantum chemistry algorithms available in these codes and used in this thesis, references are provided as needed.

1.2.1 Hartree-Fock

The Hartree-Fock (HF) method is the general starting point for wavefunction-based quantum chemistry.[22,23] HF is based on using Slater determinants to write the wavefunction. For single determinant, or restricted HF (RHF), the N-electron determinant can be written as

$$\Psi(q_1, q_2, \ldots q_N) = \frac{1}{\sqrt{N!}} \begin{vmatrix} \Phi_1(q_1) & \Phi_2(q_1) & \cdots & \Phi_N(q_1) \\ \Phi_1(q_2) & \Phi_2(q_2) & \cdots & \Phi_N(q_2) \\ \vdots & \vdots & \ddots & \vdots \\ \Phi_1(q_N) & \Phi_2(q_N) & ... & \Phi_N(q_N) \end{vmatrix}. \tag{1.3}$$

Here, $\Phi_i(q_j)$ are spin orbitals depending on the coordinate q_j which includes both spatial (r_i) and spin (σ) coordinates and built by the respective spin functions ($\alpha(\sigma)$ or $\beta(\sigma)$). By writing the orbitals as linear combinations of atom-centred basis functions and then considering each electron to move in the average potential of the other electrons, one can

rewrite the N-electron equation as N-coupled 1-electron equations (so-called the Hartree-Fock-Roothan equations) which can be solved iteratively in a self-consistent fashion. The HF theory provides a reasonable estimate of molecular energies, structures, and, importantly, the electronic wavefunction, which is based on molecular orbitals. However, the HF method itself does not account for most electron correlation effects which arise from electron-electron interactions. Thus, to account for correlation, post-HF methods must be used to determine more accurate energies, wavefunctions, and corresponding properties.[24,25]

1.2.2 Local Coupled Cluster and Algebraic Diagrammatic Construction

Coupled cluster (CC) methods, such as coupled cluster theory with single and double excitations with perturbative triples (CCSD(T)), are generally heralded as the benchmark approaches for studying single reference dominated ground state electronic structure problems.[26] Additionally, approximate CC methods, with improved computational efficiency, have also been developed and deployed such as the second and third order approximate CC (CC2 and CC3).[27,28] The CC methods have also been extended for the determination of excited states based on the equation of motion (EOM)[29] approach or using linear response.[30]

The accuracy of CC methods does come with drawbacks, such as the high computational cost, where, for example, CCSD scales at around $\mathcal{O}(n^6)$ where n is the number of basis functions. In general, this scaling makes standard CC methods impractical for large molecules. The methods used in Chapter 2 of this thesis gain computational efficiency through two main ideas: (i) density fitting (DF), which is also known as resolution-of-identity (RI), and (ii) localization of orbitals. Density fitting involves an approximation to the two electron repulsion integrals to reduce computational cost; however, one requires an auxiliary basis set to represent the two-electron densities. The use of the auxiliary basis sets is implicit in all subsequent discussions involving the DF approximation.

The use of localized orbitals to reduce computational cost in CC2 and ADC(2) meth-

ods has been introduced and implemented in Molpro.[31,32] With localization of orbitals, the range of the correlations can be restricted, i.e., single and double excitations only occur into localized virtual orbitals located "near" the localized occupied orbitals and, thus, the number of combinations (excitations) of each electron is greatly reduced. In other words, the use of spatially localized orbitals, the number of virtual spaces can be restricted.[33] Molpro's implementation of the local CC methods for excited states are based on the Laplace transformed density fitted (LT-DF) local CC with two versions:[34] (i) the LT-DF local second order coupled cluster, referred to in this thesis as LCC2,[35] and (ii) the LT-DF local second order algebraic diagrammatic construction, referenced as LADC(2).[36] LADC(2) is derived from algebraic diagrammatic construction approach which has been shown to give similar properties to CC methods. Thus, benchmarks have shown that ADC(2) results are comparable to the standards set by CC approaches. In summary, the local CC methods aim to compute high accuracy electronic structure data with low computational cost. For the purpose of this thesis, results based on LCC(2) and LADC(2) will generally be discussed together until explicit comparisons between the two approaches are to be made.

1.2.3 Complete Active Space Self-Consistent Field

The complete active space self-consistent field (CASSCF) approach divides the occupied orbital space into two portions: the active and inactive orbitals.[37] In the active space, the electrons are free to move between orbitals (provided symmetry is retained) while inactive orbitals remain doubly occupied, which reduces the number of configurations which must be considered. This procedure generates multiple configurations which can then be taken into account for computation, where one optimizes both orbitals and weights of configurations in a self-consistent fashion. If one considers several electronic states simultaneously, one obtains a set of orbitals optimized to describe all states (rather than a set optimized for each state individually); this approach is referred to as state-averaged CASSCF (SA-CASSCF) and is the one generally adopted in this thesis. The active space used is designated as

CASSCF(m,n) where m is the number of active orbitals and n the number of active electrons. The accuracy and computational speed of CASSCF depends on the size of the active space selected, including both the number of orbitals along with the number of electrons considered. When all electrons and orbitals are part of the active space, one obtains the full configuration interaction result.

1.2.4 Time-Dependent Density Functional Theory

Density functional theory (DFT) solves the electronic structure problem in a different way than that pursued by wavefunction-based approaches such as those discussed above. Rather than computing the electronic wavefunction, and corresponding energy, DFT solves the problem based on the electron density.[38,39] This approach reduces the complexity of the problem from many dimensions, three per electron (four if spin is included), down to three for the molecule. Properties can then be derived from the densities, just as one can from a wavefunction-based method. In this thesis, DFT is used to determine optimized geometries and harmonic vibrational frequencies (plus corresponding normal modes) in cases where efficient optimizers and/or analytic Hessians are not available for the other methods. Time-dependent DFT (TD-DFT) is an extension of DFT where the densities are "evolved" over time, and through a well-established formalism one can obtain electronic excited states.[39]

In general, TD-DFT provides reasonable excited state energies (within 0.3 eV of experiment) and properties provided care is taken in choosing a functional appropriate for the system of interest.[40] TD-DFT is well known to have problems with specific excited states, e.g., charge transfer states (albeit corrected with range-separated functionals), those involving double excitations, and states with multi-reference character.[41,42] Moreover, standard TD-DFT cannot describe conical intersections between the first excited and ground state, see Section 1.4.2.

1.3 Electronic Absorption and Emission Spectra

Electronic spectra are a consequence of transitions between electronic states. These spectra correspond to absorption (or emission) of photons in the ultraviolet and visible ranges of the electromagnetic spectrum (UV-Vis). Electronic transitions are at the core of a multitude of interesting and important phenomena from fluorescence to vision, light emitting diodes to phosphors in tube lights.[43–47] The first step in simulating any of these phenomena is to have the molecule in question reach the excited state. Hence, the interest in UV-Vis absorbance.

The UV-Vis absorbance spectrum represents the probability, as a function of energy, a molecule, atom, or complex, etc. can absorb a photon and move from the ground electronic state to an excited electronic state. A single electronic transition can be represented by a single peak. By taking a combination of these transitions and their respective probabilities, it is possible to simulate the absorption spectrum of any molecule (or atom) given the energy differences between the electronic states involved.

The simplest method to interpret UV-Vis absorption spectra is via vertical excitation energies and their corresponding oscillator strengths.[48,49] This method uses the optimized geometry of the ground electronic state and computes the excited electronic state energies and oscillator strengths at the same geometry. In reality, molecules do not exist as static equilibrium structures, even at absolute zero due to zero-point energy effects, and thus the lines (delta functions) predicted by vertical excitation do not reflect the reality for molecules.[11,12,50] Molecular spectra will broaden due to any number of effects including temperature, vibrational coupling, pressure, Doppler effects, etc. Most importantly, for the work in this thesis, the ground state molecular vibrational wavefunction samples the ground electronic state geometry away from equilibrium and excitations at those geometries will thus contribute to the spectral broadening.

From the vertical excitation energies and oscillator strengths, one can generate UV-Vis spectra by phenomenologically broadening with a lineshape function. To obtain improved excitation energies, multiple geometry optimizations (ground and excited) and Hessian eval-

uations for vibrational energies are needed.[49,51] From this data, one can then simulate a spectrum via Franck-Condon models.[52,53]

An alternate method is to take weighted distributions of the ground state geometries using harmonic frequencies and normal modes which can be used to construct a "surface" to excite from rather than a point. To obtain a well-mapped distribution of ground state geometries that will adequately reflect the ground vibrational state of a molecule, distributions of the potential geometries a molecule takes must be sampled. One such distribution is the Wigner distribution:[43,44,54,55]

$$f(Q,P) = \frac{1}{\pi}\int_{-\infty}^{\infty} dQ' \psi(Q-Q')^* \times \psi(Q+Q') e^{-2iQ'P}. \tag{1.4}$$

Equation 1.4 presents one form of the Wigner function where Q is the coordinate and P is the momentum of the harmonic oscillator.[56] The Wigner distribution allows for the generation of a weighted distribution of geometries based on the Hessian to represent classically a vibrational wavefunction. This distribution effectively allows for the creation of a collection of initial points which can then be used to simulate a vibrational state. Through this method, one can then generate a starting set of geometries which reflects the molecule at the zero-point vibrational state, which much better reflects real molecular behaviour.[43]

Absorption cross sections ($\sigma(E)$) can then be generated from these sampled vertical excitations by summing the individual lineshapes as follows:[54]

$$\sigma_{i,p}(E) = \frac{\pi e^2 \gamma}{2mc\varepsilon_0 n} \sum_{l \neq i}^{N_{fs}} \left[\frac{1}{N_p^l} \sum_{k}^{N_p^l} f_{il}\left(\boldsymbol{R}_k\right) g\left(E - \Delta E_{il}\left(\boldsymbol{R}_k\right), \delta\right) \right] \tag{1.5}$$

where $g(E - \Delta E_{il}(\boldsymbol{R}_k), \delta)$ can be defined as either a Gaussian or Lorentzian lineshape. Equation 1.5 sums N_p^l points across N_{fs} final states (l), scaling based on the energies (ΔE_{il}) and oscillator strength (f_{il}) at the geometry ($\boldsymbol{R}$) of each current point (k). Here, i is the initial state, generally the ground state, with phenomenological broadenings of δ and the the

standard constants of elementary charge (e), electron mass (m), permittivity of free-space (ε_0), the refractive index (n), and the scaling factor of γ which is equal to $1-\exp(-E/k_BT)$ with T as temperature and k_B being the Boltzmann constant.

1.4 Molecular Dynamics

1.4.1 Adiabatic Molecular Dynamics

A trajectory for a molecule follows the evolution of nuclear positions, and their conjugate momenta, over time given a set of initial conditions (i.e., positions and momenta) and the forces acting on the nuclei. Within the BO approximation, the dynamics take place on a single potential energy surface (PES). Molecular motion is computed classically as the nuclei follow Newton's equations of motion,[14] i.e.,

$$\frac{d^2\boldsymbol{R}_m}{dt^2} = -\frac{1}{M_m}\frac{\partial E_k}{\partial \boldsymbol{R}_m} \tag{1.6}$$

where $\boldsymbol{R}_m$ is the position, M_m is the mass of nucleus m, and E_k is the potential energy of the current state k.[54] To propagate such trajectories, nuclear gradients ($\partial E_k/\partial \boldsymbol{R}_m$) are used to obtain the forces at the current geometry.[57–59] These gradients are then used with the trajectory's current velocity to generate the next step of the trajectory, i.e., the new position and momentum. In the present work, Newton's equations of motion are integrated numerically.[54]

1.4.2 Conical Intersections and Avoided Crossings

The main contribution to non-adiabatic interactions arise when two discrete electronic states become (near) degenerate and the vibrational motion of molecules can then bridge the gap between the states allowing for electronic transitions without radiation; these transitions represent the breakdown of the BO approximation as the electronic and nuclear motions

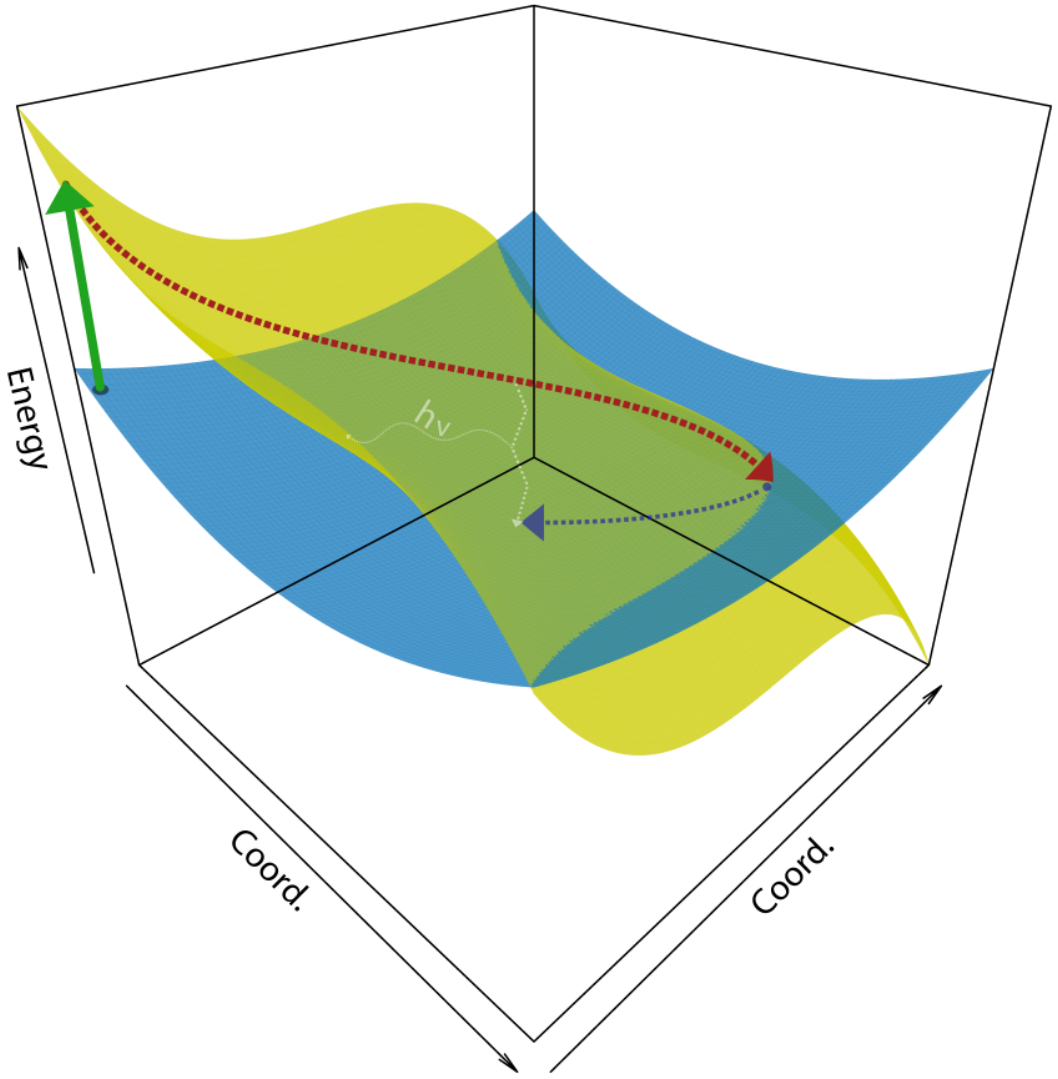

Figure 1.1: Simplified representation of a seam of a conical intersection. Degeneracies between two states can present seams in the potential energy surfaces where the two states cross over. Normal, adiabatic relaxation paradigms manifest as a radiative transition involving spontaneous emission. Conical intersections thereby provide an alternative pathway for relaxation. When the states do not actually cross, an avoided crossing can be observed with similar effects.

can no longer be separated. In most cases, these (near) degeneracies present themselves as either conical intersections or avoided crossings.[1,3,4,54,60–63] Here, the vibrational motions of the atoms are no longer insignificant as the motions of the nuclei are what allows for the non-radiative transition. As seen in Figure 1.1, conical intersections are a "funnel" from a higher energy electronic state to a lower energy one.[63–65] As such, these interactions will affect molecular dynamics and spectra due to the ultrafast nature of the transition.[65] Quantum chemistry computations to locate conical intersections are important for explaining photo-induced behaviours in molecules where light driven transitions may be quenched internally. Moreover, going beyond the static picture to consider dynamics is often necessary to determine the impact the conical intersection has on photophysical behaviour.

1.4.3 Non-Adiabatic Molecular Dynamics

The BO approximation can break down in a number of circumstances. This breakdown mainly occurs when the electrons and nuclei couple in situations of vibronic coupling.[4,66,67] In these cases, the vibrational and electronic transitions allow for ultra-fast interstate crossings making nuclear motion no longer trivial in comparison to the electronic transition timescale. These crossovers where electronic states couple form so-called conical intersections and avoided crossings, best visualized as where two PESs meet and intersect.[1,3,4,54,60–63]

To account for breakdowns in the BO approximation, non-adiabatic interactions must be kept in mind, including when performing adiabatic molecular dynamics.[3,4,60,61,68] Non-adiabatic coupling coefficients, which determine the probability of the molecule "switching" states[34,58] can be computed. The surface hopping approach to classical non-adiabatic dynamics involves two PESs which are (near) degenerate, for which a probability exists (based on the non-adiabatic coupling coefficients) for the electrons to hop across to the other PES. Molecular dynamics is studied using mixed quantum-classical methods where the motion of nuclei are classically evolved with quantum electron states superimposed.[60]

In the present work, the trajectory surface hopping method, based on Tully's fewest

switches algorithm, is used.[16,54] The hopping probability ($P_{K\to L}$) is based on the change in the population of target state ($\Delta \boldsymbol{p}_L$), corresponding to the adiabatic population, compared to the current state ($\boldsymbol{p}_K$),[14,16,54,69] i.e.,

$$P_{K\to L} = \frac{\Delta \boldsymbol{p}_L(K, \Delta t)}{\boldsymbol{p}_K}. \tag{1.7}$$

As $\Delta \boldsymbol{p}_L$ is dependent on the non-adiabatic coupling vector between K and L, this trajectory can then be propagated along a single PES until non-adiabatic factors take over and allow for the exchange (hop) between the two considered PESs. The semi-classical trajectory obtained thereby represents the non-adiabatic dynamics for the molecule.

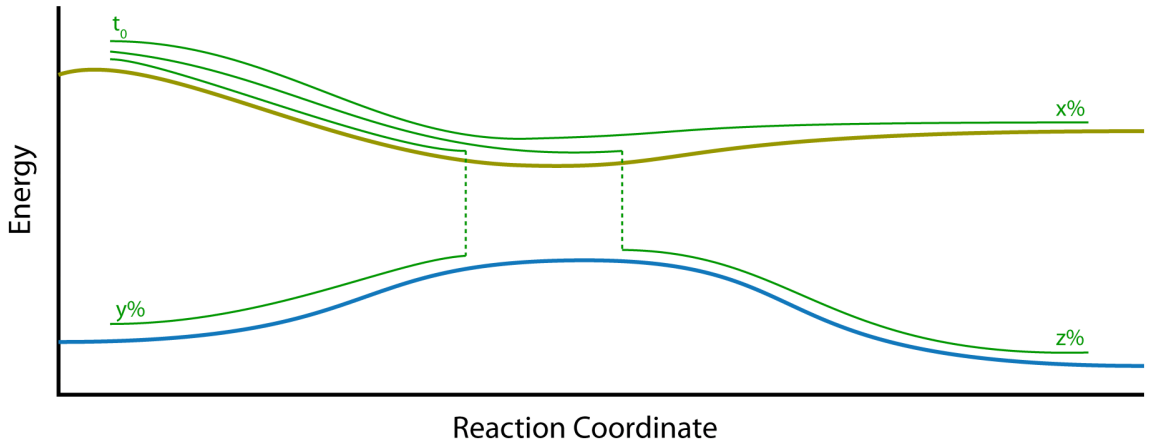

Figure 1.2: A classical molecular trajectory is traversed one state at a time. When two states begin to couple, the hopping probability is computed and the trajectory is updated to hop to the other surface when applicable.

Overall, surface hopping is conceptually straightforward and the name summarizes the important process. One can visualize surface hopping akin to two parallel roads where one traverses one path until an opportune crossing presents itself (Figure 1.2), thereby allowing one to cross the road and travel on the other. Replacing the roads by PESs and crossroads with regions of non-adiabatic coupling, surface hopping is a relatively straightforward method to implement; moreover, the algorithm has been developed, and used, in software packages such as Newton-X,[54,69] where one just requires the appropriate nuclear gradients and non-

adiabatic coupling vectors.

As mentioned above, to compute the probability for surface hopping, non-adiabatic coupling vectors must be determined. For Molpro, these vectors are obtained as derivatives of the wavefunction with respect to nuclear position and can either be determined numerically or analytically for CASSCF or MRCI wavefunctions.[34,58] The coupling vectors are then used to obtain the probability for transitions between PESs. Using Tully's algorithm, the trajectory is checked at each time step to ascertain which state is appropriate for progression, thus creating the desired hops across the non-adiabatic regions.[16,54]

1.5 Thesis Overview

This thesis describes the creation of an interface between Newton-X,[54,69] a software package focused on ab initio molecular dynamics (AIMD) including non-adiabatic dynamics (trajectory surface hopping), and Molpro,[19,20] an electronic structure computation package. Through this interface, the routines and quantum chemistry algorithms found in Molpro can be used to expand and augment Newton-X's available methods for simulating absorption and emission spectra as well as for performing excited state dynamics.

This thesis includes the development and testing of the Molpro/Newton-X interface for three types of quantum chemistry methods: LCC2, LADC(2), and CASSCF. Included in the thesis is the implementation algorithm for the underlying Perl interface used to connect Newton-X and Molpro. The implementation relies heavily on matching Molpro output flags to data requested by Newton-X and then parsing output as well as converting the data to the format required by Newton-X. Also included in the technical description are the environmental setup requirements for running such jobs, where extra parameters are passed to the software to function reliably.

For LCC2 and LADC(2), UV-Vis absorption spectra were computed using thiophene and a tellurophene as examples; the results from thiophene are similar to simulations demon-

strated previously using different quantum chemistry methods.[12] The sampling of the ground state distribution for computing the UV-Vis spectra uses two different approaches: sampling from a Wigner distribution as well as geometries sampled from classical trajectories. The development and testing of the Molpro/Newton-X interface to generate LCC2 and LADC(2)-based UV-Vis spectra are outlined in Chapter 2.

With CASSCF, excited state trajectories were examined to verify the functionality of the non-adiabatic programs. Test computations were carried out with methaniminium (CH_4N^+), where benchmark results are available based on the Gaussian 09/Newton-X interface. The non-adiabatic dynamics of thiophene were then explored with reference to prior examinations,[70] hence, connecting with the UV-Vis spectrum discussed in Chapter 2. The development of the interface and these test results are discussed in Chapter 3.

The final chapter of the thesis summarizes the present software development for the Molpro/Newton-X interface. Remaining challenges, including the use of local methods for adiabatic dynamics, are highlighted. Finally, future directions for extending the functionality of the Molpro/Newton-X interface are outlined.

Chapter 2

Computing Absorption Spectra: Thiophene and Tellurophene B-Te-6-B

2.1 Introduction

Molecules do not exist as a single stationary equilibrium structure due to the effects of zero point energy, i.e., the lowest energy state involves the ground state vibrational wavefunction. Alternatively, thinking classically, their natural vibrations deform the geometry even at 0 K. Therefore, electronic excitation does not involve simply one ground state geometry but rather a set of geometries sampling the ground state vibrational wavefunction. To treat a molecule as static, with a single equilibrium structure, in computation does indeed reduce computational cost but for some molecules, does not belay their true nature.[11,12] Thus computations aiming to portray accurately molecular properties must also take this quantum mechanical nature, or motion, into account.

While a number of computational methods have been devised to evaluate molecular properties under experimental conditions, this chapter is focused on expanding two related methods for determining UV-Vis absorption spectra. First, using a molecular Hessian, it is possible to represent the vibrational modes of a molecule with a Wigner distribution func-

tion.[43,44,54,55] The resulting classical map of the quantum mechanical probability can then be sampled to generate a weighted spectrum accounting for the vibrational distortions.[11,54] Alternatively, a molecular mechanics based classical trajectory can be propagated over time on the ground state potential energy surface (PES) and likewise sampled. By sufficiently populating trajectories to encompass the expected PES, either by running fixed energy (NVE) or fixed temperature (NVT) trajectories, one can follow the vibrational behaviour of a molecule over time and, therefore, sample the various structures from which it can be excited.

In this chapter, the capabilities of two accurate local quantum chemistry methods were investigated for determining UV-Vis absorption spectra. Two select methods for computing excited states, local second order algebraic diagrammatic construction (LADC(2))[36] and local second order approximate coupled cluster (LCC2) quantum chemistry methods,[35] are used along with techniques implemented in Newton-X (NX) by Barbatti et al.[54,69] to investigate the capabilities of these local methods for determining excited state spectra. To carry out these investigations, an interface between Newton-X and the Molpro quantum chemistry package,[19,20] where LCC2 and LADC(2) are available, was implemented. To highlight the new implementation, two example molecules are considered: thiophene and the B-Te-6-B tellurophene (Figure 2.1).

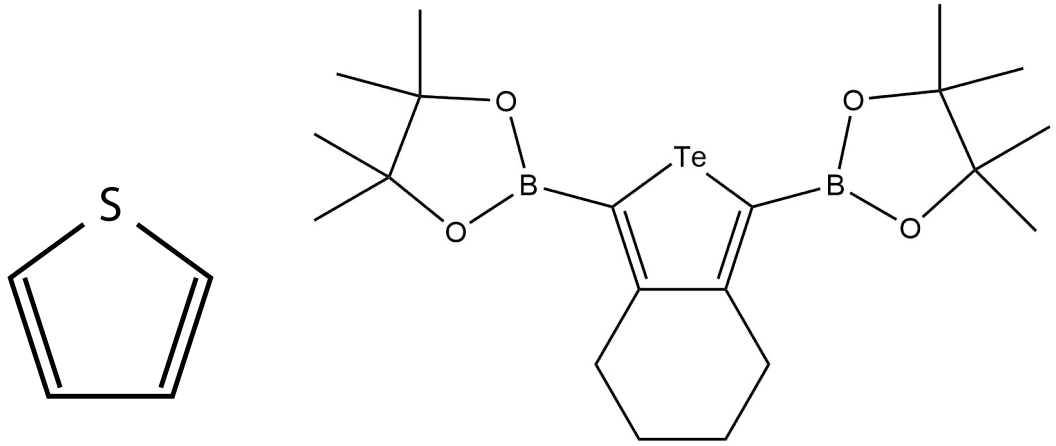

Figure 2.1: Structures of thiophene (left) and the B-Te-6-B tellurophene (right). Hydrogens omitted for clarity.

The electronic absorption spectrum of thiophene was investigated as a test of the Molpro/Newton-

X interface. Thiophene is a heterocyclic aromatic compound which, while small, presents a number of interesting excited electronic state phenomena to investigate. Also, thiophene has a fairly involved electronic spectrum with overlapping peaks corresponding to excited states of different symmetries.[45,46,71] Thiophene itself is also a common subunit in many extended molecular systems, including ones involved in photochemical events and non-linear absorption phenomena.[45,70,72–78] As such, inspecting the dynamics, both adiabatic and non-adiabatic, will greatly improve the understanding of its role in photoluminescent media. Here, UV-Vis spectra based on both sampling a Wigner distribution and adiabatic ground state trajectories were investigated to examine the use of local methods (LCC2 and LADC(2)) in describing the low-lying excited states.

Pinacolboronate containing tellurophene heterocycles, such as B-Te-6-B, show strong phosphorescence in the solid-state.[79–81] Comparatively, hydrogen capped H-Te-6-H tellurophenes are non-emissive. The principles behind the differences in tellurophene heterocycles have thus far only been investigated using time dependent density functional theory (TD-DFT).[79] As such, analysis using other quantum chemistry methods is desirable to explain the emissivity of B-Te-6-B, as well as other analogous species. Using the local CC methods, the absorption spectra were computed and correlated with experimental measurements. Through this analysis one can better characterize the intrinsic electronic transitions. This study of absorption is the first step to understand the behaviour behind the increased luminescence of pinacolboronate containing species.

2.2 Computational Methods

Geometry optimization was carried out for thiophene via the Gaussian 16 software package[21] using density functional theory (DFT) with the CAM-B3LYP functional[82] and the cc-pVDZ basis set (sometimes designated in this thesis as VDZ).[83,84] Similarly, the frequencies and normal modes required for sampling the ground state Wigner distribution were obtained

at the same level of theory (CAM-B3LYP/cc-pVDZ). Due to the limitation on methods to obtain analytical Hessians in Molpro,[19,20,34] DFT Hessians from Gaussian were chosen to generate the Wigner distribution. To determine the UV-Vis spectrum, excited states (energies and oscillator strengths) were then computed using second order local methods, local algebraic diagrammatic construction (LADC(2))[36] and local approximate coupled cluster (LCC2)[35], using the cc-pVDZ or aug-cc-pVDZ (aVDZ)[83] basis sets, as implemented in Molpro 2015.[19,20,34]

The B-Te-6-B tellurophene geometry was obtained from the literature with geometries optimized using the B3LYP functional[85–88] and the cc-pVDZ basis set for all atoms except for tellurium, where the pseudopotential and basis set cc-pVDZ-PP[89] was used; this combination is designated as cc-pVDZ(pp) throughout the thesis. As with thiophene, DFT (B3LYP/cc-pVDZ(pp)) was also used to obtain frequencies and normal modes for generating the Wigner distribution. LCC2 and LADC(2) computations to obtain excitation energies and oscillator strengths were conducted with the same basis set.

To obtain a UV-Vis spectrum, three different methods were considered: (i) vertical excitation energies and oscillator strengths used as bases for simple line-shape functions to phenomenologically broaden the spectrum, (ii) sampling ground state geometries from the Wigner distribution (eq. 1.4) with excitation energies and oscillator strengths determined at each geometry, and (iii) similarly sampling but using fixed energy molecular dynamics trajectories to obtain a distribution of geometries. For method (i), only a single point needs to be sampled at the ground state equilibrium geometry. For methods (ii) and (iii), the spectral intensity for a given excited state i at an excitation energy E, $S_i(E)$, is obtained as

$$S_i(E) = \sum_{n=1}^{N_{points}} P_n(F) g(E - \Delta E_n, \sigma) \tag{2.1}$$

where S is the sum of N_{points} line shape functions g given height P and broadening σ as a function of the excitation energy E. The intensities are then summed over excited states

i to obtain the spectrum (see also Equation 1.5). For method (ii), the N_{points} geometries were sampled from a Wigner distribution as calculated by the respective electronic structure software packages using Newton-X.[54,69] For the required excited state computations, Newton-X was custom integrated with Molpro for the local methods while the available Gaussian implementation was used for the TD-DFT comparison.[90]

For method (iii), the required initial conditions (geometries and momenta) for the trajectories are derived from sampling the Wigner distribution (see Section 1.3), where one requires the Hessian at the equilibrium geometry. These initial conditions were then fed as inputs for adiabatic dynamics on the ground state PES to produce trajectories sampling the geometries over time. Dynamics computations were carried out using LADC(2) and LCC2 with the cc-pVDZ basis set. The adiabatic trajectories were then bound by the zero-point energy (see discussion in Section 2.3.1.3) with the excitation energies and oscillator strengths determined at the sampled geometries. These sets of excitation data from were then convoluted with Lorentzian lineshape functions to generate electronic spectra for the thiophene molecule (Equation 2.1).[54]

2.3 Results and Discussion

The following sections discuss the computationally determined UV-Vis spectra of thiophene and B-Te-6-B with the use of LCC2 and LADC(2) quantum chemistry methods as implemented in Molpro. Results are compared to those obtained with TD-DFT and experiment.

2.3.1 Thiophene

To determine the excited states which are important for examining the absorption spectrum, the vertical excitation energies and respective oscillator strengths were computed. The resulting data are then compared to results from the literature.[42,46] As per Table 2.1, thiophene consistently shows two peaks within the first five excitations that display sizable

(>0.05) oscillator strengths. These two peaks are centred around 6 eV. This assignment is reinforced by Table 2.2 with literature values, where one notes two bright states arising from the excitations, HOMO to LUMO forming the B_2 transition and HOMO-1 to LUMO as the A_1 transition.[42] As the C_{2v} symmetry does not exist when the structure deviates from equilibrium (e.g., breaking the planarity of thiophene), no symmetry is used for the thiophene computations reported in this chapter.

The LCC2 and LADC(2) results are similar to each other in terms of energies and oscillator strengths. Increasing the basis set from cc-pVDZ to aug-cc-pVDZ decreases the excitation energies by approximately 0.2 eV; moreover a dark state with no significant oscillator strength now occurs between the two bright states. These local values also agree well with their canonical counterparts from Table 2.2 despite using substantially smaller basis sets as well as localization approximations. For the DFT-based results, the gap between the bright states is smaller than that determined by the wavefunction-based methods as observed previously.[46] Additionally, Table 2.2 suggests that the transitions that contribute to the B3LYP excitations are reordered energetically in comparison with the wavefunction based methods.[42] The predicted excited states correspond well with experimental measurements which suggest there are two overlapping peaks in this spectral region.[45] As expected due to the relatively modest basis sets used for the LCC2 and LADC(2) computations, the computed band gaps are higher than experimental measurements of 5.33 and 5.70 eV.[45,91] However, the aug-cc-pVDZ results are within 0.02 eV of the RI-CC2 and RI-ADC(2) with the much larger cc-pVQZ basis set.[42]

To compensate for states reordering or oscillator strengths increasing/decreasing when distorted from the equilibrium geometry, the first four excited states were all incorporated into Wigner and trajectory based computations of the UV-Vis spectrum. This choice results in five states (ground state plus four excited states) being computed for every sampled geometry. Since the goal of the work is to test the new Molpro/Newton-X interface, rather than the most accurate simulation of the UV-Vis spectrum of thiophene, this chapter focuses

Table 2.1: Vertical Excitation Energies and Corresponding Oscillator Strengths for the First Five Excited Singlet States of Thiophene

	cc-pVDZ					
	LCC2		LADC(2)		CAM-B3LYP	
Excitation	ΔE (eV)	Osc	ΔE (eV)	Osc	ΔE (eV)	Osc
1	5.928	0.081	5.881	0.096	6.111	0.094
2	6.368	0.106	6.358	0.117	6.180	0.084
3	6.857	0.000	6.884	0.000	7.161	0.001
4	6.900	0.000	6.948	0.000	7.249	0.000
5	7.959	0.000	7.998	0.000	7.688	0.000
	aug-cc-pVDZ				Literature[46]	
	LCC2		LADC(2)		B3LYP/aug-cc-pVTZ	
Excitation	ΔE (eV)	Osc	ΔE (eV)	Osc	ΔE (eV)	Osc
1	5.790	0.087	5.761	0.106	5.67	0.078
2	5.949	0.000	5.989	0.000	5.75	0.079
3	6.140	0.102	6.141	0.110	5.80	0.012
4	6.152	0.017	6.215	0.019	6.34	0.014
5	6.347	0.000	6.329	0.000	6.65	0.028

Table 2.2: Vertical Excitation Energies for Thiophene from Literature Showing the First Two Bright Singlet States[42] Using cc-pVQZ

	RI-CC2		RI-ADC(2)		B3LYP	
Excitation	ΔE (eV)	Osc	ΔE (eV)	Osc	ΔE (eV)	Osc
A_1	5.78	0.078	5.75	0.093	5.79	0.074
B_2	6.13	0.094	6.12	0.105	5.69	0.078

	EOM-CCSD		CASPT2[42,92]	
Excitation	ΔE (eV)	Osc	ΔE (eV)	Osc
A_1	5.83	0.081	5.85	0.067
B_2	6.18	0.085	6.14	0.109

on the more computationally efficient cc-pVDZ results.

2.3.1.1 UV-Vis Spectrum from Phenomenological Broadening

The UV-Vis spectrum can be simulated most simply by considering the vertical excitation energies and oscillator strengths of the molecule each broadened by a single lineshape function, then summed to generate the overall spectrum. Spectra generated in this manner, using the data from Table 2.1 and a Gaussian lineshape with a FWHM of 0.1 eV can be seen in Figure 2.2. The larger difference in energies for the first and second excited states

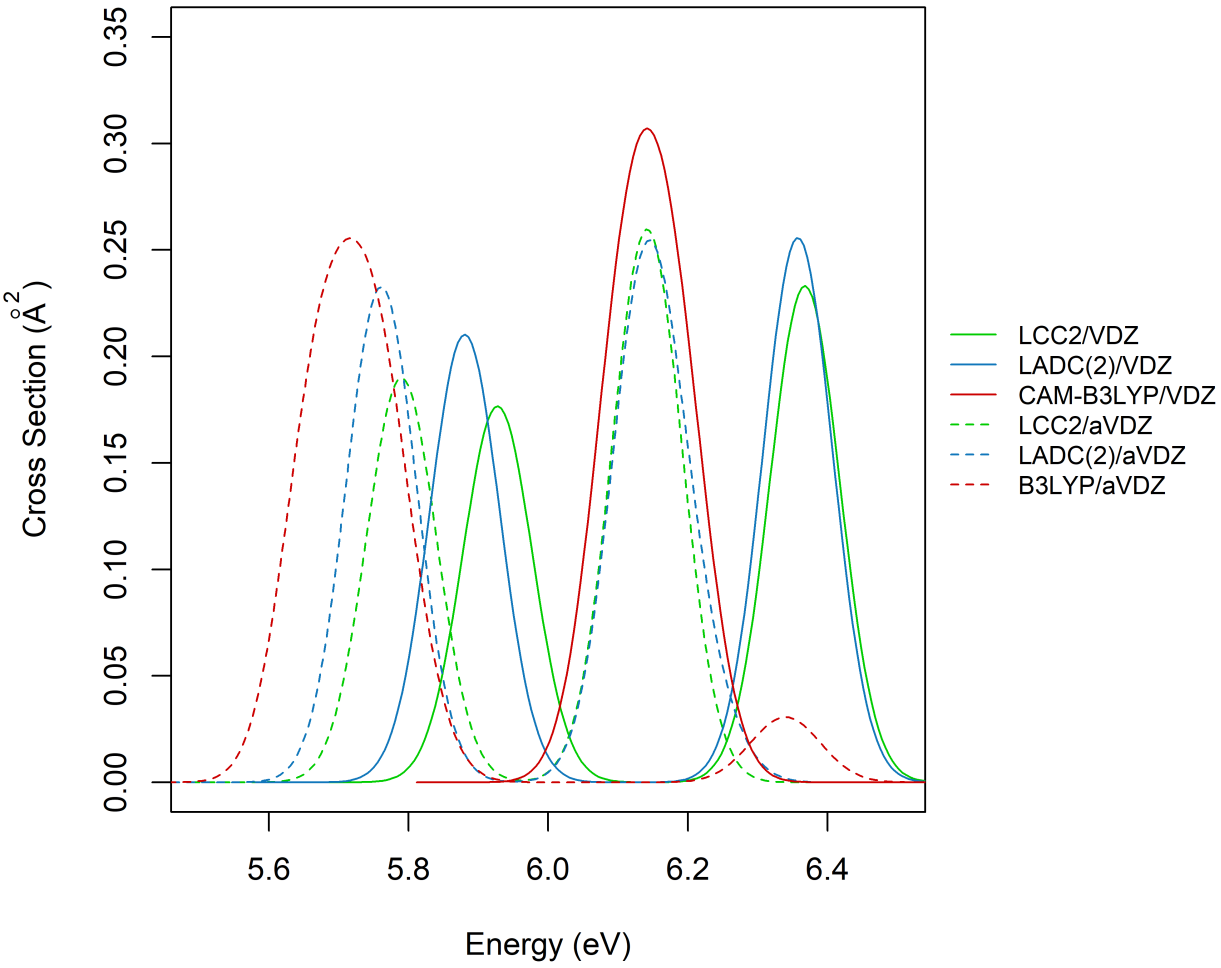

Figure 2.2: Thiophene spectrum generated through phenomenological broadening of the vertical excitations, see Table 2.1, using a Gaussian line shape with FWHM = 0.1 eV. Solid lines are from cc-pVDZ while dashed are from aug-cc-pVDZ. LCC2 is in green, LADC(2) in blue, and DFT (CAM-B3LYP and B3LYP, respectively) values in red.

for the local methods relative to the TD-DFT values is reflected in the bimodal spectra; of course, the two components could be made to overlap by increasing the FWHM. Comparatively the TD-CAM-B3LYP/cc-pVDZ spectrum appears to have only one peak due to the close spacing of the vertical excitation energies of the first two excited states (<0.1 eV); this dependence of the state separation on quantum mechanical approach is consistent with prior research.[42] As reported previously,[42,46] the TD-DFT spectrum resolves to two components using B3LYP/aug-cc-pVDZ.

2.3.1.2 UV-Vis Spectrum from the Wigner Distribution

As discussed in Section 1.3, spectra can also be generated by sampling geometries based on the ground state (harmonic) vibrational wavefunction. Incorporating the first four excited states, spectra were obtained sampling 500 geometries from a Wigner distribution, as determined from CAM-B3LYP/cc-pVDZ normal modes with excited states determined at the LCC2/cc-pVDZ, LADC(2)/cc-pVDZ, and TD-CAM-B3LYP/cc-pVDZ levels of theory. Figure 2.3 displays the spectra determined incorporating the four lowest energy excitations. As these geometries are sampled from the same initial seed for the random number generation and normal modes determined at the same level of theory, the three sets of geometries used to obtain the spectra are identical; hence, any differences in spectra reflect those for the methods used to obtain the excited states. Also of note is that the spectra determined from sampling the Wigner distribution lie slightly lower than their respective equilibrium excitations, more evident in Figures 2.4 - 2.6. This shift is due to how the Wigner sampling incorporates geometries away from the equilibrium structure thus reducing (or increasing) the energy gap between states the further the geometry sampled is away from the equilibrium structure. Despite the shift to lower energy compared to the vertical excitation energies, all three methods used here tend to predict spectra shifted to higher energies relative to the experimental spectrum as measured in the gas phase.

While it appears that there is reasonable agreement between the computed spectra (Figure 2.3) and the expectations from vertical excitation energies alone as well as decent overlap between the quantum chemical methods considered, having a benchmark spectrum does aid in the assessment of the new Molpro/Newton-X implementation and the use of local methods. Experimental data measuring thiophene's photoelectron and UV-Vis spectra in the gas phase suggests that a single peak between 5 and 6 eV is expected, composed of two overlapping bands peaking at 5.33 and 5.70 eV.[45,91] This two-banded nature, which one sees in the asymmetry of the experimental absorption spectrum, is not reflected in the TD-DFT spectrum, even with Lorentzian broadenings reduced to values <0.001 eV. LADC(2) and

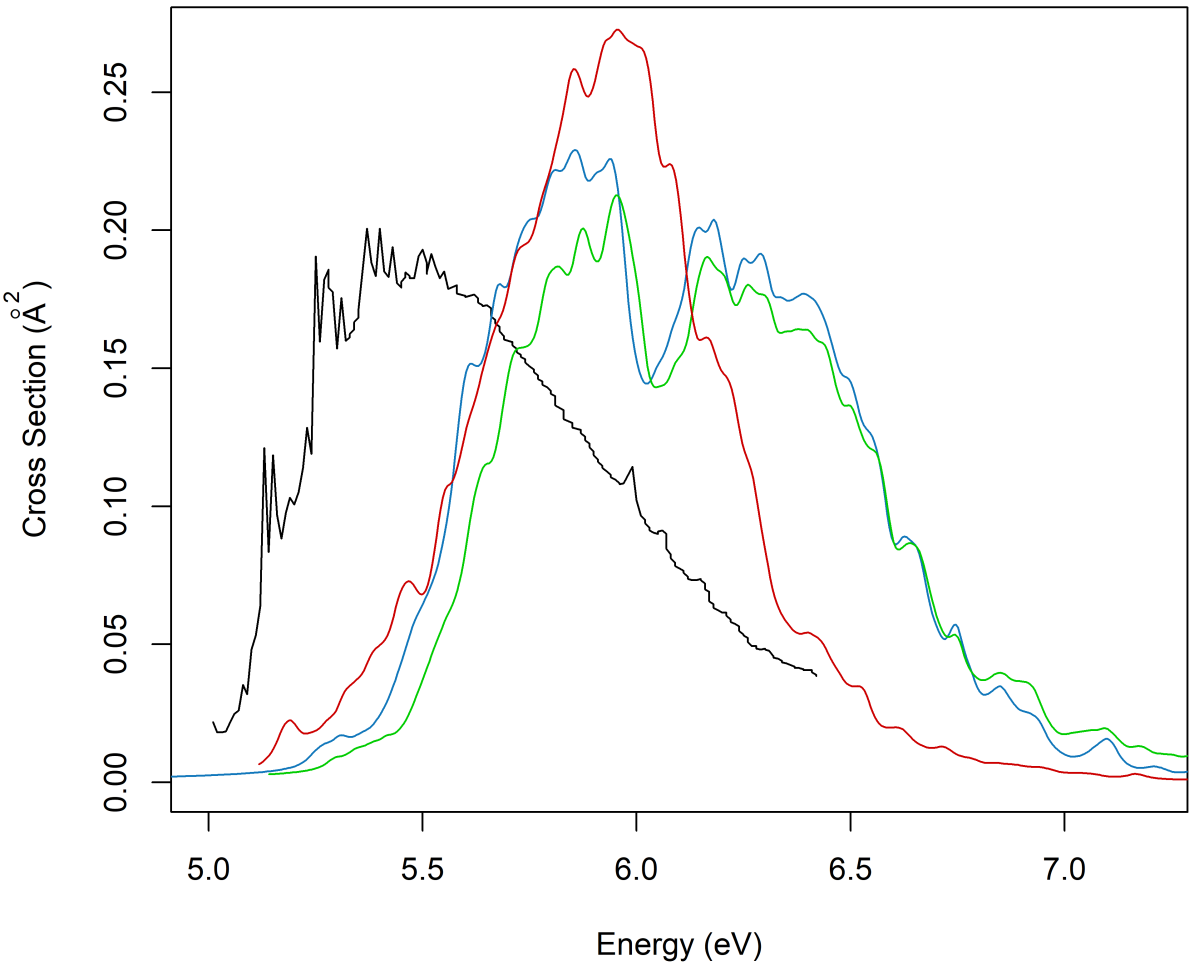

Figure 2.3: Thiophene spectrum generated via a Wigner distribution of 500 initial conditions according to normal modes with a phenomenological broadening of 0.05 eV per Lorentzian line incorporating the first four excited states. Spectra generated with TD-CAM-B3LYP/cc-pVDZ (red), LCC2/cc-pVDZ (green), LADC(2)/cc-pVDZ (blue), and experimental measurement (black).[45]

LCC2, however, do display the ∼0.4 eV separation between the two contributions although both are blue-shifted 0.5 eV compared to experiment. To further understand the spectra, it is worthwhile to consider the individual excited state contributions for each of the quantum chemistry methods used.

Decomposing the single TD-DFT peak into its major components allows for the observation of the overlap between the contributions from these two lowest-lying excited states. Presenting spectra comprised of the lowest two, three, and four excited states shows the con-

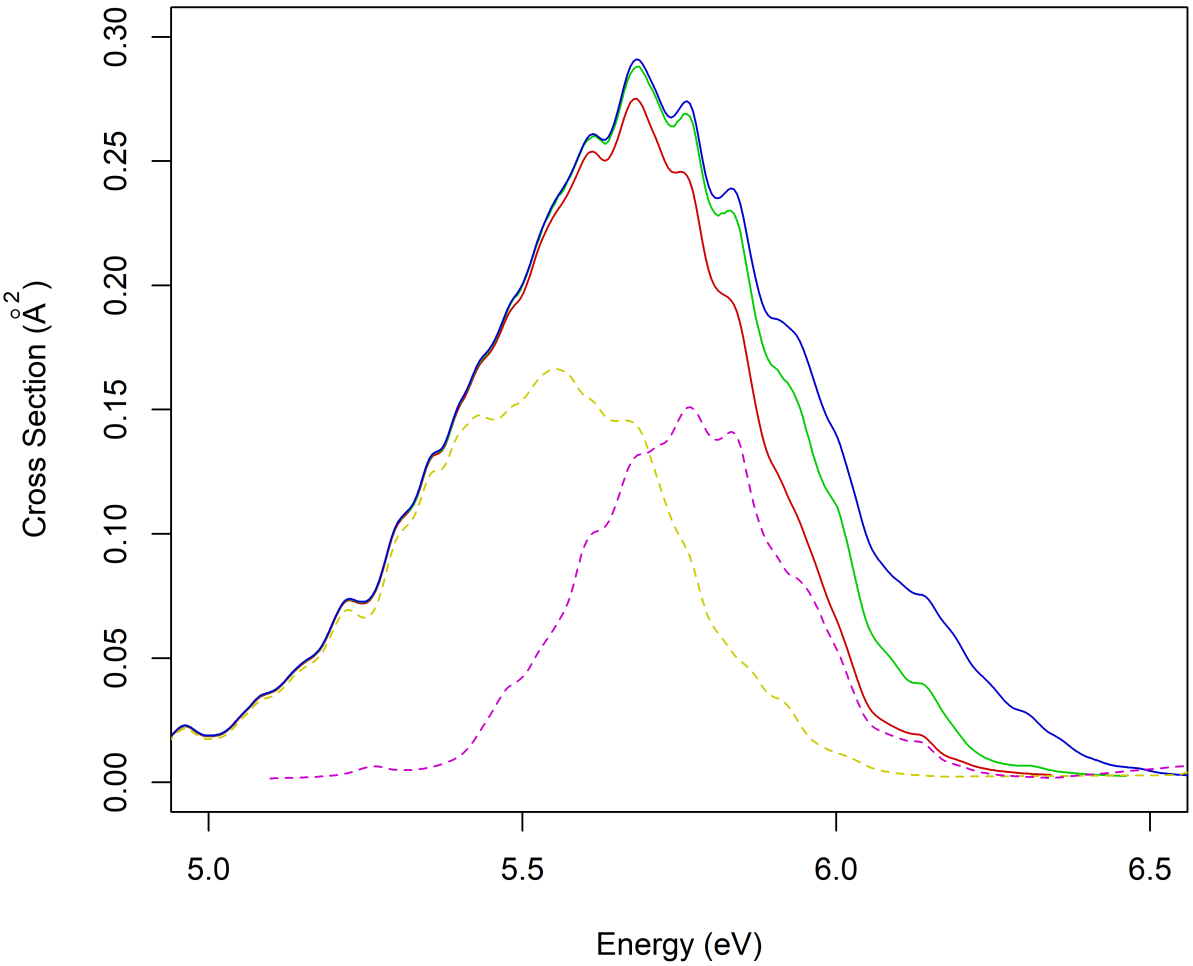

Figure 2.4: TD-CAM-B3LYP/cc-pVDZ spectral components, i.e., excitation to S_1 and S_2, from the Wigner distribution. The two main component peaks are yellow and magenta (individual S_3 and S_4 contributions not illustrated) with the sums of states as the other lines: red for two states, green for three, and blue for four

tribution each of the states makes to the overall spectrum. From Figure 2.4, the peaks for the first two excited states, which have maxima at around 5.55 and 5.77 eV, overlap to form the apparent single peak with a maximum at 5.6 eV. These peak maxima can be compared to the vertical excitation energies of 6.11 and 6.18 eV, respectively (Table 2.1). The third excited state has a modest, but non-negligible contribution to the total spectrum, as seen by the gap between the sums of two versus three states, and thus the oscillator strength appears to gain in strength away from the equilibrium geometry, see Table 2.1.

As mentioned previously, states beyond the first and second excited states were consid-

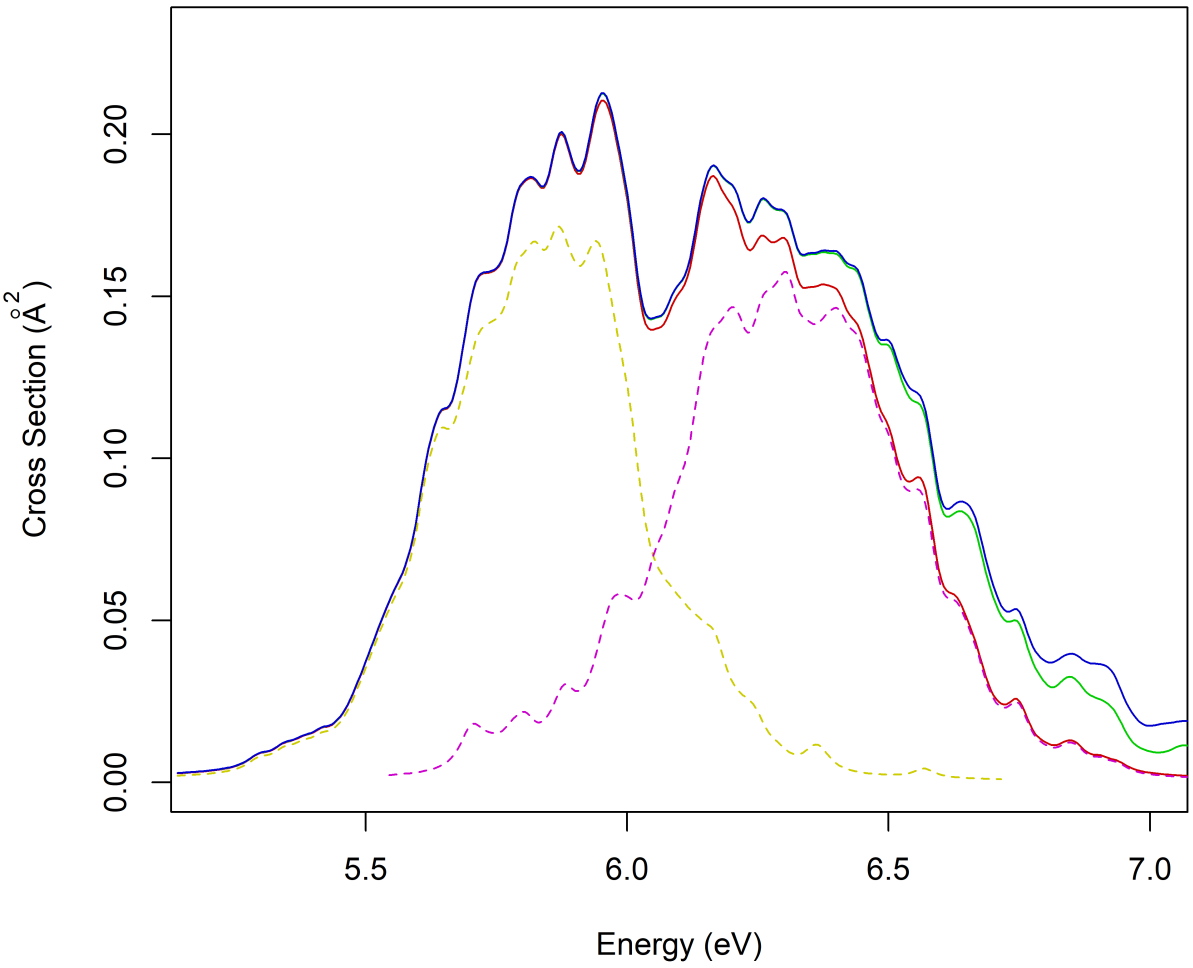

Figure 2.5: LADC(2)/cc-pVDZ spectral components, i.e., excitation to S_1 and S_2, from the Wigner distribution. The two component peaks are yellow and magenta (individual S_3 and S_4 contributions not illustrated) with the sums of states as the other lines: red for two states, green for three, and blue for four.

ered in spectral generation. Based on the computed vertical excitation energies, see Table 2.1, the need to include additional states for LCC2 and LADC(2) approaches is exacerbated for computations with the aug-cc-pVDZ basis set (not considered in the present work) due to the "dark" second excited state and the small, but non-negligible, oscillator strength of the fourth excited state transition. While there are advantages to including states beyond the third excited state for the cc-pVDZ basis, the improvements acquired are not significant in comparison to the spectra obtained with two or three states. From Figures 2.5 and 2.6, which illustrate the LCC(2)/cc-pVDZ and LADC(2)/cc-pVDZ spectra, respectively, gener-

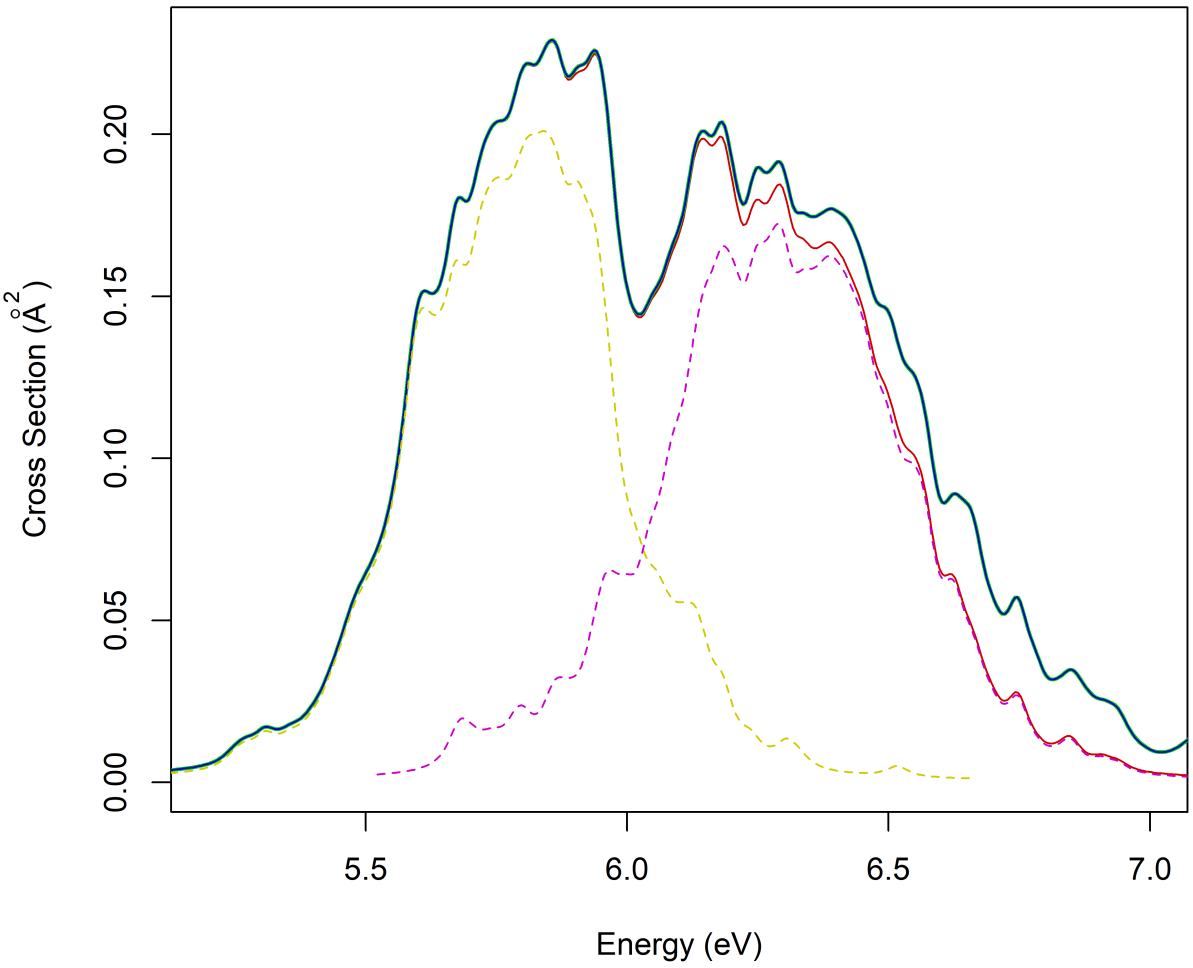

Figure 2.6: LCC2/cc-pVDZ spectral components, i.e., excitation to S_1 and S_2, from the Wigner distribution. The two component peaks are yellow and magenta (individual S_3 and S_4 contributions not illustrated) with the sums of states as the other lines: red for two states, green for three, and blue for four. Note that the spectra incorporating three and four states overlap.

ated incorporating two, three, or four excited states, it can be seen that incorporating the fourth excited state into the spectrum effectively overlaps with the sum of three excitations. Comparatively, there is a small increase in intensity for the spectra above 6.2 eV when including the third excited state. This change can be attributed to the third excited state gaining oscillator strength at these geometries, as alluded to in Table 2.1 in the discrepancy between cc-pVDZ and aug-cc-pVDZ oscillator strengths. Additionally, there are also small differences between LCC2/LADC(2) computations where three, four, and five total states

(two, three, and four excited states) are taken into account. Considering that most of these differences between the spectra for the number of states considered are small for energies less than 6.2 eV (2 versus 3 states) and 6.5 eV (3 versus 4 states), considering two excited states is sufficient when determining the spectrum using the cc-pVDZ basis; additional states would have to be considered if diffuse functions (aug-cc-pVDZ) are to be used.

2.3.1.3 UV-Vis Spectrum from Trajectory Based Sampling

As an alternative to generating spectra from geometries sampled from the Wigner distribution, geometries from the ground state could be sampled from molecular dynamics trajectories. From the initial conditions (geometries and momenta) obtained from the Wigner distribution, ground state adiabatic dynamics were obtained using LADC(2) and LCC2, both using the cc-pVDZ basis set. Default energy and oscillator strength screening from Newton-X selects approximately 300 trajectories from 500 initial conditions. Trajectories, where the normalized relative transition probability (f/f_{max}) are greater than normally distributed threshold probabilities to avoid oversampling, are then selected to reduce bias and computational load. Each trajectory was propagated for 100 femtoseconds with 0.5 fs steps for 200 total time steps. Total energies that deviate outside 0.5 eV from the initial energy are terminated due to energy conservation loss.

Tracing the energy contributions for the trajectories (see Figure 2.7) reveals a fundamental flaw in the ground state adiabatic trajectories based on LCC2 and LADC(2) methods. In theory, the total energy, i.e., the sum of the kinetic and potential energies of the system should be (near, depending on the integration scheme used) constant. However, it is clear that energy is not conserved and, hence, many trajectories are terminated before propagating for 100 fs. Further investigation propagated as many trajectories as possible beyond the 0.5 eV threshold. This divergence suggests that the LCC2/LADC(2) ground state nuclear gradients have numerical problems; gradients for LCC2 and LADC(2) have primarily been obtained for excited states using Molpro. This problem is further evidenced by a comparison

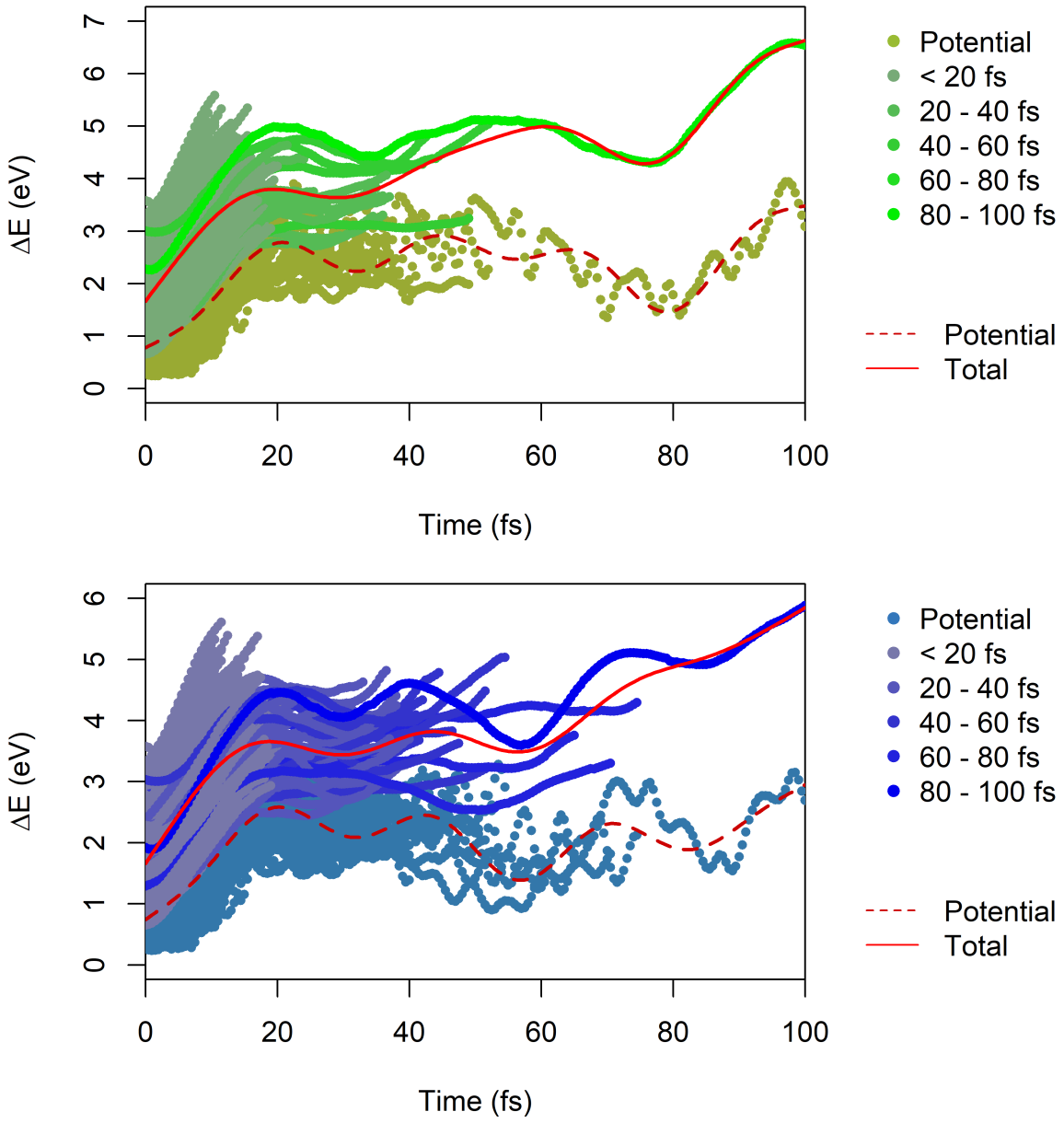

Figure 2.7: Trace of total (brighter, multiple) and potential energies (darker, single) for LCC2/cc-pVDZ (green) and LADC(2)/cc-pVDZ (blue) adiabatic dynamics trajectories. Energy is zeroed at the respective equilibrium ground state geometries. Due to stepwise filtering, most trajectories terminate before the full 100 fs computation due to rapid energy jumps with longer trajectory total energies being more saturated. Red trendlines show the energy climb with the total energy (solid line) and the potential energy (dashed line).

with energies obtained along a DFT-based ground state trajectory, see Figure 2.8. Here, a CAM-B3LYP/cc-pVDZ trajectory of thiophene was generated from a given set of initial conditions (geometry and momenta). Using the same starting conditions, a LADC(2)/cc-pVDZ

trajectory was also evolved. The DFT total energy remains relatively flat as compared to the constantly rising LADC(2) total energy.

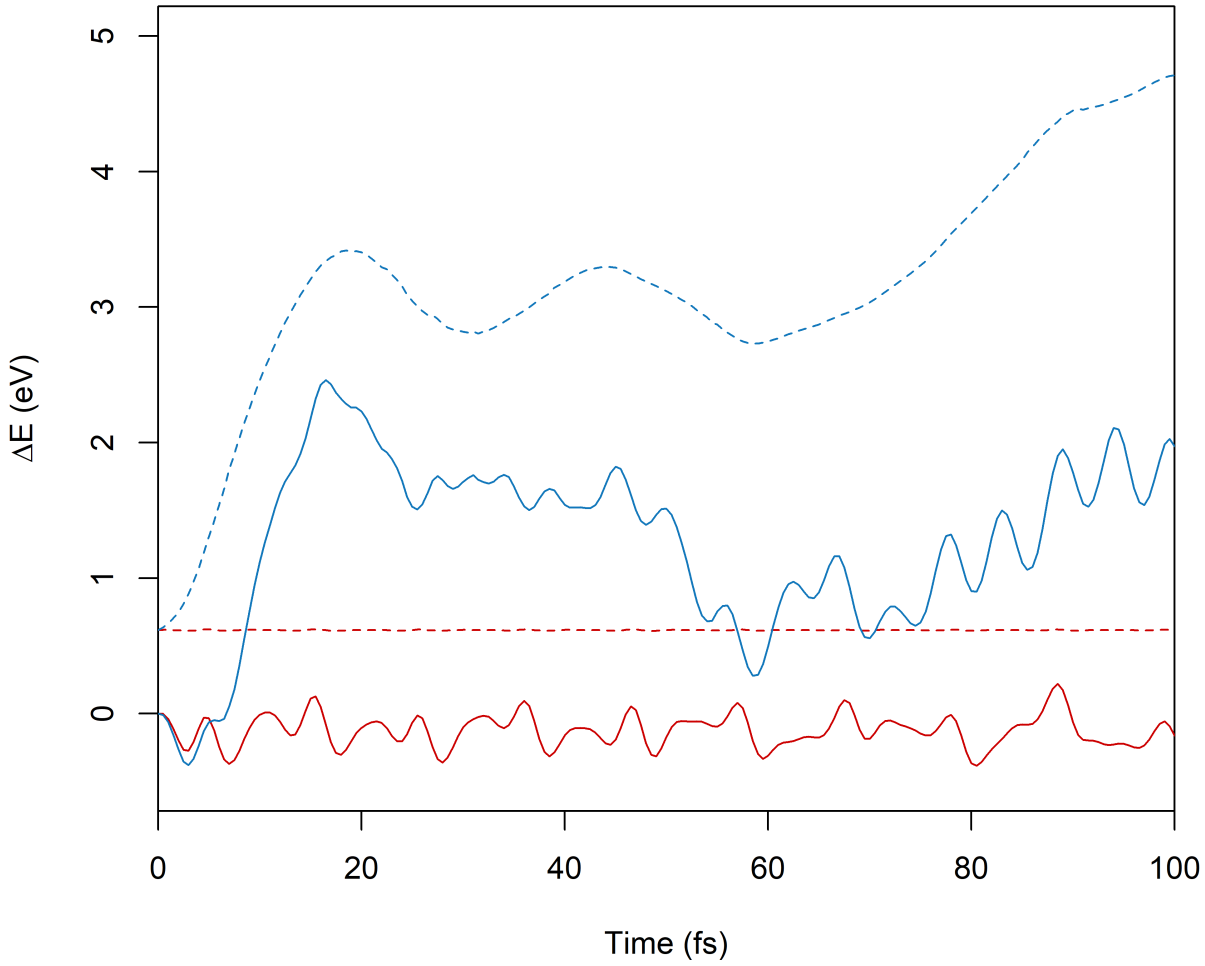

Figure 2.8: Comparison of potential (solid) and total (dashed) energy deviations for a single CAM-B3LYP/cc-pVDZ (red) and corresponding LADC(2)/cc-pVDZ (blue) adiabatic ground state trajectory of thiophene from the initial geometry.

While LCC2 and LADC(2) are methods that theoretically are applicable for both ground and excited states, the present implementations in Molpro might not compute the ground state gradients correctly. Access to these gradients is not documented in the manual but can be accessed via less well documented input keywords.[34] This problem is exemplified through the lack of concurrent computing of ground and excited state properties for the LCC2 and LADC(2) methods, i.e., one can only obtain either ground or excited state properties but not

both simultaneously. A comparison test with LMP2/cc-pVDZ[93,94] (see Figure 2.9) also shows a similar steep climb in the total energy suggesting that the localization may cause numerical problems with the ground state gradients. Hence, while the present LCC2 and LADC(2) Molpro/Newton-X integration is capable of generating UV-Vis spectra, there appears to be problems with the nuclear gradients and thus LCC2 and LADC(2) are not currently suited for adiabatic dynamics based on Molpro 2015; future testing of their use for dynamics could be warranted if these methods continue to be developed in future Molpro releases.

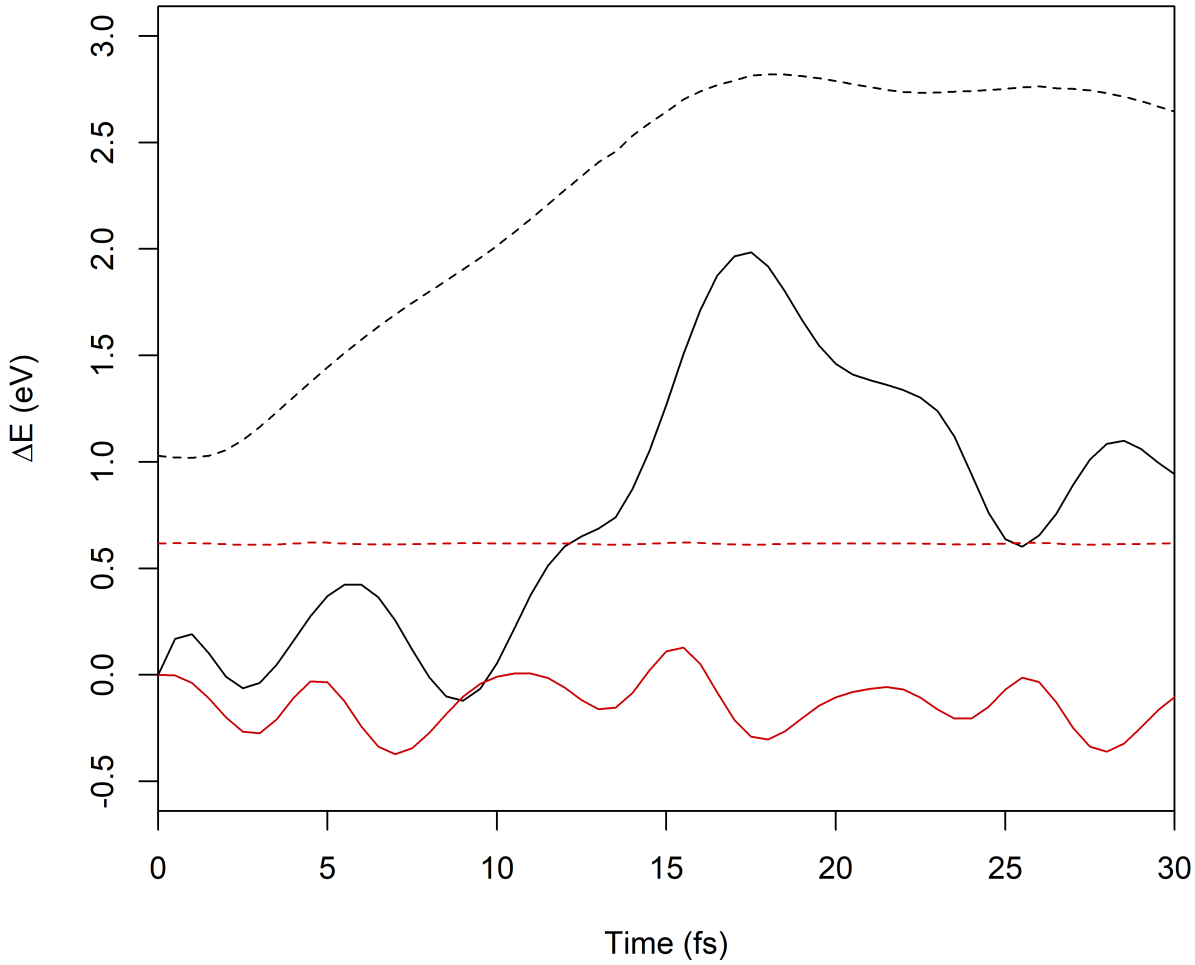

Figure 2.9: Potential (solid) and total (dashed) energy deviations for a single LMP2/cc-pVDZ (black) trajectory compared with a CAM-B3LYP/cc-pVDZ (red).

Although there were energy conservation problems along the trajectory, one could use the sampled geometries to generate a UV-Vis spectrum. To obtain a spectrum from the

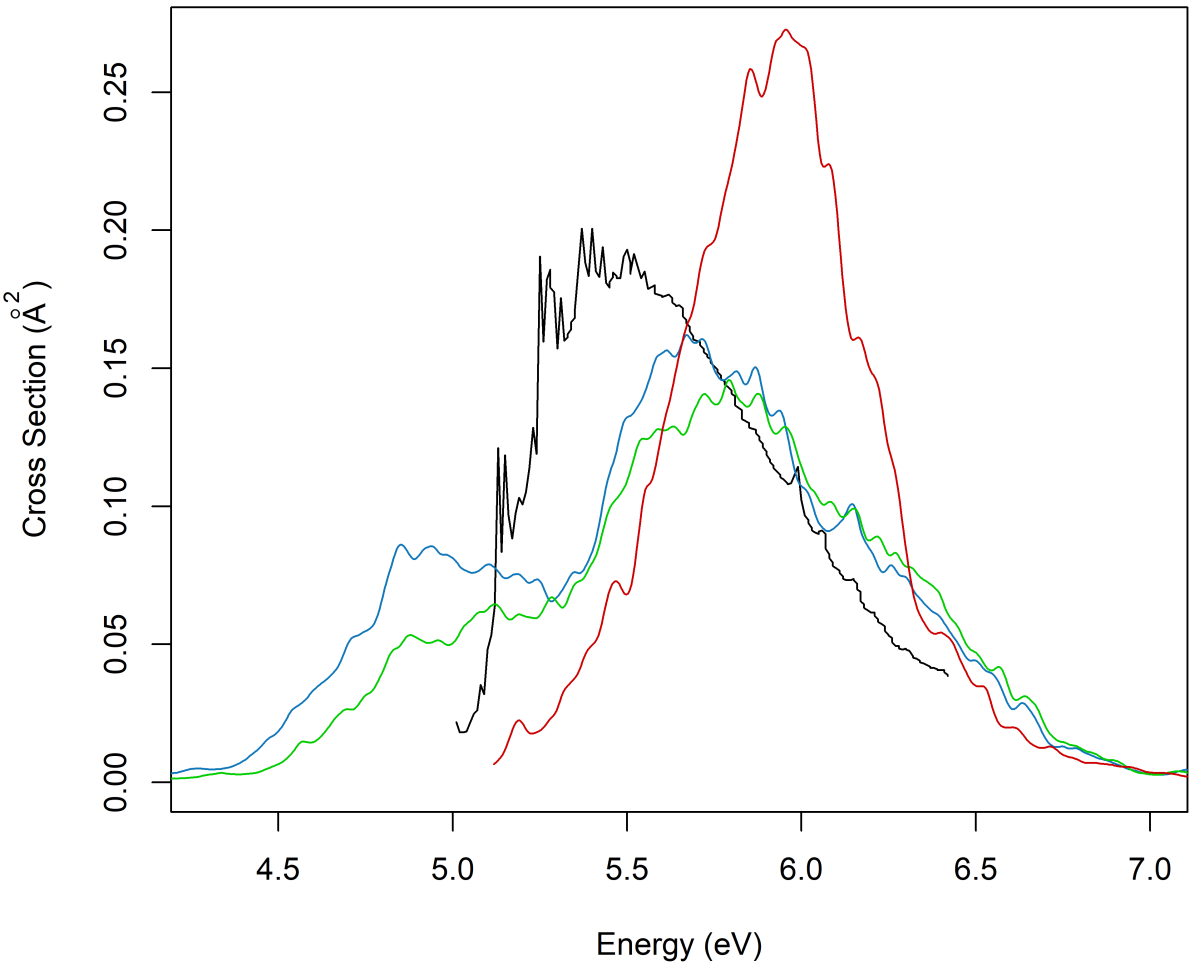

Figure 2.10: Thiophene spectrum generated via sampling a set of ground state trajectory generated geometries, where vertical excitations and their respective oscillator strengths were determined, see main text for details. The TD-CAM-B3LYP/cc-pVDZ (red) and experimental spectrum[45] (black) is are included for comparison. LCC2/cc-pVDZ data is in green while LADC(2)/cc-pVDZ is in blue.

trajectories, the vertical excitation energies and their respective oscillator strengths were determined at sampled geometries and then compiled. To reduce correlation between sampled geometries, only every 10th trajectory step (every 5 fs) was sampled. This sampling was further restricted to geometries within 1.8 eV of the energy of the ground state at the equilibrium geometry; this value of 1.8 eV corresponds to the harmonic zero point energy. The energy filtering was required due to the energy convergence issues with the LCC2/LADC(2) trajectories leading to sampling of very high energy regions of the ground state potential

energy surface. From Figure 2.10, it is evident that the peaks are substantially red-shifted compared to Figure 2.3 by ∼0.5 eV for the higher energy peak and ∼1 eV for the lower energy peak. This appears to better fit the experimental spectrum's description of the 5.33 and 5.70 thiophene peaks. However, this improvement may be somewhat fortuitous due to the procedures used to sample the energy non-conserving trajectories.

2.3.2 B-Te-6-B

Using the methods outlined above, the UV-Vis absorption spectrum for the B-Te-6-B tellurophene was also generated to further test the methodology and to compare to the experimental measurement.[79,95] To start, the vertical excitation energies of the first four singlet states along with their respective oscillator strengths were computed at the LCC2/cc-pVDZ(pp) and LADC(2)/cc-pVDZ(pp) levels of theory; these results could be compared to the previously published values. Looking at Table 2.3, there are two excitations with significant oscillator strengths below 5 eV. If broadened (Figure 2.11), it can be seen that the local wavefunction-based methods display more intense peaks spread apart more widely than the TD-B3LYP results (0.9 - 1.1 eV gap as compared to 0.6 eV).

Table 2.3: Singlet Vertical Excitation Energies and Corresponding Oscillator Strengths of B-Te-6-B. All Results Determined Using cc-pVDZ(pp)

	B3LYP		LCC2		LADC(2)	
Excitation	ΔE (eV)	Osc	ΔE (eV)	Osc	ΔE (eV)	Osc
1	3.692	0.070	3.839	0.091	3.641	0.108
2	4.200	0.000	4.426	0.000	4.392	0.000
3	4.303	0.366	4.744	0.439	4.706	0.426
4	4.772	0.000	5.232	0.000	5.393	0.001

Using Wigner sampling of the ground state (based on B3LYP/cc-pVDZ(pp) optimized geometries and normal modes), the low energy peak in the LADC(2) and LCC2 spectra agrees modestly well in terms of position and intensity with the experimental data, see Figure 2.11. However, at present, the higher energy peak intensity is too low. Figure 2.11 was generated with 197 initial geometries for LCC2 and 173 with LADC(2); however, the

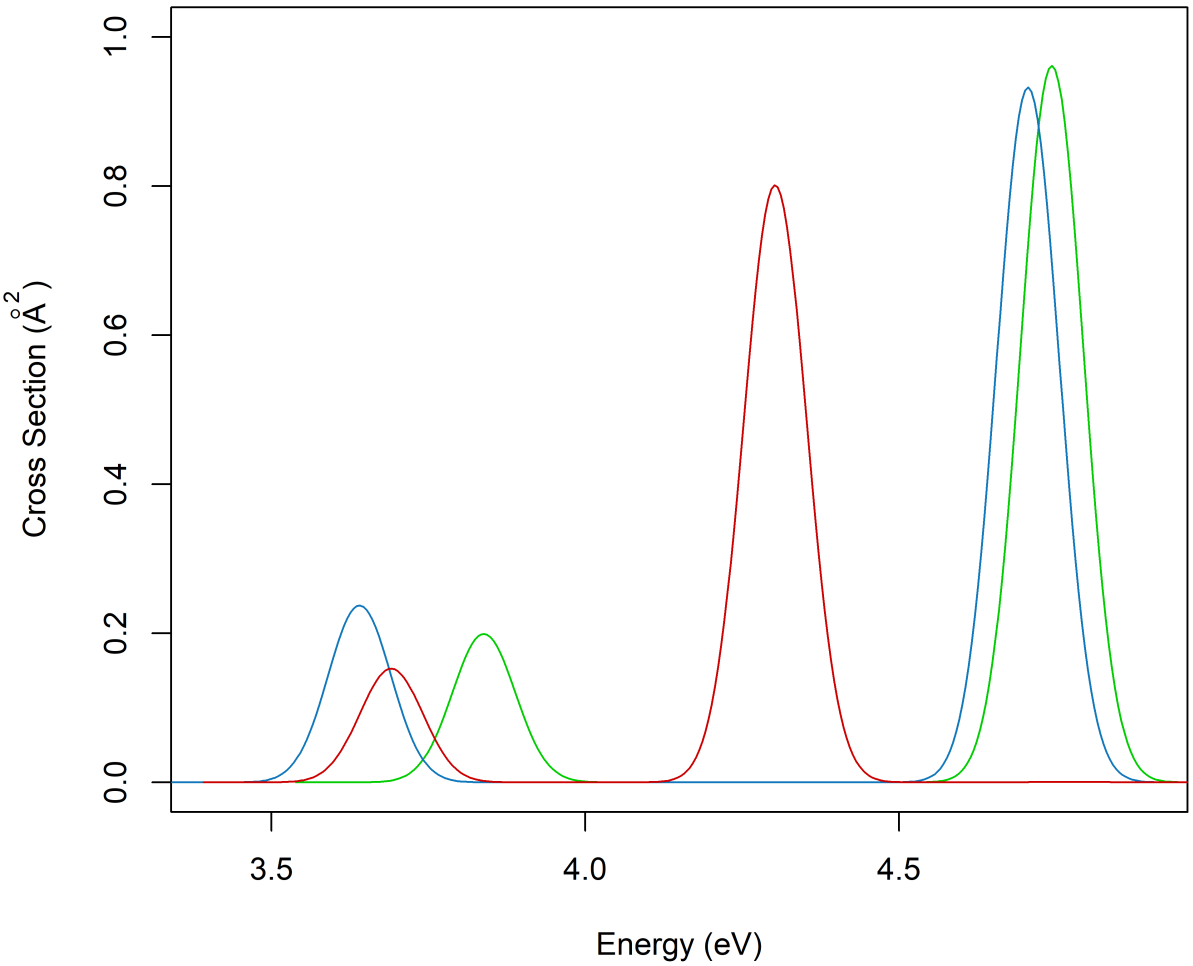

Figure 2.11: B-Te-6-B spectrum generated through phenomenological broadening of the vertical excitations using a Gaussian line shape (FWHM = 0.1 eV). LCC2 data is in green, LADC(2) in blue, and CAM-B3LYP in red; all with cc-pVDZ(pp).

present spectra only account for the first two excited states. The LCC2 peaks manifest at 3.80 and 4.41 eV while with LADC(2) the peaks are at 3.59 and 4.30 eV. Both peaks are significantly smaller in intensity in comparison with the experimental data.[79,95] However, the two peaks are relatively well matched in position compared to the experimental values of 3.50 and 4.25 eV, e.g., the peaks in the LCC2 spectrum are blue-shifted by approximately 0.3 and 0.5 eV, respectively.

However, large peaks around the 4.3 eV region were not expected for the present computation as only the first two excited states were considered; at the equilibrium geometry, the

second excited state has an oscillator strength of zero. This suggests that there is substantial "swapping" between the second and third excitations which causes oscillator strengths to increase for the second excited state. Incorporating the third state into the simulation should result in significant intensity increase for the second peak. Considering that the ground to third transition has a much higher oscillator strength, future work will involve an expanded excited state search in Newton-X encompassing the higher energy states, i.e., excited states 3 and 4, which were omitted in the present work due to computational cost.

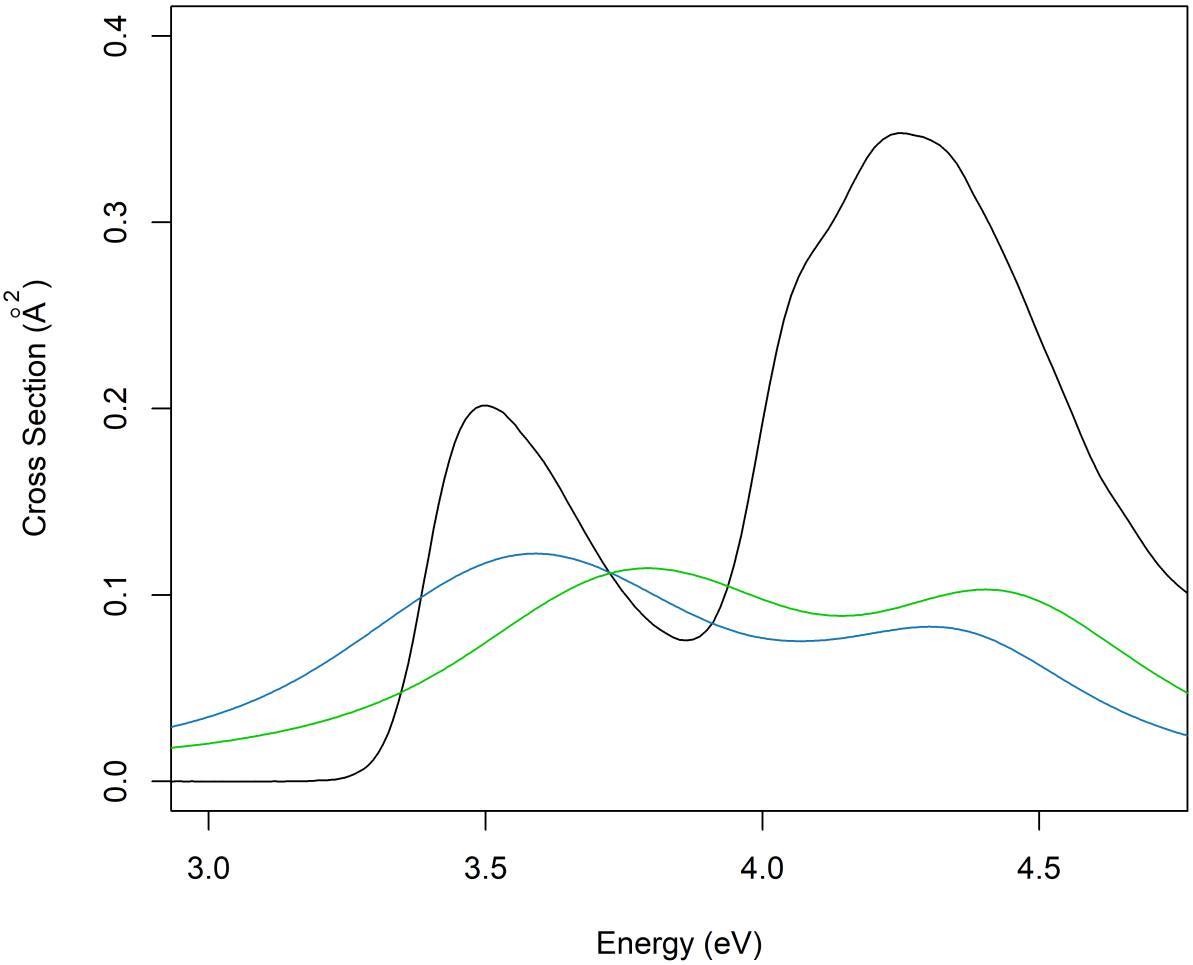

Figure 2.12: B-Te-6-B spectrum from Wigner distributions with experimental reference[79,95] in black, LCC2/cc-pVDZ(pp) in green, and LADC(2)/cc-pVDZ(pp) in blue. Spectra determined considering excitations to the two lowest singlet states.

2.4 Conclusions

Integration of Molpro via input-output interfacing with Newton-X was completed for LCC2 and LADC(2) methods. Implementation allows for initial conditions generation, adiabatic dynamics, and spectrum generation. Adiabatic dynamics integration should also be portable for any other quantum chemistry methods using the standard nuclear gradients program layout for Molpro. The new implementation was tested on two model systems: thiophene and the B-Te-6-B tellurophene.

The electronic spectrum of thiophene was determined using LADC(2) and LCC2 approaches with the cc-pVDZ basis set. Three different methods for evaluating the UV-Vis spectrum were assessed and contrasted. The first generated the spectrum based on vertical excitation energies (and oscillator strengths) with phenomenological lineshapes and broadening. The second uses a Hessian-based Wigner distribution of the ground state structures. The third involves using adiabatic dynamics to sample the ground state potential energy surface. Dynamics computations were run for 100 fs with the geometry sampled every 5 fs for vertical excitations; geometries were only considered for energies within thiophene's harmonic zero-point energy range. The total energies provided by Newton-X, from the ground state LCC2 and LADC(2) computations were not conserved, and thus the trajectories are not likely to be reflective of the true dynamics. At present, the source of this problem for the ground state has not been identified (i.e., local approximations, implementation of gradients for the ground state) and thus ground state dynamics for LCC2 and LADC(2) cannot be used; excited state dynamics remains to be investigated. Although problems with the ground state dynamics remain, with some energy-filtering of the dynamics, the ground state trajectory-based sampling methodology was shown to be adequate in describing experimental spectra.

The resulting spectra for thiophene from all three approaches exhibit bimodal character although with larger linewidths, a single peak (as observed experimentally) could be observed. The Wigner based spectra (LCC2/LADC(2)) are blue-shifted by $\sim$0.5 eV compared

to experimental data. The trajectory based spectrum, however, had the higher energy peak well aligned, while the lower energy peak was red-shifted by ∼0.5 eV. Based on relative ranges, the trajectory based method shows better accuracy in comparison to both direct vertical excitations in addition to the Wigner distributed spectrum's range; however, this agreement may be fortuitous.

Furthermore, the electronic spectrum of the B-Te-6-B tellurophene was also generated using ground state geometries sampled from a Wigner distribution, while corresponding excited state properties were determined with either LCC2/cc-pVDZ(pp) or LADC(2)/cc-pVDZ(pp). While the intensities for the two observed peaks are smaller than the experimental measurements, this difference for the higher energy peak is accounted for in the potential for the reordering of the second (dark) and third (bright) excited states at geometries away from equilibrium. Due to computational cost, the third state was not yet accounted for in the present simulations. For this much larger molecule, the inclusion of additional states is computationally expensive, but the present results suggest that further examination into the extended excitations of the tellurophene will be required for better comparisons to experiment.

Overall, a new computational tool using the LCC2 and LADC(2) quantum chemistry methods in Molpro has been developed for spectral simulations in Newton-X. Tests on thiophene and the B-Te-6-B tellurophene have highlighted the use of the newly implemented methodology. The present implementation for the wavefunction-based LCC2 and LADC(2) approaches are complementary to the TD-DFT, non-local (canonical) CC2 and ADC(2), multi-reference configuration interaction methods, and multi-reference self-consistent field methods currently available in Newton-X for determining UV-Vis spectra.

Chapter 3

Non-adiabatic Dynamics with CASSCF

3.1 Introduction

In the simplest conceptual model, molecular electronic spectra (absorption and emission) involve two simple processes: (i) a molecule absorbs a photon and an electron is excited to a higher energy electronic state and (ii) after possible geometric rearrangement of the molecule, the electron relaxes back down to the ground state, releasing a photon. However, this simplistic picture fails to account for more sophisticated treatments of the excited state, such as multiple single, double, and higher order electron excitations, and discounts many other interactions that may exist between the excited and ground electronic states. Conical intersections and avoided crossings are examples of such interactions which can cause population transfer between potential energy surfaces (PESs) while avoiding the release of a photon in non-radiative relaxation. In such cases, the corresponding energies of the excited and ground state PESs are either very close in the case of avoided crossings, or degenerate at the seam of conical intersection. Therefore, investigating such transitions, either statically or dynamically, is helpful in evaluating the efficiency and potential time scales of non-radiative

relaxation, as well as photochemical events, e.g., bond forming/breaking.

One of the most widely used quantum chemistry methods for studying photodynamics on excited electronic state PESs, which can be coupled to each other and/or the ground state, is the complete active space self-consistent field (CASSCF) approach. Therefore, CASSCF functionality, based on the Molpro software package[37] is also useful to integrate with Newton-X; CASSCF functionality based on the Gaussian 09,[90] GAMESS-US,[96] COLUMBUS,[97,98] and, recently, BAGEL[99,100] software packages is presently available in Newton-X. CASSCF, as a multi-reference method, provides a fairly accurate representation of molecular properties, including energies and non-adiabatic couplings, for and between electronic states. Moreover, it is the starting point for other quantum chemistry approaches such as multi-reference configuration interaction (MRCI)[101,102] and second-order complete active-space perturbation theory (CASPT2).[103–108] By computing electronic states for a chosen active space (see Section 1.2.3), CASSCF already provides a qualitative to semi-quantitative representation of a system's excited state properties, albeit one lacking dynamic electron correlation. The largest challenge within the CASSCF approach, then, is the selection of a suitable active space for accuracy versus computational cost. The difficulty of this choice is exacerbated by the general requirement of large active spaces for aromatic systems, a motif which is common in photoactive compounds.[71,109,110]

For simplicity of comparison to existing computations based on CASSCF (with Gaussian 09)[90] provided by Newton-X in introductory tutorials, initially the focus is on the molecule methaniminium (CH_4N^+). Comparing with sample outputs from a working interface (Gaussian 09/Newton-X), allows the testing of the newly developed code for Newton-X using Molpro. Methaniminium is a small amine fragment which is a component of a number of organic compounds usable as ligands and as a reaction by-product.[111–113] Due to its small size, methaniminium acts as a simple molecule for investigation to save computational cost during implementation and testing of the new Molpro/Newton-X interface for CASSCF. The generated Molpro/Newton-X interface is then applied to exploratory computations for

thiophene, which is one of a series of building blocks for polymers for future study.[78]

3.2 Computational Methods

As the goal of the project was to integrate Molpro[19,20] CASSCF functionality into Newton-X,[54,69] these two software packages were used for CASSCF quantum chemistry computations and dynamics, respectively.[37] Reference CASSCF computations of excited state trajectories for methaniminium were computed using the Newton-X provided Gaussian 09 interface.[90] Reference initial conditions, i.e., geometries and momenta, for methaniminium were taken from the Newton-X provided examples for benchmarking. For testing the integration of Molpro with Newton-X, excited state dynamics were first conducted using state-averaged CASSCF (SA-CASSCF, averaging over the ground and first excited states) with 4 electrons in 3 orbitals (CASSCF(4,3)) to minimize computational cost. Note that all CASSCF computations presented in this chapter involve state-averaging over the number of states under consideration; however, this will be referred to as CASSCF for simplicity. The Pople basis set 6-31G was used for the computations.[114]

As considered in Chapter 2 when computing UV-Vis absorption, here thiophene is the sample molecule when examining excited state dynamics. The ground state geometry was optimized, and corresponding harmonic frequencies and normal modes computed, using DFT at the CAM-B3LYP/cc-pVDZ level of theory, i.e., the same ground state information used in Chapter 2. Initial computations for thiophene were performed with CASSCF(4,4) as this very small active space (and inadequate for quantitative study of thiophene) permitted rapid testing of the dynamics as well as consistency checks on the interface comparing with methaniminium trajectories. The excited state dynamics computations were conducted with the 6-31G(d) basis set.[114,115]

The developed Molpro/Newton-X interface was then used to compute a thiophene UV-Vis spectrum and excited state dynamics using CASSCF(10,10)/6-31G(d). This active space

was chosen due to previous studies[71,109,110] suggesting larger active spaces being required for five-membered rings to simulate accurately their excited state phenomena. Equilibrium geometries and normal modes were also computed in Molpro with CASSCF(10,10)/6-31G(d) for consistency. Normal modes were stored in the Molden format for ease of access.[116]. Using the Molpro/Newton-X interface, first UV-Vis spectra, based on sampling a ground state Wigner distribution, and incorporating different numbers of excited states were computed and then non-adiabatic trajectories initiated on the first excited singlet state were investigated. UV-Vis spectra were determined incorporating (up to) the first five states (ground plus four excited) to account for state reordering events events as well as potential changes in oscillator strengths for dark bands while dynamics followed the first singlet excited state and the ground state.

3.3 Results

Implementation of CASSCF non-adiabatic dynamics using Molpro as the quantum chemistry driver was first tested using Newton-X preloaded sample cases for methaniminium. The choice of initial test was inspired by the provided Gaussian 09 integration and uses an identical quantum chemistry approach (notwithstanding the differences in the back-end numerical implementations) and initial conditions for the dynamics. The methaniminium example benchmarks the Molpro integration against a well-tested approach so that conclusive determination of the veracity of the new implementation can be drawn from the comparison. Following this initial testing, the standalone Molpro integration was then used to compute dynamics for thiophene; the same molecule used for examining the LCC2 and LADC(2) approaches for UV-Vis spectra detailed in Chapter 2. Compared to the previous chapter, more focus is on non-adiabatic dynamics initiated on the first excited state rather than the ground state adiabatic dynamics considered previously. As such, most of the discussion is on electronically excited states and, most importantly, the surface hopping between the first

excited state and the ground state. For ease of reference, the ground state will hereby be referred to as S_0 with each subsequent excited state denoted by S_n where n is the state's number in increasing energetic order; the present work only concerns singlet states hence the designation S.

3.3.1 Methaniminium

Output files for CASSCF-based dynamics for methaniminium using Gaussian 09 are found in Newton-X's distributed sample calculations. Methaniminium consists of six atoms, four of which are hydrogen and thus the cation is fairly small making it a suitable model for testing non-adiabatic trajectories; here a single trajectory known to exhibit surface hopping is tested. The trajectory takes into account two electronic states, S_0 and S_1, where the upper state is initially populated. The dynamics are propagated for 100 fs with a time step of 0.5 fs. Along the trajectory the non-adiabatic coupling vectors are computed to predict surface hops (i.e., transfers from S_1 to S_0 or, in principle, S_0 back to S_1). To promote surface hopping, the threshold energy gap below which a hop can made is set to the maximum value of 100 eV. For much smaller values of this threshold, which represents the S_1 to S_0 energy gap below which a hop is considered as possible, surface hopping is less probable.

The output from the CASSCF(4,3)/6-31G trajectory computed with the existing Gaussian 09/Newton-X interface is illustrated in Figure 3.1. The surface hopping events, where the trajectory moves from the S_1 to S_0 states, visible in Figure 3.1 at $\sim$11 and 51 fs, then, are the main target for the testing phase of the Molpro/Newton-X implementation. The output from a CASSCF(4,3)/6-31G trajectory computed using the newly developed Molpro/Newton-X interface is shown in Figure 3.2. The initial geometry and atomic momenta are identical to those used in Figure 3.1. Examining Figure 3.2, one can see the characteristic surface hopping as the illustrated trajectory swaps from the excited to the ground state several times. It is evident that surface hopping is therefore successfully implemented in the Molpro/Newton-X integration although there are differences between the

trajectories for the two different quantum chemistry engines although the initial conditions are identical and both are based on the CASSCF(4,3)/6-31G level of theory.

In the Gaussian sample, only one hop, where the trajectory remains on the new PES, occurs around 51 fs; at 11 fs the trajectory hops to the ground state but immediately returns to the excited state PES. In comparison, the Molpro generated trajectory hops back and forth between the ground and excited states three times at around 11, 48, and 54 fs. This qualitative change results most likely from small numerical differences in computing the CASSCF wavefunction and corresponding non-adiabatic coupling vectors in Molpro versus

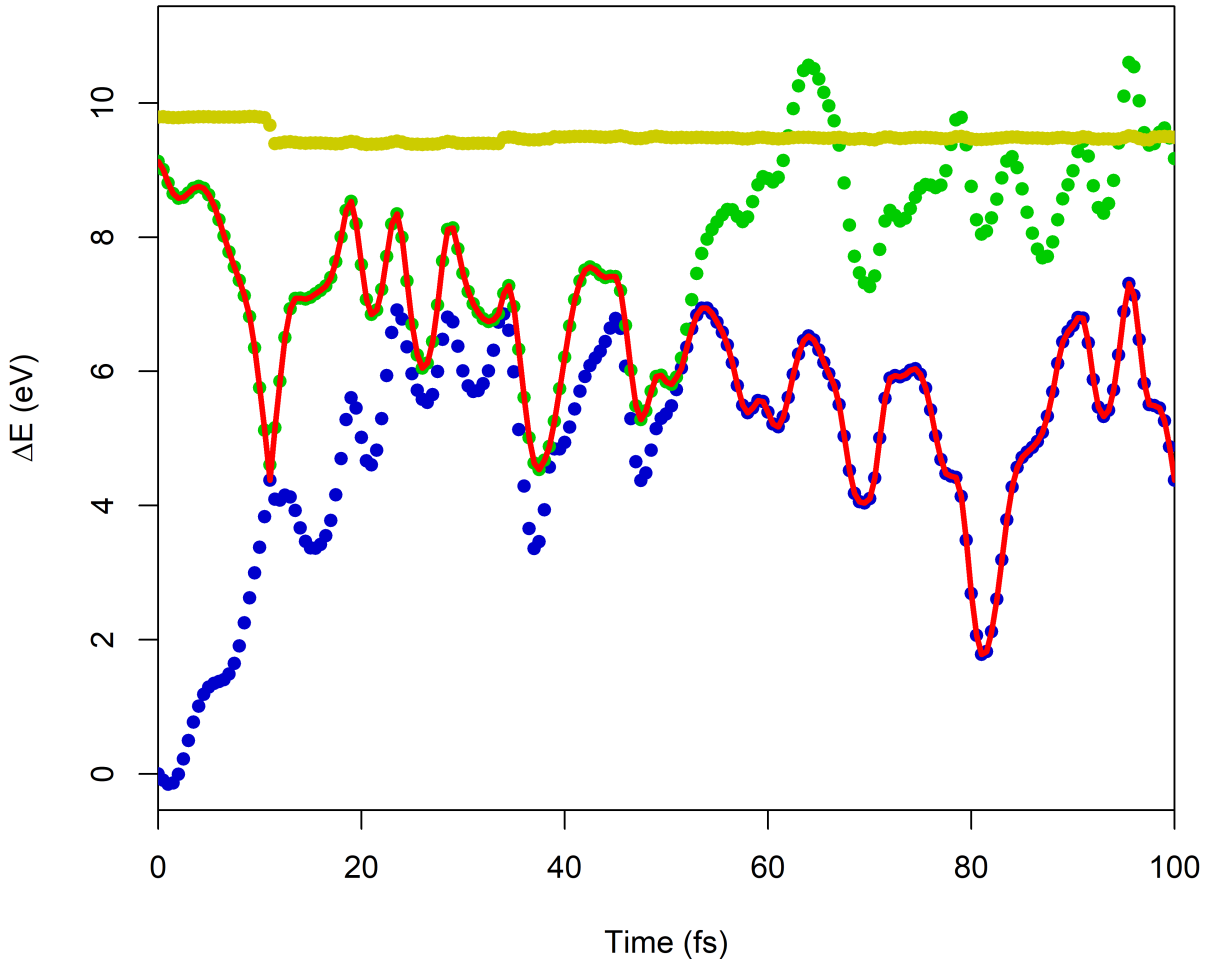

Figure 3.1: Non-adiabatic trajectory energies for methaniminium from Gaussian CASSCF(4,3)/6-31G. The ground (S_0) and excited state (S_1) energies are given by blue and green, respectively, with total energy in yellow. The red trace indicates the currently populated state.

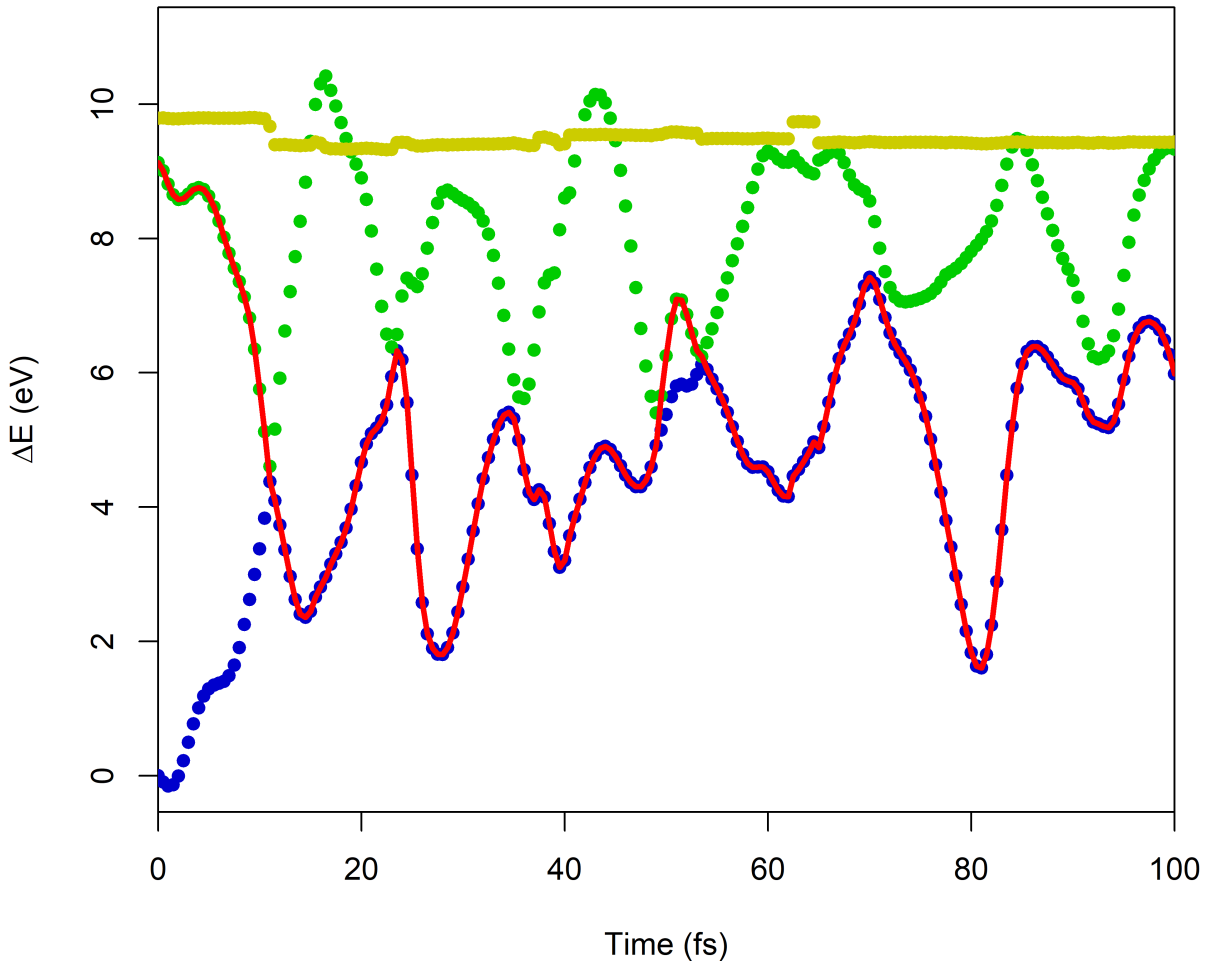

Figure 3.2: Non-adiabatic trajectory energies for methaniminium from Molpro CASSCF(4,3)/6-31G implementation. Same as Figure 3.1, where blue is S_0, green is S_1, red is the populated state, and yellow is the total energy.

Gaussian. These differences can manifest from convergence thresholds or the underlying numerical algorithm but, most importantly, can drastically change the projected path. Here, the main difference manifests at ∼11 fs where the Gaussian trajectory transfers onto S_0 from S_1 for a single timestep before returning to S_1 while the Molpro trajectory remains on S_0 after the initial transition. Of course, the two trajectories then diverge after this point. Nonetheless, this is a positive result showing that non-adiabatic trajectories can be investigated further using the Molpro/Newton-X interface.

3.3.2 Thiophene

Table 3.1: Vertical Excitation Energies and Corresponding Oscillator Strengths of Thiophene as Determined at the CASSCF(n,m)/6-31G(d) Level of Theory

	(4,4)		(10,10)	
Excitation	ΔE (eV)	Osc	ΔE (eV)	Osc
1	6.88	0.000	6.17	0.075
2	6.89	0.000	6.41	0.000
3	7.83	0.449	6.74	0.005
4	7.95	0.694	6.79	0.000
5	12.47	0.000	6.79	0.004
6	12.48	0.008	7.15	0.079
7	12.92	0.000	8.11	0.100
8	13.91	0.000	8.36	0.000
9	14.98	0.000	8.89	0.001

The study of thiophene was focused on the first few excited states as discussed previously in Chapter 2, see Table 2.1. For this investigation of dynamics in the excited state, CASSCF vertical excitation energies and corresponding oscillator strengths have been determined, see Table 3.1. From experimental measurements, the low lying absorptions are located around 5.3 and 5.7 eV,[45] while both the CASSCF(4,4) and CASSCF(10,10) values are significantly overestimated due to the lack of dynamical correlation. Also, as noted in Chapter 2 for the LCC2 and LADC(2) spectra, the vertical excitation energies are larger than those obtained when determining the spectrum from ground state sampling. Moreover, the oscillator strengths change significantly depending on the choice of active space. As such the CASSCF(10,10) data suggests the importance for the spectrum of excitations to S_1 and S_3, at 6.17 and 6.74 eV, respectively. These three lowest states, with S_2 being dark, are qualitatively similar to the LCC2 and LADC(2)/aug-cc-pVDZ results. CASSCF(4,4), as expected, does not show a state with a reasonable oscillator strength until 7.83 eV, which is significantly above the experimental values for the lowest energy aborption. This observation agrees with expectations about active spaces needed for five membered rings.[71,109,110] However, the CASSCF(4,4) computations are still useful for testing and exploring the Molpro/Newton-X interface due to their computational efficiency.

For CASSCF(4,4)/6-31G(d) testing, the dynamics was initiated on the first excited state as it has a non-zero, albeit small, oscillator strength ($f = 2.3 \times 10^{-4}$). For the final CASSCF(10,10)/6-31G(d) computation, the first five states will be considered for the generation of a UV-Vis spectrum as S_2 to S_5 have comparable energies at the equilibrium geometry (Table 3.1) and thus could be reordered at different geometries sampled from the Wigner distribution. Once again, dynamics initiated on the first excited state will be examined.

3.3.2.1 Thiophene CASSCF(4,4)

CASSCF(4,4)/6-31G(d) non-adiabatic trajectories of thiophene along S_1 (Figure 3.3) were generated from 208 initial conditions (geometries and momenta) sampled from a Wigner distribution based on the CAM-B3LYP/cc-pVDZ equilibrium geometry. Trajectories were then run for 100 fs with a time step of 0.5 fs for S_1 of thiophene. Relatively flat total energies, see Figure 3.3, show that the total energy is conserved for the majority of the trajectories; an example of one specific trajectory is shown in Figure 3.4. A small number of trajectories exhibit sharp energy changes which then terminate the given trajectory; these types of divergences are commonly encountered for CASSCF-based trajectories (albeit for a small percentage of a large number of trajectories that are run). Most of the trajectories show little to no surface hopping (non-adiabatic behaviour) between the excited and ground state with only one of the 208 trajectories having more than a 50% hopping probability at 68%, represented as the adiabatic population of the ground state by Newton-X. Sadly, the trajectory also shows a very strong energy divergence at the hop and thus it is discarded from the final analysis. The rest of the trajectories stay under 0.2% population exchange with those that survive the full 100 fs below 0.02% probability.

Investigating a typical trajectory such as the one visualised in Figure 3.4 shows why there is no crossover (surface hopping) between S_1 and S_0; clearly the energy gap is too large along the trajectory for hopping to occur. This large energy separation is a consequence of the active space being too small to describe the energies and non-adiabatic couplings

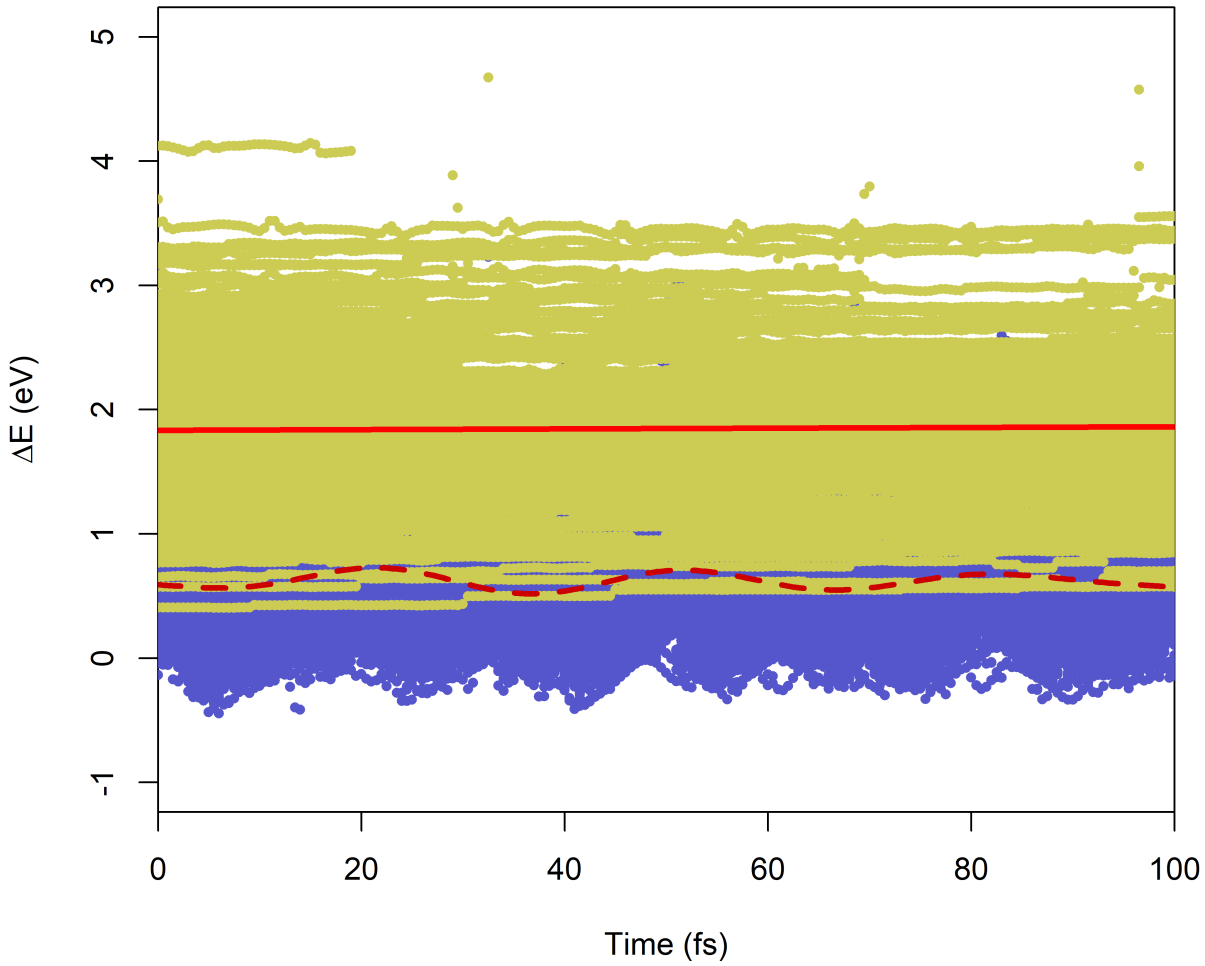

Figure 3.3: Non-adiabatic trajectory energies obtained via CASSCF(4,4)/6-31G(d) for the first excited state of thiophene. Trace is comprised of potential energy (blue) and total energy (yellow) zeroed at the potential energy determined by the DFT optimized equilibrium geometry. Red trendlines show the energy fitted with the total energy (solid line) and the potential energy (dashed line).

properly. This qualitative failure of the modest, but computationally efficient, (4,4) active space necessitates the expansion of the active space to the (10,10) active space used in the next section.

3.3.2.2 Thiophene CASSCF(10,10)

Initially, the UV-Vis spectrum at the CASSCF(10,10)/6-31G(d) level of theory was determined to compare with the previous LCC2 and LADC(2) results, see Chapter 2. The ge-

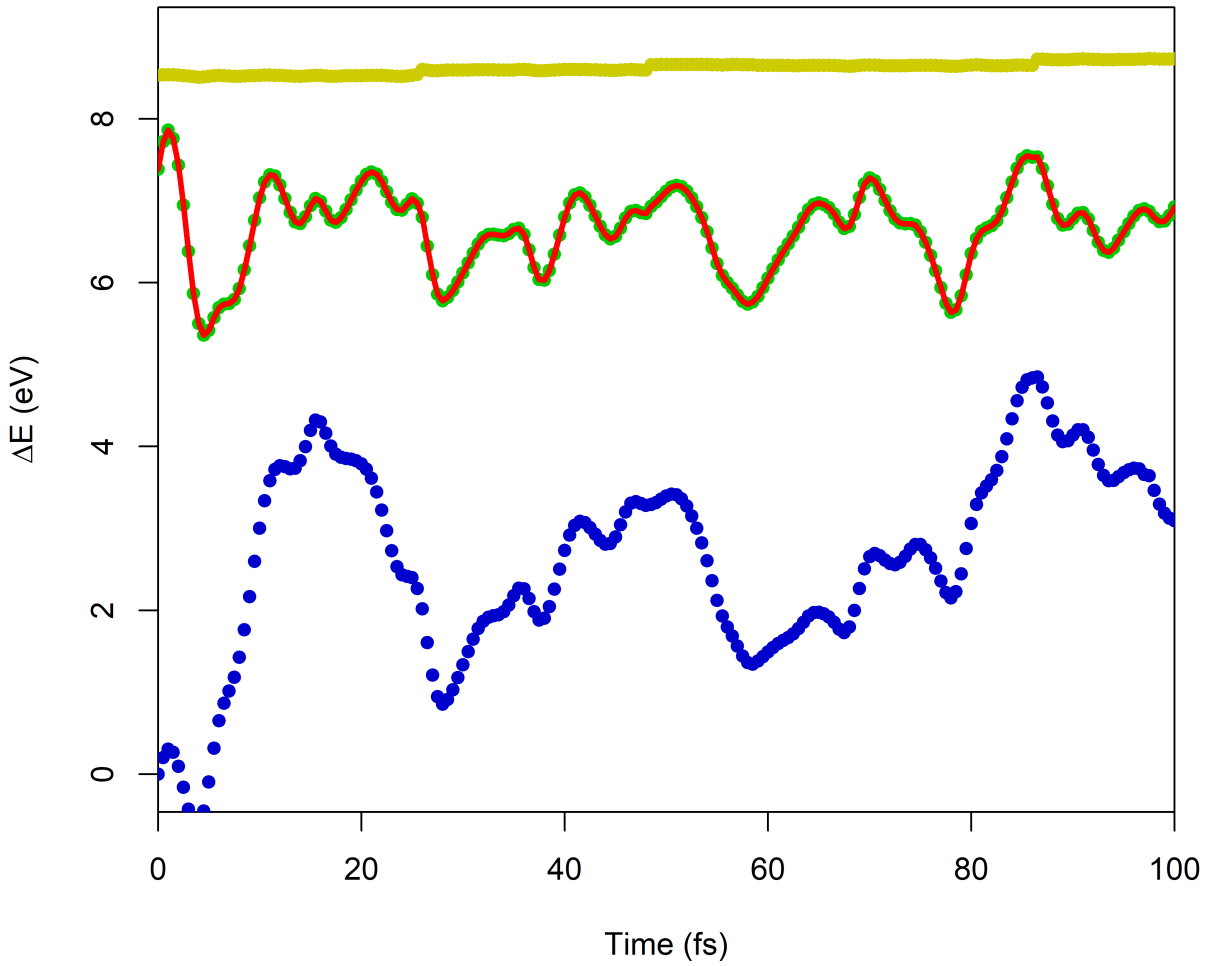

Figure 3.4: Trace of a typical thiophene CASSCF(4,4)/6-31G(d) trajectory (trajectory 150). Total energy is in yellow with S_1 (green) obscured by the data showing the populated state along the trajectory (red). Ground state potential energy is in blue.

ometries were sampled based on a Wigner distribution from the CASSCF(10,10)/6-31G(d) equilibrium structure, harmonic frequencies, and corresponding normal modes. The first excited states with significant oscillator strengths are S_1 and S_3 (Table 3.1); however, up to four excited states were taken into consideration to account for any switches in energy order between S_3 to S_4 at geometries displaced from equilibrium. Once again, this procedure allows for the generation of a Wigner based UV-Vis absorbance spectrum. Figure 3.5 shows the spectra accounting for two, three, and four excited states as well as the component peaks of interest.

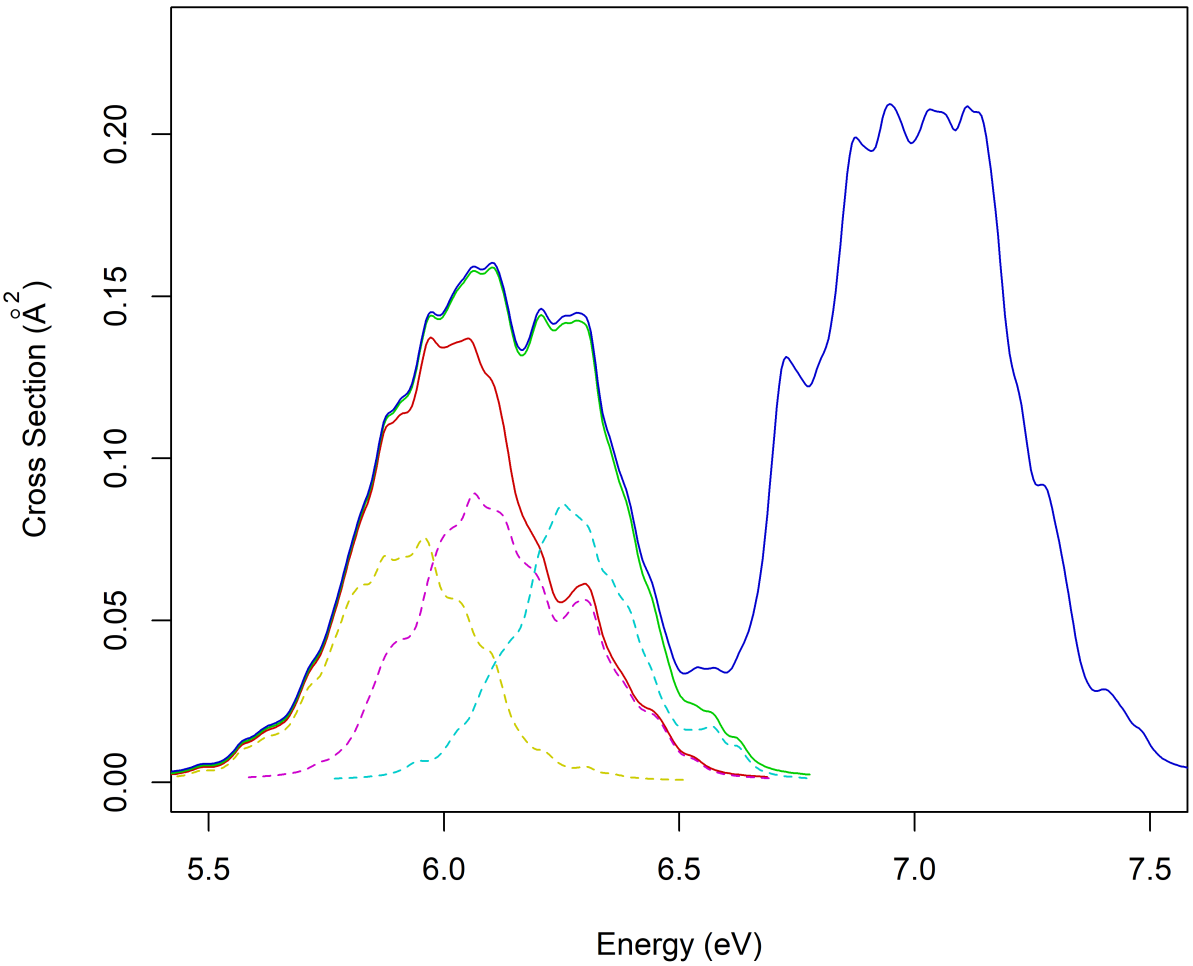

Figure 3.5: UV-Vis spectrum obtained via CASSCF(10,10)/6-31G(d) and sampling the ground state Wigner distribution (500 points) for thiophene. Red is the sum of two excited states, green three, and blue is four. Peaks shown for contributing states (dashed): S_1 in yellow, S_2 in magenta, and S_3 in cyan.

Comparing to the LCC2 and LADC(2) spectra, the CASSCF(10,10)/6-31G(d) spectrum generated from sampling a Wigner distribution of 500 ground state geometries with 0.05 ev line widths behaves as expected with two peaks blue-shifted relative to the experimentally measured spectrum. Similar to the local methods discussed in Chapter 2, there is substantial energetic re-ordering of the bright and dark states as observed by the difference between summing two and three excitations. By examining the individual state contributions to the spectrum in Figure 3.5, the existence of an absorption peak for the S_2 excitation which has a negligible oscillator strength at the equilibrium geometry strongly suggests state re-

ordering at geometries away from equilibrium. The addition of the 4th excited state begins to probe into the second set of peaks. Overall, the CASSCF(10,10)/6-31G(d) spectrum adequately reproduces the experimental spectrum; while there is a notable blue-shift due to a lack of dynamical electron correlation, similar, albeit smaller, blue-shifts are also seen in the spectrum computed with LCC2 and LADC(2) approaches, see Figures 2.3 and 2.10.

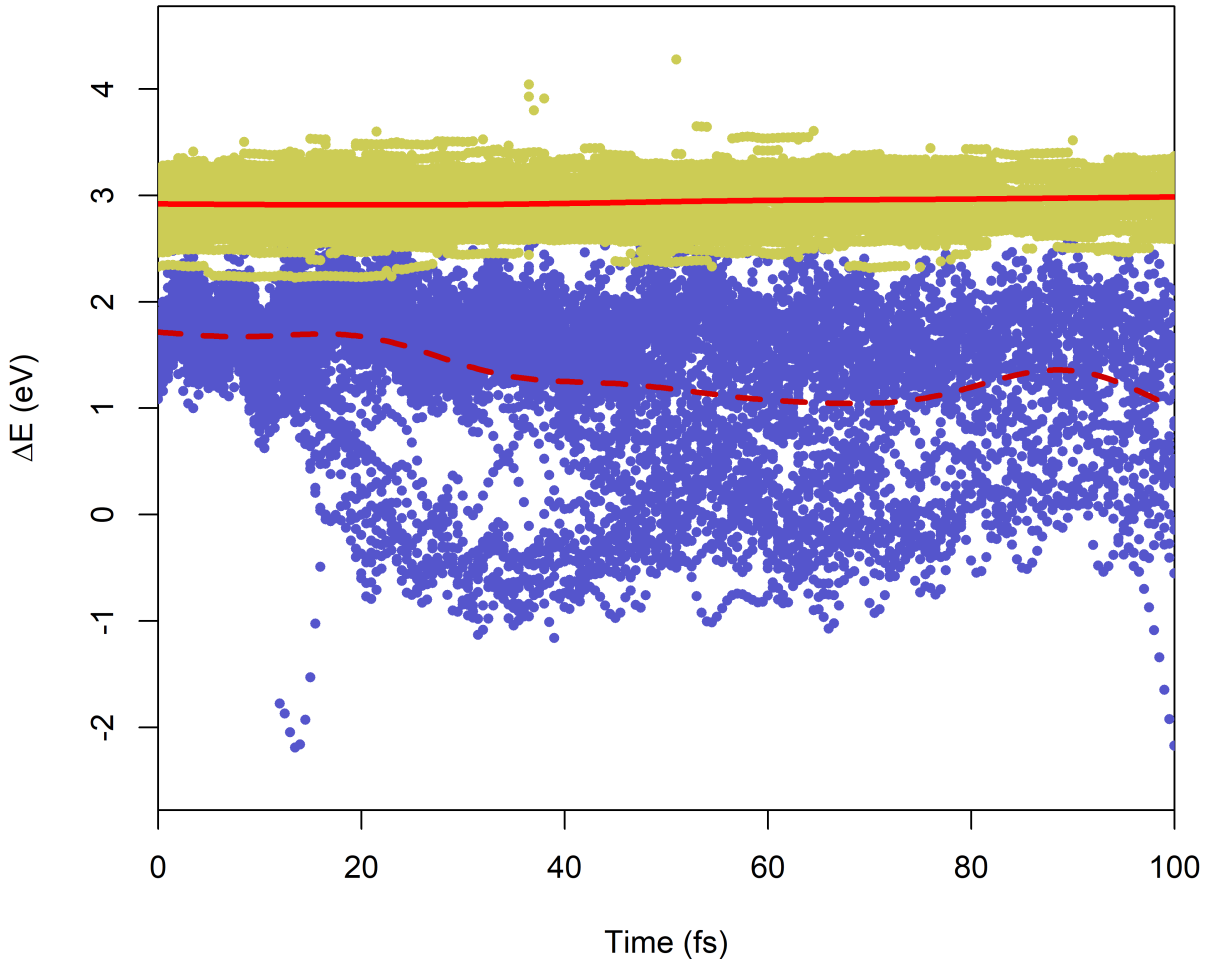

Figure 3.6: Non-adiabatic trajectory energies obtained via CASSCF(10,10)/6-31G(d) for the first excited state of thiophene. Trace is comprised of potential energy (blue) and total energy (yellow) zeroed at the potential energy determined at the CASSCF(10,10)/6-31G(d) optimized equilibrium. Red trendlines show the energy fitted with the total energy (solid line) and the potential energy (dashed line).

Non-adiabatic trajectories were conducted with CASSCF(10,10)/6-31G(d) energies ($E_{potential}$ and E_{total}, see Figure 3.6) initially populating the first excited state. These 125 trajectories

were run for 100 fs with a time step of 0.5 fs. The initial conditions (geometries and momenta) were sampled from the previous CASSCF(10,10)/6-31G(d) Wigner distribution and filtered by energy restriction windows (unlimited in this case) and screened where the normalized relative transition probability (f/f_{max}) is greater than a randomly selected threshold probability to reduce bias and computational load. The currently considered propagation time is relatively short as the excited state lifetime is measured to be 80±10 fs[74] but the 100 fs propagation time was used for computational efficiency. Examining the full set of energies (Figure 3.6), total energies are relatively conserved suggesting good pathfinding over the 100 fs of the trajectories with 41 of the trajectories reaching the full 100 fs. Of the 125 trajectories evolved, 27 contained hopping probabilities (ground state adiabatic populations) of above 1% with 16 reaching 99%. This shows strong coupling between the S_0 and S_1 states exists as expected from experimentally measured S_1 lifetimes (80±10 fs)[74] and from previous theoretical studies of the excited state dynamics.[70]

It has been suggested based on prior CASSCF computations[70] that a thiophene ring opening is caused by a crossing between the S_1 and S_0 states. When inspecting trajectories with substantial population transitions, a similar ring opening was identified. In focus is trajectory 43 which shows a transition from S_1 to S_0 at ∼34 fs (Figure 3.7). Visualising the molecular geometry along the trajectory depicts the referenced ring opening, see Figure 3.8. Clearly the present results confirm the qualitative aspects (lifetime and products) of the excited state dynamics available from literature.[70,74,75] Moreover, these trajectories demonstrate the utility of the Molpro/Newton-X interface for studying non-adiabatic dynamics based on CASSCF electronic structure for determining gradients and analytical non-adiabatic coupling vectors.

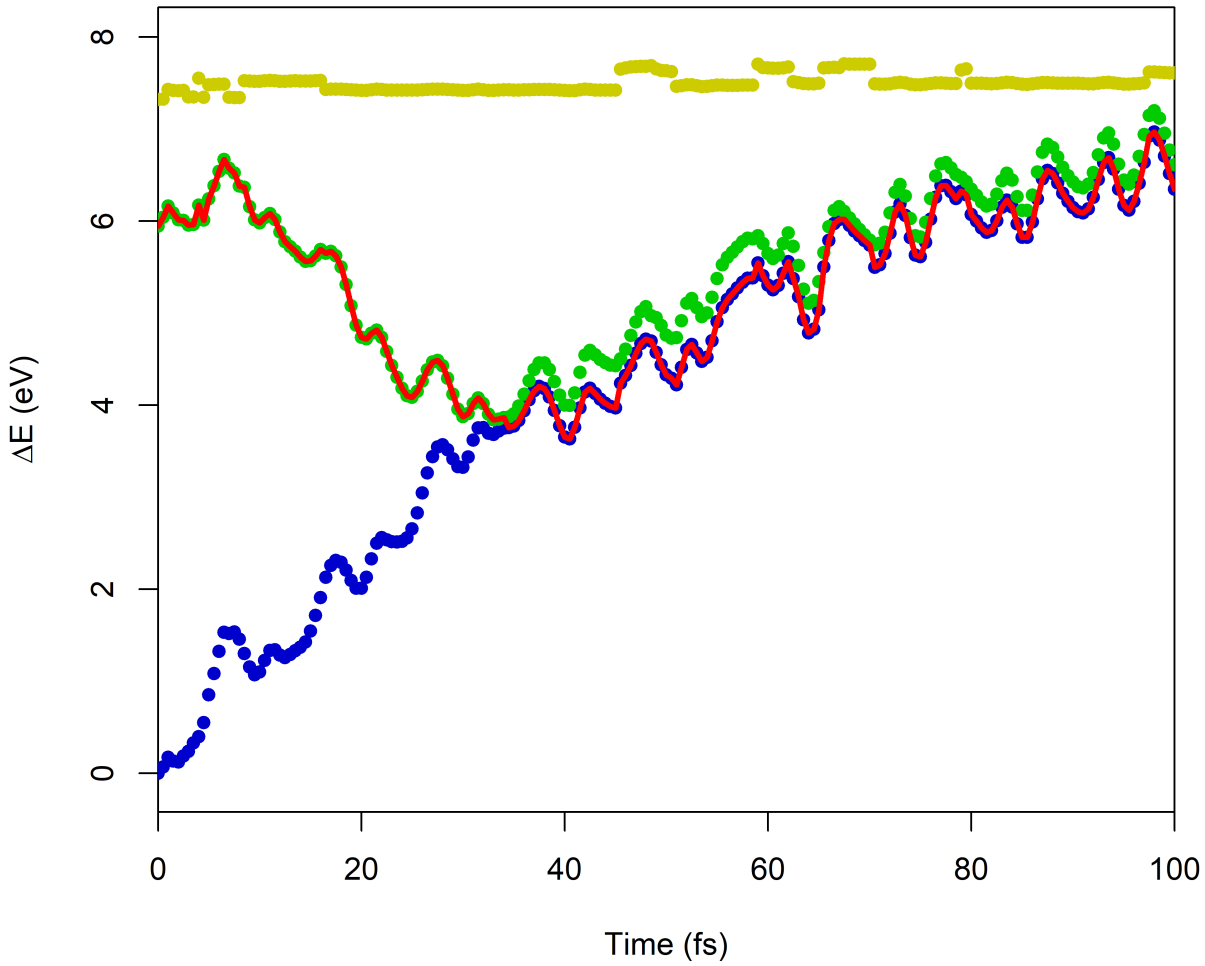

Figure 3.7: CASSSCF(10,10)/6-31G(d) trajectory showing a surface hopping event. Trajectory shows a transition from the S_1 (green) to S_0 (blue) states as indicated by the currently populated state (red). The total energy is shown in yellow as a guide.

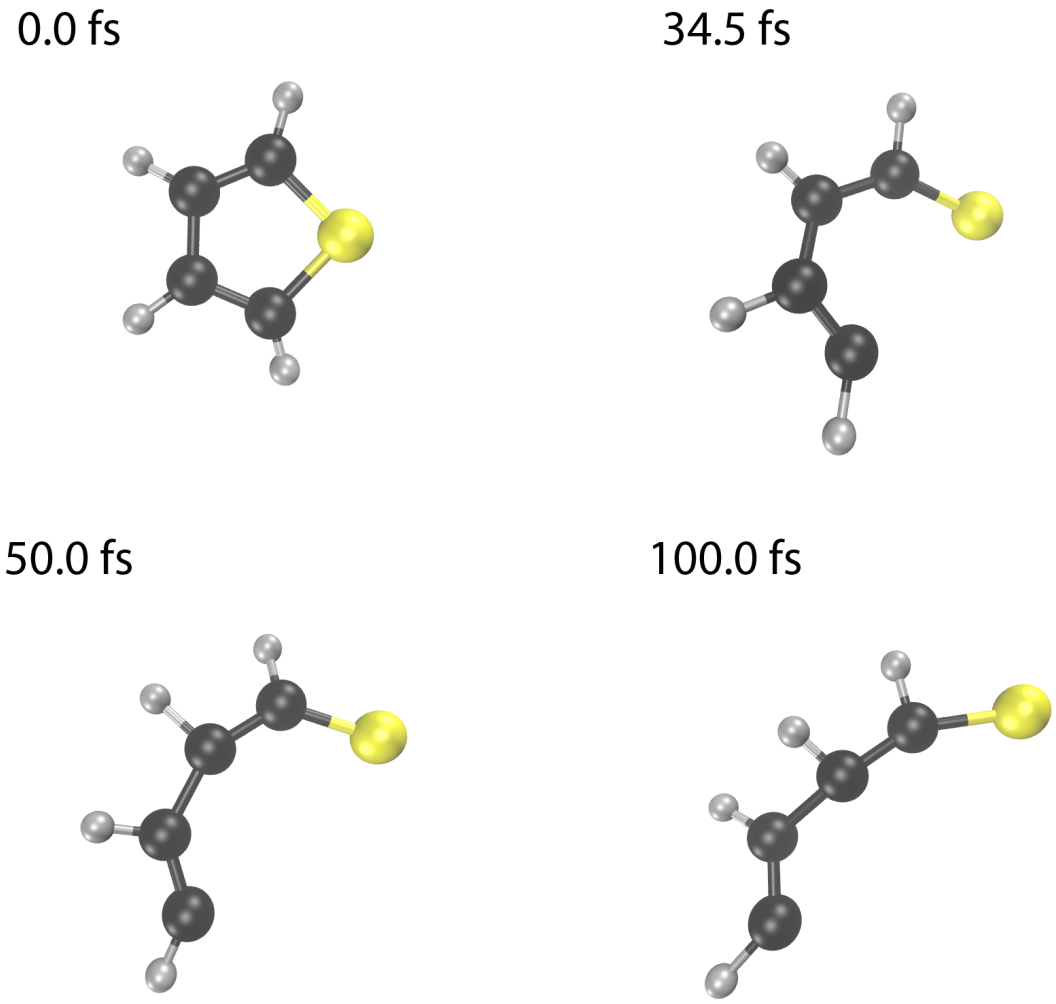

Figure 3.8: Visualization of the ring opening event depicted in CASSCF(10,10)/6-31G(d) trajectory 43. The transition between S_1 and S_0 occurs at 34.5 fs.

3.4 Conclusion

Integration of Molpro 2015 into Newton-X was completed for the CASSCF quantum chemistry method including UV-Vis spectrum determination and non-adiabatic dynamics. The present implementation has been used to replicate the provided sample CASSCF dynamics using Gaussian 09 for computation on methaniminium. Deviations between the present results and those observed previously have been attributed to small numerical differences between the wavefunction and, hence, gradients as well as non-adiabatic coupling vectors determined within the Molpro and Gaussian software packages.

Subsequent analysis with thiophene was conducted with positive returns. CASSCF(4,4) preliminary testing showed the ability for the present implementation to produce trajectories with appropriate sampling of initial conditions and energy conservation; however, the small active space did not replicate the full features of thiophene's excited state potential energy surface. Increasing the active space to (10,10) allowed for the determination of a semi-quantitative UV-Vis spectrum and study of excited state dynamics including the replication of a ring opening event which has been observed previously in non-adiabatic simulations.[70,74,75]

Chapter 4

Conclusions and Future Work

4.1 Summary of Thesis Research

This thesis aimed to (i) develop an interface between Newton-X, an ab initio molecular dynamics software package focused on non-adiabatic processes (trajectory surface hopping), with Molpro as the electronic structure back-end, (ii) implement methods for computing UV-Vis spectra based on the local methods LCC2 and LADC(2) along with CASSCF, and (iii) further add non-adiabatic dynamics functionality for the CASSCF integration. The interface was then used to analyse the absorbance spectra of thiophene and the B-Te-6-B tellurophene using the local methods which were then compared to ones determined by TD-DFT. The non-adiabatic dynamics of thiophene was further examined with CASSCF(10,10)/6-31G(d) which replicated literature results[70,74,75] of the thiophene ring opening that results from a S_1 to S_0 non-adiabatic transition.

Chapter 2 outlined the integration of Molpro and Newton-X for LCC2 and LADC(2) and demonstrated how absorbance spectra could be generated. The examples presented used sampling of a ground state Wigner distribution generated from B3LYP/cc-pVDZ normal modes while LCC2 and LADC(2) (with the cc-pVDZ basis set) were used for energies of the excited states and the corresponding oscillator strengths. LCC2 and LADC(2) were not used

for the ground state sampling due to the current lack of analytic Hessians for these methods. Thiophene absorbance spectra generated from a Wigner distribution compare well to experimental data. The spectra generated for B-Te-6-B from B3LYP/cc-pVDZ(pp) ground state data and LCC2/LADC(2) excitation energies with the same basis set compare moderately well with experiment; more quantitative agreement would require larger basis sets and the inclusion of one (or more) additional excited states at significant additional computational cost. For comparison, absorbance spectra were also generated by using phenomenologically broadened vertical excitations with oscillator strengths dictating intensities. This approach is the simplest as it only requires computation at a single geometry; however, it may not capture all features of the absorbance spectrum. A third alternative to generating a UV-Vis spectrum involved sampling ground state geometries with adiabatic dynamics. Further progress using molecular dynamics based on LCC2 and LADC(2) to sample the ground state was hampered by the apparent inconsistencies of nuclear gradients which caused substantial non-conservation of total energy. This problem appears to be an issue with localization of orbitals as sample calculations with LMP2 also exhibited this non-conservation of energy.

In Chapter 3, the framework created in Chapter 2 was expanded upon to allow for excited state dynamics using CASSCF, focusing on non-adiabatic effects. Non-adiabatic dynamics using surface hopping were integrated using CASSCF to determine the required nuclear gradients and non-adiabatic coupling vectors analytically. This method was applied first to a sample test methaniminium trajectory provided by Newton-X using an interface to Gaussian 09. The second example was, again, thiophene. Similar to Chapter 2, an absorption spectrum for thiophene was generated using CASSCF(10,10)/6-31G(d) to obtain the ingredients for the ground state Wigner distribution as well as the excitation energies and corresponding oscillator strengths. Dynamics modelling was based on using CASSCF(4,4)/6-31G(d) and CASSCF(10,10)/6-31G(d) approaches. The very computationally efficient CASSCF(4,4)/6-31G(d) approach was used for initial testing but the active space was too small for quantitative study of thiophene. From the CASSCF(10,10)/6-31G(d) trajectories, the ring opening

of thiophene as it relaxes from the first excited state to the ground state via the dissociation of a carbon-sulphur bond was observed; this observation is consistent with previous results seen with thiophene.[70,74,75]

In this thesis, a framework for the inclusion of Molpro functionality into Newton-X for specific tasks (spectra and dynamics) and quantum chemistry methods (LCC2, LADC(2), and CASSCF) was developed and tested. Thiophene was used in this study as a test case due to its small size and the extensive background literature versus which the present results could be compared. Testing with B-Te-6-B shows that it is possible, although computationally costly, to compute spectra for much larger systems. With this integration of Newton-X and Molpro, the ability to use preferential electronic structure software has broadened for non-adiabatic dynamics. While this thesis only provides two functioning interfaces, there is potential for the expansion of the integration to other methods available in Molpro; discussed further below.

4.2 Future Directions

The understanding of non-adiabatic effects is important for proper insight into the photophysical and photochemical properties of molecules. Molecules that interact with photons need predictable behaviours if they are to be used for applications (e.g., biophysical imaging, photovoltaic devices). However, potential non-radiative relaxation pathways can both promote and hamper desired properties. Therefore, the simplest extension beyond this thesis is to simulate the excited state dynamics of other molecules beyond the small examples used here to test the new Molpro/Newton-X interface. Due to computational cost, exploring B-Te-6-B CASSCF dynamics was deemed prohibitive for the timeframe of this thesis. Moreover, the most interesting properties of this molecule would require the incorporation of spin-orbit couplings, as accomplished in the software package SHARC.[117–119] Once implemented, extended computation of B-Te-6-B for excited state dynamics could be conducted

along with similar molecules. Indeed, the computational framework generated in this work is applicable to any molecule, provided the available quantum chemistry methods are suitable.

In the context of LCC2 and LADC(2), further understanding of the effects of localization parameters on the nuclear gradients is necessary for continuing any development of adiabatic dynamics for the ground state, which can be used for sampling for UV-Vis spectra, or the natural extension to excited state dynamics. As Molpro does not offer analytical non-adiabatic coupling vectors for the local methods, different approaches would be required for non-adiabatic dynamics.[90,96–100] One possible direction is to compare a canonical CC integration (presently available in Newton-X via Turbomole)[120] to the current one and determine the changes to the gradients obtained. This development would have the added benefit of creating support for the more computationally expensive but potentially more accurate methods.

As the CASSCF non-adiabatic integration was successful, extending functionality to other multi-reference methods would be useful. While the current integration has the capabilities to support other Molpro multi-reference methods (CASPT2,[103–106] CASPT-F12,[121] and MRCI[101,102]), small modifications would be required for portable support. This implementation would allow for exploitation of benefits garnered from the methods built upon CASSCF such as CASPT2 and the like; note that during the writing of this thesis, a new BAGEL/Newton-X interface for both CASSCF and XMS-CASPT2 was developed and published.[99,100] Molpro's CASPT2 shares much of the same functionality with CASSCF (although, at present, non-adiabatic coupling vectors cannot be computed either numerically or analytically) and thus should be able to be called with minimal edits to search parameters in the interface. The details of the interface can be further explored in the Appendices A and B.

Additionally, Molpro's continued updates to newer editions may add new features which could ease program optimization. The current integration uses Molpro 2015 as the base which was current at the beginning of the work. At time of writing, Molpro has released

a 2019 version which has improved energy gradients for LCC2 and LADC(2) and improved CASSCF functionality; both features may affect the accuracy and behaviour of the interface. It is expected that the Molpro version update should not break the interface but minor changes to the internal syntax may be needed for smooth running of the code.

Bibliography

[1] Polli, D.; Altoè, P.; Weingart, O.; Spillane, K. M.; Manzoni, C.; Brida, D.; Tomasello, G.; Orlandi, G.; Kukura, P.; Mathies, R. A.; Garavelli, M.; Cerullo, G. *Nature* **2010**, *467*, 440–443.

[2] Barbatti, M.; Aquino, A. J. A.; Szymczak, J. J.; Nachtigallová, D.; Hobza, P.; Lischka, H. *Proc. Natl. Acad. Sci. U. S. A.* **2010**, *107*, 21453–21458.

[3] Jasper, A. W.; Zhu, C.; Nangia, S.; Truhlar, D. G. *Faraday Discuss.* **2004**, *127*, 1–22.

[4] Worth, G. A.; Cederbaum, L. S. *Annu. Rev. Phys. Chem.* **2004**, *55*, 127–158.

[5] Kamtekar, K. T.; Monkman, A. P.; Bryce, M. R. *Adv. Mater.* **2010**, *22*, 572–582.

[6] Hagfeldt, A.; Boschloo, G.; Sun, L.; Kloo, L.; Pettersson, H. *Chem. Rev.* **2010**, *110*, 6595–6663.

[7] Jensen, F. *Introduction to Computational Chemistry*; John Wiley & Sons, Incorporated: New York, United Kingdom, 2017.

[8] Roos, B. O.; Lindh, R.; Malmqvist, P. Å.; Veryazov, V. *Multiconfigurational Quantum Chemistry*; John Wiley & Sons, Incorporated: Hoboken, New Jersey, 2016.

[9] Cramer, C. J. *Essentials of computational chemistry : theories and models, 2nd ed.*; John Wiley & Sons, Incorporated: Chichester, West Sussex, England, 2004.

[10] Bunge, C. F. In *Novel Electronic Structure Theory: General Innovations and Strongly Correlated Systems*; Hoggan, P. E., Ed.; Advances in Quantum Chemistry; Academic Press, 2018; Vol. 76; pp 3 – 34.

[11] Zobel, J. P.; Heindl, M.; Nogueira, J. J.; González, L. *J. Chem. Theory Comput.* **2018**, *14*, 3205–3217.

[12] Zobel, J. P.; Nogueira, J. J.; González, L. *J. Phys. Chem. Lett.* **2015**, *6*, 3006–3011.

[13] Tully, J. C. *J. Chem. Phys.* **2012**, *137*, 22A301.

[14] Barbatti, M.; Crespo-Otero, R. In *Density-Functional Methods for Excited States*; Ferré, N., Filatov, M., Huix-Rotllant, M., Eds.; Springer International Publishing: Cham, 2016; pp 415–444.

[15] Herman, M. F. *J. Chem. Phys.* **1984**, *81*, 754–763.

[16] Tully, J. C. *J. Chem. Phys.* **1990**, *93*, 1061–1071.

[17] Li, X.; Tully, J. C.; Schlegel, H. B.; Frisch, M. J. *J. Chem. Phys.* **2005**, *123*, 084106.

[18] Ding, F.; Goings, J. J.; Liu, H.; Lingerfelt, D. B.; Li, X. *J. Chem. Phys.* **2015**, *143*, 114105.

[19] Werner, H.-J. et al. MOLPRO, version 2015.1, a package of ab initio programs. 2015; see http://www.molpro.net.

[20] Werner, H.-J.; Knowles, P. J.; Knizia, G.; Manby, F. R.; Schütz, M. *Wiley Interdiscip. Rev. Comput. Mol. Sci.* **2012**, *2*, 242–253.

[21] Frisch, M. J. et al. Gaussian 16 Revision B.01. 2016; Gaussian Inc. Wallingford CT.

[22] Hartree, D. R. *Math. Proc. Camb. Philos. Soc.* **1928**, *24*, 89–110.

[23] Fock, V. *Z. Phys.* **1930**, *61*, 126–148.

[24] Hartree, D. R.; Hartree, W. *Proc. R. Soc. Lond. A* **1935**, *150*, 9–33.

[25] Slater, J. C. *Phys. Rev.* **1930**, *35*, 210–211.

[26] Deegan, M. J.; Knowles, P. J. *Chem. Phys. Lett.* **1994**, *227*, 321 – 326.

[27] Christiansen, O.; Koch, H.; Jørgensen, P. *Chem. Phys. Lett.* **1995**, *243*, 409 – 418.

[28] Schreiber, M.; Silva-Junior, M. R.; Sauer, S. P. A.; Thiel, W. *J. Chem. Phys.* **1994**, *128*, 134110–134134.

[29] Stanton, J. F.; Bartlett, R. J. *J. Chem. Phys.* **1993**, *98*, 7029–7039.

[30] Monkhorst, H. J. *Int. J. Quantum Chem.* **1977**, *12*, 421–432.

[31] Kats, D.; Korona, T.; Schütz, M. *J. Chem. Phys.* **2006**, *125*, 104106.

[32] Pipek, J.; Mezey, P. G. *J. Chem. Phys.* **1989**, *90*, 4916–4926.

[33] Ledermüller, K.; Kats, D.; Schütz, M. *J. Chem. Phys.* **2013**, *139*, 084111.

[34] Verner, H. J.; Knowles, P. J. MOLPRO User Manual. 2015.

[35] Kats, D.; Schütz, M. *J. Chem. Phys.* **2009**, *131*, 124117.

[36] Schütz, M. *J. Chem. Phys.* **2015**, *142*, 214103.

[37] Siegbahn, P. E. M.; Almlöf, J.; Heiberg, J.; Roos, B. O. *J. Chem. Phys.* **1981**, *74*, 2384 – 2396.

[38] Hohenberg, P.; Kohn, W. *Phys. Rev.* **1964**, *136*, B864–B871.

[39] Gross, E. K. U.; Dobson, J. F.; Petersilka, M. In *Density Functional Theory II: Relativistic and Time Dependent Extensions*; Nalewajski, R. F., Ed.; Springer Berlin Heidelberg: Berlin, Heidelberg, 1996; pp 81–172.

[40] Laurent, A. D.; Jacquemin, D. *Int. J. Quantum Chem.* **2013**, *113*, 2019–2039.

[41] Tozer, D. J. *J. Chem. Phys.* **2003**, *119*, 12697–12699.

[42] Prlj, A.; Curchod, B. F. E.; Fabrizio, A.; Floryan, L.; Corminboeuf, C. *J. Phys. Chem. Lett.* **2015**, *6*, 13–21.

[43] Crespo-Otero, R.; Barbatti, M. *Theor. Chem. Acc.* **2012**, *131*, 1237.

[44] Lukeš, V.; Šolc, R.; Barbatti, M.; Lischka, H.; Kauffmann, H.-F. *J. Theor. Comput. Chem.* **2010**, *09*, 249–263.

[45] Holland, D. M. P.; Trofimov, A. B.; Seddon, E. A.; Gromov, E. V.; Korona, T.; de Oliveira, N.; Archer, L. E.; Joyeux, D.; Nahon, L. *Phys. Chem. Chem. Phys.* **2014**, *16*, 21629–21644.

[46] Jones, D. B.; Mendes, M.; Limão-Vieira, P.; Ferreira da Silva, F.; Jones, N. C.; Hoffmann, S. V.; Brunger, M. J. *J. Chem. Phys.* **2019**, *150*, 064303.

[47] Kang, H.; Lee, K. T.; Jung, B.; Ko, Y. J.; Kim, S. K. *J. Am. Chem. Soc.* **2002**, *124*, 12958–12959.

[48] Adrover, M.; Frau, J.; Caldés, C.; Vilanova, B.; Donoso, J.; Muñoz, F. *J. Photochem. Photobiol. A* **2010**, *209*, 19 – 26.

[49] Adamo, C.; Jacquemin, D. *Chem. Soc. Rev.* **2013**, *42*, 845–856.

[50] Milonni, P. W. In *The Quantum Vacuum*; Milonni, P. W., Ed.; Academic Press: San Diego, 1994; pp 1 – 33.

[51] Denis, J.; Aurélien, P.; Carlo, A.; Benedetta, M. *J. Chem. Theory Comput.* **2012**, *8*, 2359–2372.

[52] Condon, E. *Phys. Rev.* **1926**, *28*, 1182–1201.

[53] Franck, J.; Dymond, E. G. *Trans. Faraday Soc.* **1926**, *21*, 536–542.

[54] Barbatti, M.; Ruckenbauer, M.; Plasser, F.; Pittner, J.; Granucci, G.; Persico, M.; Lischka, H. *Wiley Interdiscip. Rev. Comput. Mol. Sci. 4*, 26–33.

[55] Wigner, E. *Phys. Rev.* **1932**, *40*, 749–759.

[56] Dahl, J. P.; Springborg, M. *J. Chem. Phys.* **1988**, *88*, 4535–4547.

[57] Schütz, M. *J. Chem. Phys.* **2015**, *142*, 214103.

[58] Busch, T.; Esposti, A. D.; Werner, H. *J. Chem. Phys.* **1991**, *94*, 6708–6715.

[59] Lindh, R. *Theor. Chem. Acc.* **1993**, *85*, 423–440.

[60] Barbatti, M. *Wiley Interdiscip. Rev. Comput. Mol. Sci.* **2011**, *1*, 620–633.

[61] Tavernelli, I.; Tapavicza, E.; Rothlisberger, U. *J. Chem. Phys.* **2009**, *130*, 124107.

[62] Plasser, F.; Barbatti, M.; Aquino, A. J. A.; Lischka, H. *Theor. Chem. Acc.* **2012**, *131*, 1073.

[63] Levine, B. G.; Coe, J. D.; Martínez, T. J. *J. Phys. Chem. B* **2008**, *112*, 405 – 413.

[64] Malhado, J. P.; Bearpark, M. J.; Hynes, J. T. *Front. Chem.* **2014**, *2*, 1 – 21.

[65] Domcke, W.; Yarkony, D. R. *Annu. Rev. Phys. Chem.* **2012**, *63*, 325 – 352.

[66] Nakamura, H. *Advances in Chemical Physics*; John Wiley & Sons, Ltd, 2008; Chapter 3, pp 95–212.

[67] Azumi, T.; Matsuzaki, K. *Photochem. Photobiol.* **1977**, *25*, 315–326.

[68] Menger, M. F. S. J.; Plasser, F.; Mennucci, B.; González, L. *J. Chem. Theory Comput.* **2018**, *14*, 6139–6148.

[69] Barbatti, M.; Ruckenbauer, M.; Plasser, F.; Queen, R. C.; Granucci, G.; Persico, M.; Pittner, J.; Lischka, H. NEWTON-X: A package for Newtonian dynamics close to the crossing seam. Version 2. 2016; `www.newtonx.org`.

[70] Pederzoli, M.; Pittner, J. *J. Chem. Phys.* **2017**, *146*, 114101.

[71] Schnappinger, T.; Kölle, P.; Marazzi, M.; Monari, A.; González, L.; de Vivie-Riedle, R. *Phys. Chem. Chem. Phys.* **2017**, *19*, 25662–25670.

[72] Saika, T.; Irie, M.; Shimidzu, T. *J. Chem. Soc., Chem. Commun.* **1994**, 2123–2124.

[73] Vivas, M. G.; Nogueira, S. L.; Silva, H. S.; Barbosa Neto, N. M.; Marletta, A.; Serein-Spirau, F.; Lois, S.; Jarrosson, T.; De Boni, L.; Silva, R. A.; Mendonca, C. R. *J Phys. Chem. B* **2011**, *115*, 12687–12693.

[74] Salzmann, S.; Kleinschmidt, M.; Tatchen, J.; Weinkauf, R.; Marian, C. M. *Phys. Chem. Chem. Phys.* **2008**, *10*, 380–392.

[75] Wu, X.-F.; Zheng, X.; Wang, H.-G.; Zhao, Y.-Y.; Guan, X.; Phillips, D. L.; Chen, X.; Fang, W. *J. Chem. Phys.* **2010**, *133*, 134507.

[76] Wan, J.; Hada, M.; Ehara, M.; Nakatsuji, H. *J. Chem. Phys.* **2001**, *114*, 842–850.

[77] Haberkern, H.; Asmis, K. R.; Allan, M.; Swiderek, P. *Phys. Chem. Chem. Phys.* **2003**, *5*, 827–833.

[78] González, D. M.; Raftopoulos, K. N.; He, G.; Papadakis, C. M.; Brown, A.; Rivard, E.; Müller-Buschbaum, P. *Macromol. Rapid Commun.* **2017**, *38*, 1700065.

[79] Braun, C. A.; Zomerman, D.; de Aguiar, I.; Qi, Y.; Delgado, W. T.; Ferguson, M. J.; McDonald, R.; de Souza, G. L. C.; He, G.; Brown, A.; Rivard, E. *Faraday Discuss.* **2017**, *196*, 255–268.

[80] He, G.; Torres Delgado, W.; Schatz, D. J.; Merten, C.; Mohammadpour, A.; Mayr, L.; Ferguson, M. J.; McDonald, R.; Brown, A.; Shankar, K.; Rivard, E. *Angew. Chem.* **2014**, *53*, 4587–4591.

[81] Torres Delgado, W.; Shahin, F.; Ferguson, M. J.; McDonald, R.; He, G.; Rivard, E. *Organometallics* **2016**, *35*, 2140–2148.

[82] Yanai, T.; Tew, D. P.; Handy, N. C. *Chem. Phys. Lett.* **2004**, *393*, 51–57.

[83] Dunning Jr., T. H. *J. Chem. Phys.* **1990**, *90*, 1007–1023.

[84] Woon, D. E.; Dunning Jr., T. H. *J. Chem. Phys.* **1993**, *98*, 1358–1371.

[85] Stephens, P. J.; Devlin, F. J.; Chabalowski, C. F.; Frisch, M. J. *J. Phys. Chem.* **1994**, *98*, 11623–11627.

[86] Becke, A. D. *J. Chem. Phys.* **1993**, *98*, 5648–5652.

[87] Lee, C.; Yang, W.; Parr, R. G. *Phys. Rev. B* **1988**, *37*, 785–789.

[88] Vosko, S. H.; Wilk, L.; Nusair, M. *Can. J. Phys.* **1980**, *58*, 1200–1211.

[89] Peterson, K.; Figgen, D.; Goll, E.; Stoll, H.; Dolg, M. *J. Chem. Phys.* **2003**, *119*, 11113–11123.

[90] Frisch, M. J. et al. Gaussian 09 Revision B.1. Gaussian Inc. Wallingford CT 2009.

[91] Igarashi, N.; Tajiri, A.; Hatano, M. *Bull. Chem. Soc. Jpn.* **1981**, *54*, 1511–1516.

[92] Stenrup, M. *Chem. Phys.* **2012**, *397*, 18 – 25.

[93] El Azhary, A.; Rauhut, G.; Pulay, P.; Werner, H.-J. *J. Chem. Phys.* **1998**, *108*, 5185–5193.

[94] Schütz, M.; Werner, H.-J.; Lindh, R.; Manby, F. R. *J. Chem. Phys.* **2004**, *121*, 737–750.

[95] He, G. Frontier Institute of Science and Technology, Xi'an Jiaotong University, Xi'an, People's Republic of China. Personal Communication, 2018.

[96] Schmidt, M. W.; Baldridge, K. K.; Boatz, J. A.; Elbert, S. T.; Gordon, M. S.; Jensen, J. H.; Koseki, S.; N.Matsunaga,; Nguyen, K. A.; Su, S. J.; Windus, T. L.; M.Dupuis,; J.A.Montgomery, General Atomic and Molecular Electronic Structure System. 1993.

[97] Lischka, H. et al. COLUMBUS, an ab initio electronic structure program, release 5.9.2. 2008.

[98] Lischka, H.; Shepard, R.; Pitzer, R. M.; Shavitt, I.; Dallos, M.; Müller, T.; Szalay, P. G.; Seth, M.; Kedziora, G. S.; Yabushita, S.; Zhang, Z. *Phys. Chem. Chem. Phys.* **2001**, *3*, 664–673.

[99] BAGEL, Brilliantly Advanced General Electronic-structure Library. `http://www.nubakery.org`, under the GNU General Public License.

[100] Shiozaki, T. *Wiley Interdiscip. Rev. Comput. Mol. Sci.* **2018**, *8*, e1331.

[101] Werner, H. J.; Knowles, P. J. *J. Chem. Phys.* **1988**, *89*, 5803–5814.

[102] Knowles, P. J.; Werner, H. J. *Chem. Phys. Lett.* **1988**, *145*, 514–522.

[103] Werner, H. J. *Mol. Phys.* **1996**, *89*, 645–661.

[104] Celani, P.; Werner, H.-J. *J. Chem. Phys.* **2000**, *112*, 5546–5557.

[105] Shiozaki, T.; Győrffy, W.; Celani, P.; Werner, H.-J. *J. Chem. Phys.* **2011**, *135*, 081106.

[106] Györffy, W.; Shiozaki, T.; Knizia, G.; Werner, H.-J. *J. Chem. Phys.* **2013**, *138*, 104104.

[107] Andersson, K.; Malmqvist, P. A.; Roos, B. O.; Sadlej, A. J.; Wolinski, K. *J. Phys. Chem.* **1990**, *94*, 5483–5488.

[108] Andersson, K.; Malmqvist, P.; Roos, B. O. *J. Chem. Phys.* **1992**, *96*, 1218–1226.

[109] Ilkhani, A. R. *Quím. Nova* **2017**, *40*, 491 – 495.

[110] Ilkhani, A. R. *Chem. Pap.* **2019**, *73*, 85–94.

[111] Karami, K.; Abedanzadeh, S.; Hervés, P. *RSC Adv.* **2016**, *6*, 93660–93672.

[112] Abiramasundari, A.; Sudarsanam, V.; Vasu, K. K. *Anal. Methods* **2015**, *7*, 7659–7673.

[113] Lee, Y. H.; Tang, Y.; Verwilst, P.; Lin, W.; Kim, J. S. *Chem. Commun.* **2016**, *52*, 11247–11250.

[114] Hehre, W. J.; Ditchfield, R.; Pople, J. A. *J. Chem. Phys.* **1972**, *56*, 2257.

[115] Hariharan, P. C.; Pople, J. A. *Theor. Chim. Acta* **1973**, *28*, 213–222.

[116] Schaftenaar, G.; Vlieg, E.; Vriend, G. *J. Comput. Aided Mol. Des.* **2017**, *31*, 789–800.

[117] Mai, S.; Richter, M.; Heindl, M.; Menger, M. F. S. J.; Atkins, A.; Ruckenbauer, M.; Plasser, F.; Oppel, M.; Marquetand, P.; Gonzales, L. SHARC2.0: Surface Hopping Including Arbitrary Couplings — Program Package for Non-Adiabatic Dynamics. sharc-md.org, 2018.

[118] Mai, S.; Marquetand, P.; González, L. *Wiley Interdiscip. Rev. Comput. Mol. Sci.* **2018**, *8*, e1370.

[119] Richter, M.; Marquetand, P.; González-Vázquez, J.; Sola, I.; González, L. *J. Chem. Theory Comput.* **2011**, *7*, 1253–1258.

[120] Ahlrichs, R.; Bär, M.; Häser, M.; Horn, H.; Kölmel, C. *Chem. Phys. Lett.* **1989**, *162*, 165–169.

[121] Shiozaki, T.; Werner, H.-J. *J. Chem. Phys.* **2010**, *133*, 141103.

[122] Barbatti, M.; Granucci, G.; Persico, M.; Ruckenbauer, M.; Vazdar, M.; Eckert-Maksić, M.; Lischka, H. *J. Photochem. Photobiol. A* **2007**, *190*, 228–240.

Appendix A

Implementation Details

A.1 Introduction

Newton-X (NX) interfaces with quantum chemistry software (QCS) packages via parsing their outputs into standardized formats which NX then reads and processes. The majority of the NX-QCS interface is written in Perl and consists of generating geometries for the QCS, setting up the input environment, initiating the QCS, reading and extracting output, and repeating these steps as needed, e.g., for generating a molecular dynamics trajectory. By varying the input geometries as dictated by the QCS output (e.g., gradients which are needed for the numerical solution of Newton's equations of motion), NX is capable of mapping out the requisite trajectories and potential energy surfaces upon which dynamics takes place. Of relevance to this thesis, three major tasks are outlined: the generation of initial conditions, running trajectories along an adiabatic potential energy surface, and the corresponding non-adiabatic case involving surface hopping.

As Molpro is the QCS under consideration for the purposes of the code development reported in this thesis, the program calling function is consistent throughout all the job types. Molpro is simply called via the command line with an appropriate input file that is provided through NX. Conveniently, Molpro accepts molecular geometry input as an imported XYZ

file. By setting the input template to point at a specific XYZ file (geom.xyz as generated by NX), the first function for generating geometries is trivial. The major impediments then are setting up the template input file which Molpro will run and extracting the relevant data from output generated. These two issues will be outlined in the following sections.

Due to the differences in function calling between the local methods, LCC2 and LADC(2), and CASSCF, the NX-Molpro integration was separated as two distinct program modes. This choice is mainly due to the differences in output file structure when calling the different quantum chemistry methods within Molpro. Molpro's native input language is capable of some input-output manipulations allowing for grouping of certain sets of variables. The main use of this capability was to collate the energies of the states into a single table under `E_NEWTONX` to avoid issues where multiple energy entries could potentially confuse the script and to better preserve state ordering. For LCC2 and LADC(2), excited state energies were stored as vertical excitations which needed to be converted to total energies before processing.

In addition to the NX-Molpro interface scripts, additional modifications were required for NX to recognize Molpro as a module for running purposes. Here, Molpro was simply populated in the two called forms into the indices which make up the list of QCS packages recognized by NX. The interface scripts were created as separate modules following NX guidelines. This setup allows for the use of NX's built-in input generator for creating most of the non-Molpro input.

A.2 Initial Conditions and Spectra Generation

The initial conditions job generates a set of geometries, and corresponding momenta, from which trajectories are processed. For generating these initial conditions (geometries, and, for dynamics, velocities), NX offers a selection of methods which include sampling from normal modes (Wignter distribution), sampling from previously computed trajectories, and sampling velocities at a preselected geometry. Of these, only the normal mode based generation

gives the option for use of an external QCS package to generate a UV-Vis spectrum and thus Molpro integration focuses on this task. Initial conditions generation for NX requires Molpro to output only energies and corresponding oscillator strengths are needed for UV-Vis spectra for the quantum chemistry method selected. Therefore, the Molpro input file only requires the energy of the states collected after a single point computation. Otherwise, the required input files are standard as per other QCS integrations included in NX: Gaussian, COLUMBUS, Turbomole, etc.

A general walkthrough of the relevant spectrum generation algorithm can be summarized as follows. NX calls the interface script. The interface script is then provided with the current geometry and the general Molpro input template. The script assembles the input and calls Molpro. Molpro then undertakes a single point calculation at the provided geometry. The script then reads the output to assemble the energies and the corresponding oscillator strengths. Internal files are generated and then written to output before control is handed back to the main NX code. This process iterates as needed to populate the initial conditions setup, e.g., if one is sampling a Wigner distribution.

A.2.1 Energies

As stated earlier, energies are collated via Molpro's internal variable system allowing for potential energies to be saved to `E_NEWTONX` which is then printed as a table at the end of the Molpro output. These values are collected and stored in the NX internal file `epot`. Energies are stored as atomic units (hartree) and are converted to other units as needed for other in-file requirements. For CASSCF, energies can be stored directly via the command, "`E_NEWTONX=ENERGY`". The local methods (LCC2 and LADC(2)), however, save energies beyond the ground state as vertical excitations in eV as `OMEGA_S` and thus need to be converted back to atomic units and then added to the ground potential energy to satisfy NX formatting.

A.2.2 Oscillator Strengths

Since oscillator strengths are flagged differently between the quantum chemistry methods (LCC2/LADC(2) versus CASSCF), they will be discussed as separate cases. Oscillator strengths are to be read by internal NX functions and thus are read when required. Output files are searched to find the keywords flagging the locations of the (numerical) oscillator strengths and returned as values to be handled by NX.

For LCC2 and LADC(2), the oscillator strengths are conveniently listed under numbered state outputs making it trivial to extract them by location. However, CASSCF only lists transition moments rather than oscillator strengths directly which complicates matters. The transition moment between the desired states is recorded for each Cartesian coordinate axis. The transition moment components are then grouped and converted to an oscillator strength (f_i) via

$$f_i = \frac{2}{3}(E_i - E_0)(\mu_{xi}^2 + \mu_{yi}^2 + \mu_{zi}^2) \tag{A.1}$$

where E_i is the energy of the state of interest, E_0 is the ground state energy, and $\mu_{\alpha i}$ ($\alpha = x, y, z$) is the Cartesian component for the transition moment between the ground state and state i. In the present implementation, all excitations are initiated from the ground state ($E_0 \rightarrow E_i$) for the three methods: LCC2, LADC(2), and CASSCF.

A.3 Adiabatic Dynamics

The adiabatic dynamics job determines trajectories (i.e., molecular geometries as a function of time) by solving Newton's equations of motion from the initial conditions. To follow the trajectories, NX requires nuclear gradients in addition to energies as well as a set of initial conditions (geometries and velocities). Therefore, integrated QCS methods need to compute nuclear gradients to commence dynamics. Molpro offers these analytic gradients for both the local methods and CASSCF, among others; it should be noted that access to ground state gradients for the local methods is largely undocumented. Thus, the Molpro input file

requires commands to output the gradients in addition to energies.

Molpro writes gradients under specified headers which can be read as needed. States are classified by the state number which are stored in order in the `grad.all` file. The current state's gradients are saved in `grad` file which are loaded by NX as needed. The general algorithm effectively only adds the gradients interpreter to the initial conditions script, now in the dynamics program framework.

A.3.1 Nuclear Gradients

CASSCF gradients are produced in Molpro by invoking the `force` program after saving the desired state. Gradients are then read at the end of the file after saving. The adiabatic gradients are featured for most multi-reference methods offered by Molpro and thus are exportable for them as well. Some gradients (including CASSCF and CASPT2) are determined analytically while others would need to be found numerically.

LCC2 and LADC(2) gradients are slightly more difficult to gather if the ground state is desired. This difficulty is due to the methods having mutually exclusive calls for obtaining properties for ground versus excited states. Therefore, two function calls are required, one for the ground state and one for the excited state, with the `force` program invoked after the ground state computation but before the excited state computation.

A.4 Non-adiabatic Dynamics

NX non-adiabatic dynamics computes trajectories while tracking two electronic states, as well as determining the non-adiabatic coupling vectors. Molpro's non-adiabatic functionality is currently limited to CASSCF methods. Integration with NX is built upon the adiabatic dynamics algorithm taking non-adiabatic vectors into account. These vectors are read from the Molpro output after invoking the `force` program loaded with a saved non-adiabatic coupling matrix during CASSCF runtime.

A.4.1 Non-adiabatic Coupling Vectors

Non-adiabatic coupling vectors are first saved in Molpro with `CPMCSCF` onto a desired record before being loaded by the `force` program. The output vectors representing the non-adiabatic coupling are then saved into the internal `nad_vectors` file. As only the transition between two specific states is focused upon, the coefficients for other transitions are ignored if executed. The `nad_vectors` file is then shipped to interpolation as a `newh` file.

A.5 Additional Tools

To modify the Molpro environment within the NX call, a parameter file is set up from which to draw external data. For redundancy, parameters can also be read as non-default addenda to NX input files, where priority will be put to the input files over parameter files in the case of conflict. Spectra are generated through NX's internal spectrum generator which utilizes the nuclear ensemble approach.[122] For spectra sampling from adiabatic dynamics, intermediate Molpro data was extracted and fed into the NX spectrum generator. The Molpro implementation was confirmed by comparison with results generated with the same quantum chemistry methods in other QCS (when available) to test the veracity of implementation. These tests are covered in Chapters 2 and 3.

A.6 Summary

An interface between NX and Molpro was created for spectral simulations and the generation of adiabatic dynamics for LCC2 and LADC(2) methods as well as non-adiabatic dynamics for CASSCF. The integration searches Molpro output files for relevant data to generate the components for the job steps as required: energies, oscillator strengths, nuclear gradients, and non-adiabatic coupling vectors. The implementation has been tested with the methods previously listed but expansion to other multi-reference (e.g., CASPT2) methods are possible

for the CASSCF implementation.

Appendix B

Implementation Code

B.1 Initial Conditions Implementation

```
use strict;
use warnings;
use lib join('/',$ENV{"NX"},"lib") ;
use colib_perl;
my ($MOLPRO,$mld,$mdle);
my ($ctd,$MOLPROlog,$MOLPROpar,$epotf);
my (@prmt,$w,$type,$type_prev,$koj,$memn,$mem,$proc);
my ($nat,$istep,$nstat,$nstatdyn,$ndamp,$kt,$dt,$t,$tmax,$nintc);
my ($numat,$nact,$npoints,$fgeom,$fnmode,$fout,$fvib,$iprog);
my ($chk_e,$prog,$evert,$de,$kvert,$nis,$nfs,$seed,$methodname);
my ($prop,$value,$dx,$dy,$dz,$OOS,$mxns);
my ($lvprt,$retval);
$MOLPRO     = $ENV{"MOLPRO"};                    # MOLPRO environment
$mld        = $ENV{"NX"};                          # NX environment
$mdle       = "runmolpro-initcond.pl:";
```

```
$MOLPROlog = "molpro.out";
$MOLPROpar = "molpro.par";
$ctd       = "aux.out";
if(-e "zero"){
  $epotf    ="epot0";
} else {
  $epotf    ="epot";
}
read_par();
modify_input();
run_prog();
read_info();
cleanup();
if ($lvprt>=2) { print STDOUT "End of $mdle \n";}
sub modify_input{ #Modifies Molro input, unused except for empty
    input
        $retval=callprogsp($mld,"nx2xyz",$mdle);
        if ($retval != 0){
                die "$mdle is dying now\n";
        }
        if(! -e "molpro.mpi"){
                my ($nocc,$nelectron);
                #$memn = 800;
                open(my $INP, ">molpro.mpi") or die("Cannot create
                    input");
                open(my $geom, "geom") or die("Cannot read
                    geometry");
```

```
while(<$geom>){
        chomp;
        if(/^\s*\w(\s+-?\d+\.?\d*){5}\s*$/){
                my @i = split('_',$_);
                $nelectron += $i[1];
                next;
        }
}
$nocc = int(($nelectron + 1) / 2);
print $INP ("***,$mdle\nmemory,$mem,M\n\nsymmetry,
   nosym\norient,noorient\ngeometry=geom.xyz\
   nCARTESIAN\n");
print $INP ("basis={default,vdz\nset,mp2fit\
   ndefault,vdz/mp2fit\nset,jkfit\ndefault,vdz/
   jkfit}\n");
if($methodname eq "molpro-casscf"){
        print $INP ("\n{multi");
        if($nocc > 10){
                print $INP ("\nfrozen,", $nocc-2);
        }
        print $INP ("\nocc,", $nocc + 4,";wf,
           $nelectron,1,0\nstate,3}\n");
        print $INP ("\ne_newtonx=energy\n");
}else{
        print $INP ("{hf;occ,$nocc;wf,$nelectron
           ,1,0}\n{lt-df-ladc(2)\neom,-3.1,tranes
           =-2.1+3.1\neomprint,popul=-1,loceom
```

```
                =-1}\n");
            print $INP ("e_newtonx(1)=energy(1)\n");
            for(my $i = 2; $i < $nfs; $i++){
                print $INP ("e_newtonx($i)=
                    OMEGAF_S(", $i - 1, ")/toev+
                    energy(1)\n");
            }
        }
        print $INP ("\n{table,_e_newtonx}\n{table,_gradx,_
            grady,_gradz}\n");
        close($INP);
        close($geom);
    }
    if ($methodname eq "molpro-casscf") {
        open(WFU, '>wfu') or die "failed_to_create_wfu_
            flag_file";
        close(WFU);
    }
}
sub run_prog{ #call Molpro
  if ($lvprt>=2) {print STDOUT "$mdle_starting_Molpro_with_$proc_
      cores\n";}
  $retval=callprog("","molpro_molpro.mpi_-v_-n_$proc_-d_\$TMPDIR",
      $mdle);
  if ($retval != 0){
    die "$mdle_is_dying_now_(Molpro_call_failed)\n";
  }
```

```
}
sub read_par{ #read NX input
  $prog     = getkeyword("initqp_input","prog"    ,"1");
  $methodname=method_name($prog);
  $nis      = getkeyword("initqp_input","nis"     ,"1");
  $nfs      = getkeyword("initqp_input","nfs"     ,"2");
  $lvprt    = getkeyword("initqp_input","lvprt"   ,"1");
  $mem      = getkeyword("initqp_input","mem"     ,"500");
  $proc     = getkeyword("molpro.par","proc"    ,"1"); #par file
     sometimes does not work, initqp_input overrides
  $proc     = getkeyword("initqp_input","proc", $proc);
  $mxns = max_ns($nis,$nfs);
}
sub cleanup{
  system("rm -rf NEWPROGRAM_OLD_FILES");
}
sub read_ctd{
 open(CT, $ctd) || die "Cannot open $ctd!";
 @prmt=<CT>;
 close(CT);
 foreach $w (@prmt)
 {
  chop($w);
($numat,$nact,$npoints,$fgeom,$fnmode,$fout,$fvib,$iprog,$chk_e,
   $prog,$evert,$de,$kvert,$nis,$nfs,$seed)=
split(/,/,$w);
 }
```

```
}
sub read_info{ #read Molpro output
  print "\n  $methodname \n";
  print "\n $mdle //// ENERG \n";
  read_write_energy_trans();
  print "\n $mdle //// OOS    \n";
  read_write_oos();
}
sub read_write_energy_trans{ #read energies and transition
   strengths
  print "reading energies\n";
  open(ML, $MOLPROlog) or die "Cannot open $MOLPROlog \n";
  open(EPA,">epotaux")    or die "Cannot open epotaux";
  my ($found);
  while(<ML>) {
    chomp;
        if(/^\s*ENEWTONX\s*$/){ #energy flag ENEWTONX, save
           energies into array
                while(defined($_ = <ML>) && ($_ !~ /^\s*$/)){
                        chomp;
                        print EPA "$_\n";
                }
        }
  }
  close(EPA);
  for (my $ifs = 1; $ifs <= $mxns; $ifs++){ #duplicate energies
    if ($ifs != $nis){
```

```
      open(EPA,"epotaux")    or die "Cannot open epotaux";
      open(EP, '>', "$epotf.$ifs")     or die "Cannot open $epotf.
          $ifs: $!";
      while(<EPA>) {
        if (($. == $nis) or ($. == $ifs)) {
          print EP $_;
        }
      }
      close(EPA);
      close(EP);
    }
  }
}
sub read_write_oos{ #send to oscillator strengths calculation in
    external library
  for (my $ifs = 1; $ifs <= $mxns; $ifs++){
    if ($ifs != $nis){
      $prop  = ">oos.$ifs";
      open(PP,$prop) or die "Cannot open $prop";
      $value = osc_strength($mdle,$nis,$ifs,$prog);
      ($OOS,$dx,$dy,$dz)=split(/,/,$value);
      printf PP "%9.6f \n",$OOS;
    }
  }
}
```

B.2 Dynamics Implementation

```
use strict;
use warnings;
my ($retval);
my ($MOLPRO,$mld,$mdle,$BASEDIR,$DEBG,$RS);
my ($ctd,$MOLPROlog,$MOLPROpar);
my (@prmt,$type,$type_prev,$koj,$memn);
my ($nat,$istep,$nstat,$nstatdyn,$ndamp,$kt,$dt,$t,$tmax,$nintc);
my ($nxrestart,$thres,$killstat,$timekill,$prog,$lvprt,$etot_jump,
    $etot_drift,$proc);
my ($nstd,$nstd_2,$nstd_5,$nstd_30,$tol,$tol0,$ti,$istring,$ist);
my ($tn);
my ($var1,$var2);
my ($prop,$value,$dx,$dy,$dz,$OOS,$is,$ns);
my ($mem,$phase,$getphase,$vnadx,$vnady,$vnadz,$methodname);
use lib join('/',$ENV{"NX"},"lib") ;
use colib_perl;
$MOLPRO      = $ENV{"MOLPRO"};              # MEWPROG environment
$mld         = $ENV{"NX"};                   # NX environment
$mdle        = "run-molpro.pl:";
$BASEDIR     = `pwd`;
chomp ($BASEDIR);
$DEBG        = "DEBUG";
$RS          = "RESULTS";
$MOLPROlog = "molpro.out";
$MOLPROpar = "molpro.par";
$ctd         = "control.d";
read_ctd();          # Normally, do not need any change
```

```
read_par();          # Must be changed for MOLPRO
modify_input();      # Must be changed for MOLPRO
run_prog();          # Must be changed for MOLPRO
read_info();         # Must be changed for MOLPRO
cleanup();           # Must be changed for MOLPRO
sub modify_input{ #Modifies input, only used for empty
        $retval=callprogsp($mld,"nx2xyz",$mdle);  # convert
           geometry from NX format to MOLPRO format
        if ($retval != 0){
                die "$mdle is dying now\n";
        }
        if(! -e "molpro.mpi"){
                my ($nocc,$nelectron,%atomcount);
                print("Creating input\n");
                #$memn = 800;
                open(my $INP, ">molpro.mpi") or die("Cannot create
                   input");
                open(my $geom, "geom") or die("Cannot read
                   geometry");
                while(<$geom>){
                        chomp;
                        if(/^\s*\w(\s+-?\d+\.?\d*){5}\s*$/){
                                my @i = split(' ',$_);
                                $nelectron += $i[1];
                                $atomcount{uc $i[0]} ++;
                                next;
                        }
```

```
}
$nocc = int(($nelectron + 1) / 2);
print $INP ("***,$mdle\nmemory,$mem,M\n\nsymmetry,
    nosym\norient,noorient\ngeometry=geom.xyz\
    nCARTESIAN\n");
print $INP ("basis={default,vdz\nset,mp2fit\
    ndefault,vdz/mp2fit\nset,jkfit\ndefault,vdz/
    jkfit}\n");
if($methodname eq "molpro-casscf"){
        print $INP ("\n{multi");
         if($nocc > 10){
                print $INP ("\nclosed,", $nocc -
                    2);
         }
        print $INP ("\nocc,", $nocc + 4,";wf,
            $nelectron,1,0\nstate,", $nstat, "}\n")
            ;
        print $INP ("\ne_newtonx=energy\n");
        print $INP ("\n{rs2\nstate,1,", $nstatdyn,
             "\n");
        print $INP ("noexc}\n\n{force;varsav}\n");
}else{
        print $INP ("{hf;occ,$nocc;wf,$nelectron
            ,1,0}\n{lt-df-ladc(2)\neom,-3.1,tranes
            =-2.1+3.1\neomprint,popul=-1,loceom
            =-1}\n");
        print $INP ("e_newtonx(1)=energy(1)\
```

```
                    ne_newtonx(2)=OMEGAF_S(1)/toev+energy
                    (1)\ne_newtonx(3)=OMEGAF_S(2)/toev+
                    energy(1)\n");
                }
                print $INP ("\n{table, e_newtonx}\n{table, gradx,
                    grady, gradz}\n");
                close($INP);
                close($geom);
            }
}
sub run_prog{ #call Molpro
  if ($lvprt>=2) {print_STDOUT("$mdle starting Molpro with $proc
      cores \n");}
  $retval=callprog("","molpro -v -n $proc -t $proc -d \$TMPDIR
      molpro.mpi",$mdle);  # call MOLPRO
  if ($retval != 0){
    die "$mdle is dying now\n";
  }
}
sub read_par{ #read NX input
  $prog     = getkeyword("control.dyn","prog"    ,"1");
  $methodname=method_name($prog);
  $lvprt    = getkeyword("control.dyn","lvprt"   ,"1");
  $proc     = getkeyword("molpro.par", "proc", "1");
  $proc     = getkeyword("control.dyn", "proc", $proc);
}
```

```
sub cleanup{
   if ($lvprt>=2){
      if (!-e "../$DEBG/MOLPRO.$tn"){
         system("mkdir ../$DEBG/MOLPRO.$tn");
      }
      system("cp -rf *../$DEBG/MOLPRO.$tn/.");
   }
   system("rm -rf NEWPROG_OLD_FILES");
}

sub read_ctd{
open(CT, $ctd) or die "$mdle Cannot open $ctd!\nsystems answer was
    : $!";
   @prmt=split(/,/,<CT>);
   chomp(@prmt);
close(CT);
($nat,$istep,$nstat,$nstatdyn,$ndamp,$kt,$dt,$t,$tmax,$nintc,
$mem,$nxrestart,$thres,$killstat,$timekill,$prog,$lvprt,$etot_jump
    ,$etot_drift)=@prmt;
         $nstatdyn = int($nstatdyn);
   $tn=$t*1;
if ($lvprt>=2) {
   print_STDOUT("$mdle running in $BASEDIR\n");}
}

sub read_info{ #read sequence
   print_STDOUT("\n $mdle ////  ENERG \n");
```

```
    read_write_energy();
    print_STDOUT("\n $mdle //// OOS   \n");
    read_write_oos();
    print_STDOUT("\n $mdle //// GRAD  \n");
    read_write_grad();
    if ($thres > 0){
        print_STDOUT("\n $mdle //// NONAD \n");
      read_write_nonad();
    }
}

sub read_write_grad{ #nuclear gradients reading
        my @gd;
        if(-e "grad"){
                system("cp grad grad_old");
        }
        print("reading gradients\n");
        print_STDOUT("Gradients (current state is $nstatdyn):\n",
            $istep,$kt);
        open(my $GD, $MOLPROlog) or die("cannot open $MOLPROlog \n
            ");
        open(my $grad, ">grad") or die("cannot write to grad \n");
        my $found;
        while(<$GD>){
                chomp;
                if(/GRADIENT FOR STATE (\d).\d/){ #search for
                    gradients of specified state
```

```
                    my $i = $1;
                    print_STDOUT("$i \n");
                    $found = 1;
                    <$GD>;
                    <$GD>;
                    <$GD>;
                    while(defined($_ = <$GD>) && ($_ =~ /\d+(\
                        s+-?\d+\.?\d*){3}/)){
                            chomp;
                            my @grads = split(/\s+/,$_);
                            shift @grads;
                            shift @grads;
                            $gd[$i] .= "@grads \n";
                    }
            }
}
$found or die("No Gradient Found");
close($GD);
open(my $GDO, ">grad.all") or die("cannot write to grad.
    all");
for (my $i = 1; $i <= $nstat; $i++){ #write gradients in
    order
            if ($i == $nstatdyn){
                    print($grad "$gd[$nstatdyn]\n");
                    printf_STDOUT($istep, $kt, "$gd[$nstatdyn
                        ]\n");
                    print($GDO "$gd[$nstatdyn]\n");
```

```
                }elsif($i != $nstatdyn){
                        if(defined $gd[$i] and length $gd[$i]){
                                print($GDO "$gd[$i]\n");
                        }else{
                                for (my $ind1 = 1; $ind1 <= $nat;
                                   $ind1++) {
                                        print $GDO "0.000  0.000
                                           0.000\n";
                                }
                        }
                }
        }
        close($GDO);
        close($grad);
}


sub read_write_nonad{ #non-adiabatic coupling vectors
  my ($iaux,$jst,$ist,$vh,$kat,$dum,$found);
  my (@hx, @hy, @hz, @epot);
 if (-s "nad_vectors"){
   system("cp -f nad_vectors oldh");    # Create file to
      interpolation and phase routines
 } else {
   open(OH,">oldh")      or die "Cannot open oldh to write.";
   for (my $ia=1; $ia<=2*$nat; $ia++) {
      print OH "     0.0000000     0.0000000     0.0000000 \n";
```

```
    }
    close(OH);
}
 open(my $GD, $MOLPROlog) or die("cannot open $MOLPROlog \n");
 print("reading vectors\n");
 while(<$GD>){ #read NAD vectors
        chomp;
        if(/SA-MC NACME FOR STATES \d.\d - \d.\d/){ #search for
            vectors (NACME), two states are specified, multiple
            states should only parse first
                $found = 1;
                <$GD>;
                <$GD>;
                <$GD>;
                my $i = 0;
                while(defined($_ = <$GD>) && ($_ =~ /\d+(\s+-?\d
                    +\.?\d*){3}/)){
                        chomp;
                        my @grads = split(/\s+/,$_);
                        shift @grads;
                        shift @grads;
                        ($hx[$i], $hy[$i], $hz[$i]) = @grads;
                        $i++;
                }
        }
 }
 close($GD);
```

```
  $found or print("No NAD Vectors Found");
  $found or return;
  open(my $grad, ">nad_vectors") or die("cannot write to
     nad_vectors");
  print("Nonadiabatic coupling vector: ",$istep,$kt,"\n");
  for(my $i = 0; $i < $nat; $i++){ #write vectors
        print($grad "$hx[$i] $hy[$i] $hz[$i]\n");
        print("$hx[$i] $hy[$i] $hz[$i]\n");
  }
 if ( $lvprt >= 1 ){
   print_STDOUT("Nonadiabatic coupling vectors (a.u.):\n",$istep,
      $kt);
   open(NV,"nad_vectors") or die "$mdle Cannot find nad_vectors!";
   while(<NV>){
     print_STDOUT("$_",$istep,$kt);
   }
   close(NV);
 }
 system("cp -f nad_vectors newh");    # Create file to
    interpolation routine
 if ( $lvprt >= 2 ){
   print_STDOUT("\n $mdle //// PHASE \n",$istep,$kt);
 }
 phase_adjust();
}
sub read_write_energy{ #read energies
        if ($istep != 0){
```

```
        system("cp -f epot oldepot"); # This file will be
            used in the interpolation routine
}
print("reading energies\n");
open(my $ML, $MOLPROlog) or die("cannot open $MOLPROlog \n
    ");
open(my $EPOT, ">epot") or die("cannot write to epot \n");
my $found;
while(<$ML>){
        chomp;
        if(/^\s*E_NEWTONX\s*$/){ #search for "E_NEWTONX"
            as flag
                $found = 1;
                while(defined($_ = <$ML>) && ($_ !~ /^\s*$
                    /)){
                        chomp;
                        print ("$_\n");
                        print ($EPOT "$_\n");
                }
        }
}
$found or die("No energies found under E_NEWTONX\n");
close($ML);
close($EPOT);
if ($istep != 0){
        system("cp -f epot newepot"); # This file will be
            used in the interpolation routine
```

```
        }
}
sub read_write_oos{ #read oscillator strengths, link to external
    library
     $prop  = ">>../$RS/properties";
     open(PP,$prop) or die "Cannot open $prop to append!";
     print PP "\n TIME (fs): $t     STEP: $istep     CURRENT STATE: 
        $nstatdyn \n";
     $is = 1;
     for ($ns = 2; $ns <= $nstat; $ns++){
          $value = osc_strength($mdle,$is,$ns,$prog);
          printf STDOUT "  Oscillator strength (%d,%d) = %9.6f \n",
             $is,$ns,$value;
          if (($nxrestart == 0) or ($istep != 0) or ($lvprt >= 2)){
            printf PP " Oscillator strength (%d,%d) = %9.6f \n",$is,
               $ns,$value;
          }
     }
     print_STDOUT("\n");
}
sub phase_adjust{ #adjust phase of NADV
   $phase = 1.0;
   $getphase = &keyinfile( "sh.inp", "getphase" );
   if ( $getphase == 0 ){
     print_STDOUT("No method defined for getphase = 0. Phase will 
        not be adjusted",$istep,$kt);
   }elsif( $getphase == 1 ){
```

```
    $retval = callprogsp( $mld, "escalar", $mdle );
    if ($retval != 0){
      die "$mdle is dying now\n";
    }
    system("cp -f nadv nad_vectors");
    if ( $lvprt >= 2 ) { system("cp -f escalar.log ../$DEBG/."); }
    open( EP, "escph" ) or die "Cannot open escph to read.";
    print_STDOUT("The global phase(s) is(are):",$istep,$kt);
    while(<EP>){
      chomp;
      $_ =~ s/^\s*//;
      $_ =~ s/\s*$//;
      print_STDOUT(" $_ ",$istep,$kt);
    }
    print_STDOUT("\n\n",$istep,$kt);
    close(EP);
  }
  if($lvprt >= 1){
    open( NV, "nad_vectors" ) or die "Cannot open nad vectors to
        read.";
    print_STDOUT("Nonadiabatic coupling vectors after phase
        adjustment (a.u.):\n",$istep,$kt);
    while (<NV>){
      chomp;
      $_ =~ s/^\s*//;
      $_ =~ s/\s*$//;
      ( $vnadx, $vnady, $vnadz ) = split( /\s+/, $_ );
```

```
        printf_STDOUT($istep,$kt,"%14.7F %14.7F %14.7F \n",$vnadx,
            $vnady,$vnadz);
      }
      close(NV);
    }

    system("cp -f nad_vectors newh");      # Create file to
        interpolation routine
}
```

Appendix C

Geometries

Geometries are given in xyz format using angstroms.

C.1 Thiophene

B3LYP/cc-pVDZ

9

Thiophene B3LYP/cc–pVDZ

C	−0.0095800000	−1.2377100000	0.0000840000
C	−1.2691430000	−0.7141060000	−0.0001160000
C	−1.2691420000	0.7141060000	0.0000980000
C	−0.0095790000	1.2377100000	−0.0000390000
S	1.1952430000	0.0000000000	−0.0000120000
H	0.2820090000	−2.2853250000	0.0001320000
H	−2.1716230000	−1.3244470000	−0.0001820000
H	−2.1716220000	1.3244470000	0.0001470000
H	0.2820110000	2.2853250000	−0.0000600000

CASSCF(4,4)/6-31G(d)

9

Thiophene CASSCF(4,4)/6−31G(d)

C	−0.0113500000	−1.2449270000	0.0000250000
C	−1.2756770000	−0.7154100000	−0.0000210000
C	−1.2756760000	0.7154110000	0.0000070000
C	−0.0113490000	1.2449270000	0.0000050000
S	1.2023600000	0.0000000000	−0.0000080000
H	0.2831220000	−2.2924070000	0.0000360000
H	−2.1798480000	−1.3251870000	−0.0000340000
H	−2.1798470000	1.3251880000	0.0000180000
H	0.2831240000	2.2924070000	0.0000200000

CASSCF(10,10)/6-31G(d)

9

Thiophene CASSCF(10,10)/6−31G(d)

C	−0.0179493844	−1.2452373471	0.0002468097
C	−1.2729544926	−0.7167058282	0.0001438038
C	−1.2729539903	0.7167067506	0.0001499195
C	−0.0179485129	1.2452373954	0.0002478584
S	1.2194823833	−0.0000003887	0.0000094914
H	0.2628872416	−2.2782686457	−0.0002803608
H	−2.1642969789	−1.3148443901	−0.0001030745
H	−2.1642960660	1.3148459349	−0.0000860101
H	0.2628888000	2.2782685190	−0.0002804373

C.2 B-Te-6-B

B3LYP/cc-pVDZ + B3LYP/cc-pVDZ(pp)

59

B–Te–6–B B3LYP/cc–pVDZ + B3LYP/cc–pVDZ(pp)

Te	0.0003170000	−1.2589990000	0.0572150000
C	−1.3829670000	0.3075990000	−0.1229160000
C	1.3833770000	0.3082880000	−0.1191350000
C	−0.7234090000	1.5112280000	−0.2656450000
C	0.7236810000	1.5115870000	−0.2636260000
O	3.3664690000	−1.2984120000	0.0305720000
O	3.9107720000	0.9250590000	−0.1170560000
B	2.8922370000	−0.0060030000	−0.0713710000
C	5.1706440000	0.2038470000	−0.2594120000
C	4.7993810000	−1.2342660000	0.2801420000
C	6.2396960000	0.9420500000	0.5420170000
H	7.1948970000	0.3931660000	0.5204900000
H	6.4104750000	1.9365350000	0.1023020000
H	5.9394840000	1.0832780000	1.5885300000
C	5.5225540000	0.2231400000	−1.7520400000
H	5.5590660000	1.2677960000	−2.0956410000
H	6.5029060000	−0.2389660000	−1.9452310000
H	4.7642520000	−0.3031980000	−2.3505470000
C	5.4683430000	−2.3947810000	−0.4522210000
H	6.5641020000	−2.3463760000	−0.3469130000
H	5.1277650000	−3.3482980000	−0.0207260000
H	5.2177990000	−2.4006470000	−1.5210650000
C	4.9910170000	−1.3858540000	1.7944490000
H	4.5171000000	−2.3239280000	2.1201150000
H	6.0564120000	−1.4225080000	2.0691960000

H	4.5161770000	−0.5597650000	2.3443540000
C	0.7752910000	3.8849100000	0.5695510000
H	1.1628920000	4.8875950000	0.3253130000
H	1.1409510000	3.6514620000	1.5830100000
C	−0.7797610000	3.8864230000	0.5640910000
H	−1.1525160000	3.6584210000	1.5762470000
H	−1.1636780000	4.8888170000	0.3128530000
C	−1.3875350000	2.8611420000	−0.4183960000
H	−1.2230740000	3.2162340000	−1.4537420000
H	−2.4731760000	2.7852780000	−0.2812000000
C	1.3871420000	2.8623440000	−0.4129640000
H	2.4723760000	2.7881000000	−0.2723800000
H	1.2239780000	3.2189930000	−1.4480850000
B	−2.8918160000	−0.0070800000	−0.0800500000
O	−3.3654230000	−1.2892280000	0.1132240000
O	−3.9112380000	0.9135750000	−0.2212050000
C	−4.8030470000	−1.2780520000	−0.1162260000
C	−5.1663910000	0.2442050000	0.1019820000
C	−5.4549830000	−2.2481060000	0.8660020000
C	−5.0243190000	−1.7577700000	−1.5562580000
C	−6.2528560000	0.7912980000	−0.8201660000
C	−5.4882290000	0.5910510000	1.5608110000
H	−6.5527430000	−2.2211240000	0.7747510000
H	−5.1214190000	−3.2738810000	0.6471520000
H	−5.1828220000	−2.0203780000	1.9049090000
H	−4.5552860000	−2.7456850000	−1.6773630000
H	−6.0949170000	−1.8509960000	−1.7951450000

H	−4.5619460000	−1.0737140000	−2.2832820000
H	−7.2067190000	0.2638720000	−0.6585660000
H	−6.4156200000	1.8587910000	−0.6069180000
H	−5.9745630000	0.6976220000	−1.8780040000
H	−5.5223890000	1.6856670000	1.6676010000
H	−6.4626530000	0.1831220000	1.8706590000
H	−4.7161150000	0.2084440000	2.2447220000

C.3 Methaniminium

Starting geometry

6

Methaniminium

N	0.031321	−0.105472	0.627003
C	0.056994	0.004111	−0.645862
H	0.031004	0.682487	1.103975
H	0.086989	−0.978089	1.024804
H	0.026822	0.977677	−1.006544
H	0.135467	−0.981259	−1.322544